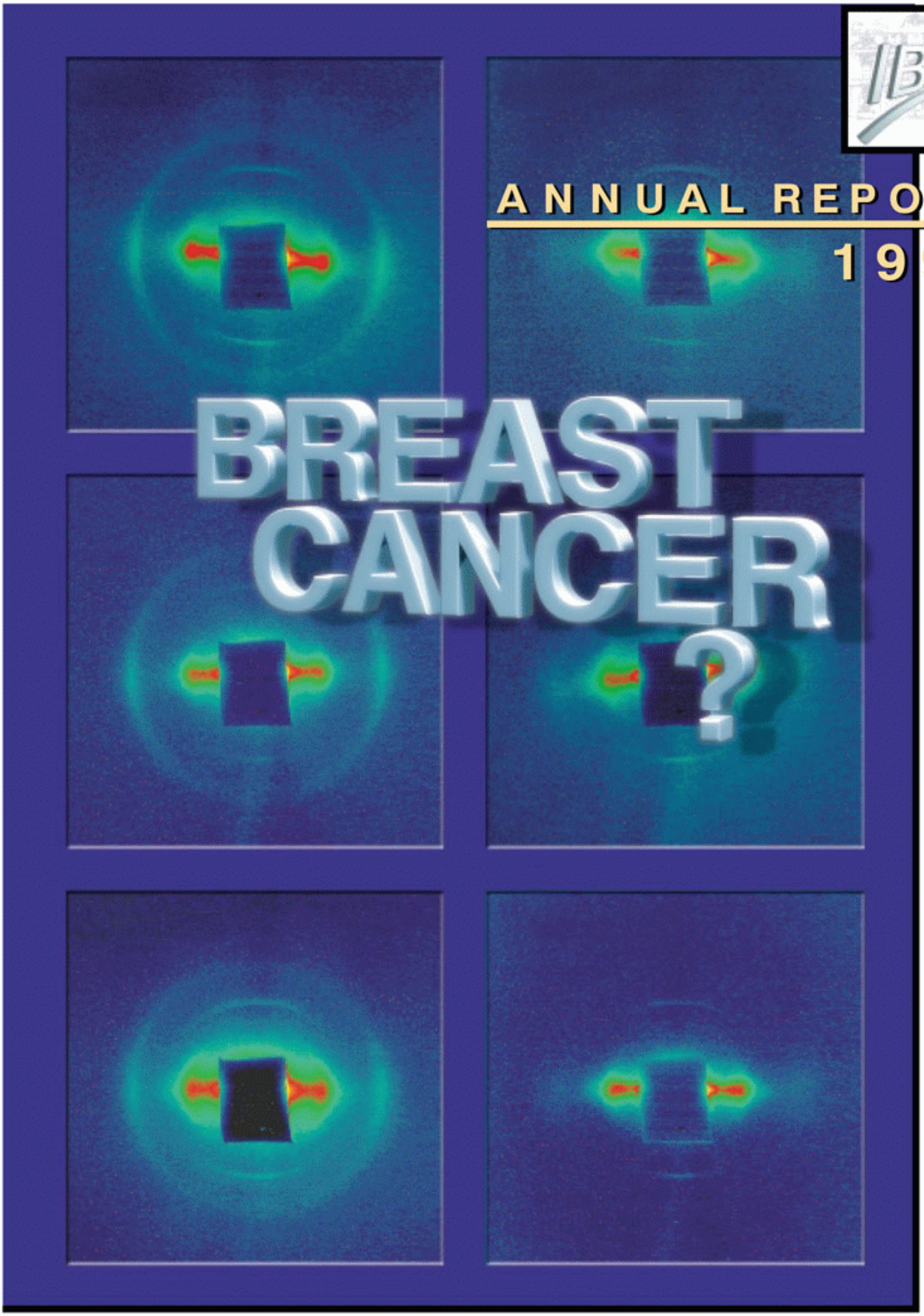

ANNUAL REPORT 1999

AUSTRIAN SAXS BEAMLINE AT elettra

Extracted from the user contribution Amenitsch et al.: *No Correlation between Breast Cancer and Hair Structure (p. 44)*

Austrian Small Angle X-ray Scattering (SAXS) Beamline at ELETTRA

Annual Report 1999

Compiled by the SAXS-Group:

- for IBR: M. Rappolt & H. Amenitsch
- for ELETTRA: S. Bernstorff

Table of Contents

Preface

The front cover of this report relates to the flop of the year: synchrotron X-ray diffraction patterns from single hair samples were reported, first in a correspondence in *Nature* and quickly afterwards in the news media around the globe, to carry promise for breast cancer screening. Only a few months later, these hopes were dispelled by several independent studies, one of them carried out at the Austrian SAXS beamline at ELETTRA. The story had all ingredients for a colorful feuilleton essay on conduct in science: politics, publicity, (over-) ambition, quest for fame, and the eagerness to justify the costs of large installations by something really important to the general public.

Scientifically and technically these 'hairy' experiments were certainly inferior to the other studies reported here. However, these remain safely within the scientific community, most of them not even sexy enough to hit the pages of *Nature*. Maybe this is not important. Science proceeds in steps, most of them being rather small, respecting the need for care as it befits the trade.

This is not the place to offer advice. My intention is to thank all the users and the staff involved for the very respectable work they have done. It encourages us to improve the facility and the access further - and we know, there is room for improvement.

This being said, I may, nevertheless, suggest that we encourage activities in a sector that is largely missing: industry. There seems to be a gap in awareness and interest. With the need for ever more refined materials and processes - keywords: nanomaterials, biotechnology, catalysis - both sides could benefit if this gap were closed or at least narrowed.

Peter Laggner
Director
Institute of Biophysics and X-Ray Structure Research
Austrian Academy of Sciences

Once again, it was a pleasure for me to read this timely and carefully prepared Annual Report of the Austrian SAXS beamline at Elettra.

In December 1999, the Elettra Scientific Advisory Council (SAC), a panel composed of distinguished international experts, reviewed the performance of several beamlines, including SAXS. The opinion of the Council about SAXS was very positive and they encouraged us to think about ways to increase the efficiency in the use of beam time in order to satisfy an even larger number of users.

The present report provides much supporting evidence for the SAC opinion. It relates the results of the experiments performed by 144 scientists of 47 different research institutes in 17 countries. The topics range from biology to complex fluids, to "soft" condensed matter and to materials science in the more traditional sense, and the quality is consistently very good.

In addition, I should like to mention the excellent cooperation between the members of the Austrian team and the Elettra staff in the daily operation of the beamline, as well as in the continuing effort to improve and upgrade the existing instrumentation. With little bureaucracy and the common desire to perform good science, most problems are solved without formalities. I believe this beamline is an example of successsful cooperation between different institutions and different countries.

I will conclude by thanking all the people involved in the success of the beamline, and wishing them, and myself, that many more "Annual Reports" will record the future achievements of this enterprise.

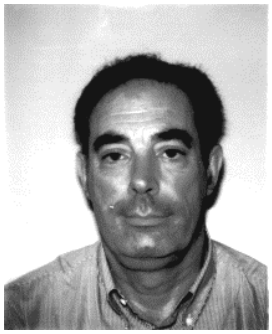

Massimo Altarelli
Director
Elettra Synchrotron Light Source

The SAXS-Group

HEAD OF PROJECT: Peter Laggner[1)]

e-mail: fibrlagg@mbox.tu-graz.ac.at

SCIENTISTS: Heinz Amenitsch[1), 3)]

e-mail: Amenitsch@Elettra.Trieste.It

Sigrid Bernstorff [2)]

e-mail: Bernstorff@Elettra.Trieste.It

POSTDOCS: Pavo Dubcek[2)]

e-mail: Pavo.Dubcek@Elettra.Trieste.It

Michael Rappolt[1), 3)]

e-mail: Michael.Rappolt@Elettra.Trieste.It

PhD-STUDENTS: Georg Pabst[1), 3)]

e-mail: Georg.Pabst@Elettra.Trieste.It

TECHNICIAN: Christian Morello[2)]

e-mail: Christian.Morello@Elettra.Trieste.It

1) Institute for Biophysics and X-ray Structure Research, Austrian Academy of Sciences, Steyrergasse 17, 8010 Graz, Austria.
Tel 0043-316-812 004
Fax 0043-316-812 367

2) Sincrotrone Trieste, Strada Statale 14, km 163.5, 34012 Basovizza (TS), Italy.
Tel 0039-040-375 81
Fax 0039-040-938 0902

3) Institute for Biophysics and X-ray Structure Research, Austrian Academy of Sciences c/o Sincrotrone Trieste

The SAXS-Beamline in General

Small Angle X-ray Scattering has become a well known standard method to study the structure of various objects in the spatial range from 1 to 1000 nm, and therefore instruments capable to perform such experiments are installed at most of the synchrotron research centers. The high-flux SAXS beamline at ELETTRA is mainly intended for time-resolved studies on fast structural transitions in the sub-millisecond time region in solutions and partly ordered systems with a SAXS-resolution of 1 to 140 nm in real-space.
The photon source is the 57-pole wiggler whose beam is shared and used simultaneously with a Macromolecular Crystallography beamline. The wiggler delivers a very intense radiation between 4 and 25 keV of which the SAXS-Beamline accepts 3 discrete energies, namely 5.4, 8 and 16 keV. The beamline optics consists of a flat double crystal monochromator and a double focusing toroidal mirror.
A versatile SAXS experimental station has been set-up, and an additional wide-angle X-ray scattering (WAXS) detector monitors simultaneously diffraction patterns in the range from 0.1 to 0.9 nm. The sample station is mounted move-able onto an optical table for optimising the sample detector distance with respect to SAXS resolution and sample size.
Besides the foreseen sample surrounding the users have the possibility to install their own specialised sample equipment. In the design phase, besides technical boundary conditions, user friendliness and reliability have been considered as important criteria.
The optimisation of the beamline with respect to high-flux and consequently high flux density, allows to perform the following experiments:

- Low Contrast Solution Scattering
- Grazing Incidence Surface Diffraction
- Micro-Spot Scanning
- X-ray Fluorescence Analysis
- Time-Resolved Studies ≥ 11 μs
- Simultaneously Performed Small- and Wide-Angle Measurements (SWAXS) on:
  - Gels
  - Liquid Crystals
  - (Bio) Polymers
  - Amorphous Materials
  - Muscles

Furthermore, using 5.4 and 16 keV energies, the beamline is widely applicable also to very thin, e.g. single muscle fibers, and optically thick (high Z) specimen, as often used in e.g., material science and solid state physics.

THE INSERTION DEVICE

The wiggler for the SAXS beamline consists of three 1.5 m long segments, each having 19 poles. The device can work with a minimum gap of 20 mm, which corresponds to K=20 at 2 GeV. The main parameters of the wiggler are:

- Critical Energy 4.1 keV
- Radiation Power 8.6 kW
- Flux 3.5×10^{14} ph/s/mrad/0.1%BW (at 400 mA)

The wiggler radiation cone has a horizontal width of 9 mrad. From this the SAXS-beamline accepts vertically 0.3 mrad, and horizontally +/-0.5 mrad at a 1.25 mrad off-axis position. The resulting source size for 8 keV photons is 3.9 x 0.26 mm^2 (horiz. x vert.).

THE OPTICS

The optics common with the diffraction beamline consists of:

- C-Filter and Beryllium window assembly to reduce the power load on the first optical elements by a factor of 2 and to separate the beamline vacuum from the storage ring.
- Beam defining slit chamber which allows to define the SAXS beam on three sides before the monochromator in order to reduce the straylight in the downstream beamline sections.

The SAXS beamline optics consists of:

- A double-crystal monochromator consisting of four individual chambers, in which three interchangeable asymmetric Si(111) crystal pairs are used to select one of three fixed energies. Each of the crystal pairs is optimised for the corresponding energy to accomplish a grazing angle of 2°. The energy resolution $\Delta E/E$ of the monochromator is in the range of 0.7 - 2.5 10^{-3}.
- A baffle chamber after the monochromator is used as an adjustable straylight fenditure.
- A segmented toroidal mirror focuses the light in horizontal and vertical direction with a 1/2.5 magnification onto the SAXS-detector.
- An aperture slit reduces the straylight after the monochromator and the toroidal mirror.
- A guard slit defines the illuminated region around the focal spot. The spot size on the detector is 1.6 mm horizontally and 0.6 mm vertically. The calculated flux at the sample is in the order of 10^{13} ph/s at 400 mA. For a maximum sample size of 5.4 x 1.8 mm^2 correspondingly a flux density of 10^{12} ph/s/mm^2 has been calculated.

SAMPLE STAGE

The multipurpose sample stage allows to perform fast time-resolved relaxation studies based on temperature- or pressure-jumps as well as stopped flow experiments. Shear jump relaxation experiments are planned. Specifically, T-jumps can be induced by an infra-red light pulse (2 ms) from an Erbium-Glass laser, raising the temperature about 20 °C in an aqueous sample volume of 10 µl. A newly designed hydrostatic pressure cell with a maximal accessible angular range of 30° for simultaneous SAXS and WAXS measurements is available. P-jumps are realised by switching fast valves between a low and a high pressure reservoir, increasing or decreasing the hydrostatic pressure in the range from 1 bar to 1.7 kbar (in future 3 kbar) within a few ms. Also a 1.5 T magnet has been installed. In an overview, the following sample manipulations are possible:

- Temperature Manipulations: Ramps, Jumps and Gradient Scans
- Pressure Manipulation: Scan and Jumps
- Stopped Flow Experiments
- SWAXS Measurements Applying Mechanical Stress
- SWAXS Measurements Applying Magnetic Fields

(For further details see also Experimental Possibilities part 1.-3.)

Scientific applications	Low Contrast Solution Scattering, Grazing Incidence Surface Diffraction, Micro-Spot Scanning, X-ray Fluorescence Analysis, Time-Resolved Studies ≥ 11 μs and Simultaneously Performed Small- and Wide-Angle Measurements (SWAXS) on: Gels Liquid Crystals (Bio) Polymers Amorphous Materials Muscles
Source characteristics	Wiggler (NdFeB Hybrid): Period: 140 mm No. full poles: 57 Gap: 20 mm B_{max}: 1.607 T Critical Energy ε_c: 4.27 keV Power (9 mrad): 8.6 kW Effective source size FWHM: 3.9 x 0.26 mm^2(HxV)
Optics	Optical elements: Double crystal monochromator: Si (111) asym. cut, water cooled. Mirror: two–segment,toroidal, Pt coated. Distance from source: 18.4 m 26.5 m Acceptance: 1 mrad/0.3 mrad (HxV) Energy (3 selectable): 5.4, 8, 16 keV (0.077, 0.154, 0.23 nm) Energy resolution ΔE/E: 0.7-2.5 x 10^{-3} Focal spot size FWHM: 1.2 x 0.6 mm^2 (HxV) Spot at Sample FWHM: 5.4 x 1.8 mm^2(HxV) Flux at sample: 5 x 10^{12} ph s^{-1}(2 GeV, 200 mA, 8 keV)
Experimental apparatus	Resolution in real space: 1-140 nm (small-angle), 0.1- 0.9 nm (wide-angle) Sample stage: temperature manipulations: ramps, jumps and gradient scans, pressure manipulation: scan and jumps, flow jump experiments, SWAXS measurements applying mechanical stress, SWAXS measurements applying magnetic fields. Detectors: 1D gas-filled detectors for simultaneous small- and wide-angle (Gabriel type), 2D CCD-detector for small-angle.
Experiment control	Beamline control: Program-units written in LabView for Windows 1 D detector control: PC-card and software from Hecus & Braun, Graz. 2 D detector control: Software from Photonic Science, Oxford.

CURRENT STATUS

The beamline has been built by the Institute for Biophysics and X-ray structure Research (IBR), Austrian Academy of Science in collaboration with staff members from Sincrotrone Trieste, and is in user operation since September 1996. The set-up of the beamline started at the beginning of January 1995 with the installation of the support structure. Until the end of 1995, the 8 keV single energy system had been realised. The upgrade to the full three energy system was finished in spring 1998. Time resolved experiments require fast X-ray detectors and data acquisition hard- and software. Depending on the desired resolution in time and in reciprocal space, on isotropic or anisotropic scattering of the sample, one-dimensional position sensitive (delay-line type) or two-dimensional area detectors (CCD-type, available since October 1998) are employed. In 1999 two more standard devices have been added to the instrumental beam line pool: the Oxford Cryostream Cooler and the for X-ray scattering experiments re-designed Bio-Logic Stopped Flow Module.
In conclusion, due to wide versatility of the beamline and the highly flexible sample stage, there are nearly no limits for the realisation of an experiment, and you are welcome by our team to propose any interesting and highlighting investigation for the benefit of material and life sciences.

Application for Beamtime at ELETTRA

1. Beamtime Policy at SAXS beamline

The agreement of setting-up a collaborating research group, and the co-operation between the Austrian Academy of Sciences and Sincrotrone Trieste concerning the SAXS beamline, has been signed on the 20th March 1998. It defines also the beamtime distribution between the partners and the beamtime policy.
The following points are of interest for users:

The available beamtime of about 5000 hours/year is distributed as follows:

- 35% for Austrian Users, type: "CRG" (Collaborating Research Group)
- 50% for Users of Sincrotrone Trieste (ST)
- 15% is reserved for beamline maintenance

In both user beamtime contingents also any industrial, proprietary and confidential research can be performed according to the "General User Policy" of Sincrotrone Trieste.

To apply for CRG and ST user beamtime proposals must be submitted according to the rules of Sincrotrone Trieste. The international review committee at ELETTRA will rank the proposals according to their scientific merit assessment. Based on this decision beamtime will be allocated according to the specific quotes for the beamtimes (CRG/ST).

2. How to apply for beamtime

There are two deadlines each year for proposals, namely August 31st and February 28th. Accepted proposals will receive beamtime either in the then following first or second half year period, respectively. The Application Form must be completed on-line according to the following instructions. In addition, one printed form is also required and must be send to:

ELETTRA USERS OFFICE
Strada Statale 14 - km 163.5
34012 Basovizza (Trieste), ITALY
Tel: +39 040 3758628 - fax: + 39 040 3758565
email: useroffice@elettra.trieste.it

INSTRUCTIONS GIVEN BY THE USERS OFFICE

In case of emergency you can also download the old application form (download at: http://www.elettra.trieste.it/Documents/Users/CallForProposal.html)

1. Read carefully the following Guidelines.

2. Connect to the virtual Users' Office: http://users.elettra.trieste.it (or http://brain.elettra.trieste.it) using your favorite browser (Netscape 3.0 or above, Internet explorer 4.0 or above, etc.) with JavaScript enabled.

3. Select the Virtual Users Office link.

4. When prompted, insert your ID and password. If you are a new user fill in the registration form with your data and choose your institution with the search button; in case your institution does not appear in the list, please contact useroffice@elettra.trieste.it giving all the details about it. When registered, you will receive an acknowledgment, i.e. your ID and password, and you will be able to continue. In case you do not remember your password, please don't register again but contact useroffice@elettra.trieste.it. At any moment you can select the help button and view more detailed instructions.

5. Select the proposals button in the User functions group.

6. Select add and fill in on-line the proposal form. Please, type your proposal in English. Repeat this procedure for each proposal you intend to submit.

7. When finished, submit the proposal electronically, selecting the save button.

8. In case of continuation proposal: a) attach the experimental report of previous measurements; b) give your previous proposal number.

9. Print the proposal form together with each related safety form.

10. Sign the safety form(s).

11. Mail one complete printed copy to the Users Office.

NOTE

For further information, e.g., financial support for travel expenses, please have a look into the web-pages http://www.elettra.trieste.it/Documents/Users/ProceduraEU.html or contact the USERS OFFICE.

List of Institutes Participating in Experiments

Austria

Austrian Academy of Science, Erich Schmid Institut für Materialwissenschaft, Leoben

Fratzl Peter
Keckes Josef
Pippan R.
Szekely E.
Zizak Ivo

Institut für Metallphysik, Montanuniversität, Leoben

Paris Oskar

Austrian Academy of Science, Institute for Biophysics and X-ray Structure Research, Graz

Amenitsch Heinz
Farkas Rita
Hickel Andrea
Jing W.
Kriechbaum Manfred
Laggner Peter
Latal Angelika
Lohner Karl
Pabst Georg
Prassl Ruth
Pregetter Magdalena
Rappolt Michael
Schwarzenbacher Robert
Staudegger Erich
Vidal Monika
Winter Ingrid

Hecus Braun, Graz

Leingartner Werner

Ludwig Boltzmann Institut for Osteology, Vienna

Grabner Barbara
Roschger Paul
Tesch Walter

Ludwig Boltzmann-Institut for Osteology, and Hanusch-Hospital, 4th Medical Department, Vienna

Klaushofer Klaus

Technische Universität Graz, Institut für Chem. & Technologie Organischer Materialien, Graz

Stelzer Franz
Viertler Karin
Wewerka A.

Technische Universität Graz, Institut für Festkoerper Physik, Graz

Gadermaier C.
Leising G.
Resel Roland
Theißl Udo

Universität Wien, Institut für Materialphysik, Wien

Kopacz Ireneusz
Schafler Erhard
Zehetbauer Michael

Belgium

Catholic University of Leuven, Laboratory of Macromolecular Structural Chemistry, Leuven Heverlee

Bongaerts Karin
Guennady Evmenenko
Rheynaers Harry
Theunissen Elisabeth
Vinck Liesel

Croatia

"Ruder Boskovic" Institute, Zagreb

Pivac Branko
Radic Nikola

University of Zagreb, Institute for Physics, Zagreb

Milat Ognjen

Czech Republic

Academy of Sciences of the Czech Republic, Institute of Macro-molecular Chemistry, Prague

Baldrian Josef
Steinhart Milos

Czech Technical University, Faculty of Nuclear Science and Physical Engineering, Prague

Horky Martin

Finland

Åbo Akademi University, Dept. of Physical Chemistry, Materials Research Group, Turku

Karlson Stefan
Linden Mika

France

CNRS UMR 8612, University Paris-Sud, Paris

Artzner Franck
Lopez Christelle
Ollivon Michel

INSERM Unite 321, Paris

Chapman M.J.
Nigon F.

European Synchrotron Radiation Facility (ESRF), Grenoble

Ferrero Claudio

Germany

BENSC-HMI, Berlin

Triolo Alessandro

Max-Planck-Institut für Kohlenforschung, Mülheim / Ruhr

Ågren Patrik
Bussian Patrik

Philipps Universität, Inst. für Physikalische und Makromolekulare Chemie, Marburg

Ruland W.
Valenca Alexander
Wendorff J. H.

Universität Erlangen-Nürnberg, Inst. für Werkstoffwissenschaften, Lehrstuhl I, Erlangen

Biermann Horst
Mughrabi H.
Pyczak Florian

Universität Siegen, Walter Flex Strasse, 57068 Siegen

Besch Hans-Juergen
Hengstebeck T.
Meissner Wolff
Orthen Andre'
Pavel Nikolaus
Sarvestani Amir
Schmidt Thomas
Wagner Hendrik
Walenta Albert Heinrich

Hungary

Eötvös Lorand University, Institute for General Physics, Budapest

Hanak Peter
Ungár Tamas

India

Bhabha Atomic Research Centre, Solid State Physics Division, Trombay, Mumbai

Aswal Vinod K.

Indian Institute of Science, Department of Organic Chemistry, Bangalore

Bhattacharya S.
De S.

Inter University Consortium for DAE Facilities, Univ. Campus, Khandwa Road, Indore

Gupta Ajay
Chaudhari Suresh Manohar
Dasannacharya B.A.
Phase D. M.

Inter University Consortium for DAE Facilities, BARC, Mumbai

Goyal Prem S.

Indian Institute of Technology, Dep. of Metallurgical Engineering and Materials State Physics, Powai, Bombay

Vitta, Satish
Major, S.S

Italy

CNR, Centro di Studio sui Meccanismi di Reazione, c/o Dept of Chemistry, Univ. La Sapienza, Rome

Borocci S.
Mancini Giovanna

Sincrotrone Trieste, Trieste

Bernstorff Sigrid
Dubcek Pavo
Menk Ralf
Morello Christian

Università di Ancona, Istituto di Scienze Fisiche,Facolta' di Scienze Matematiche Fisiche e Naturali, Ancona

Ciuchi Federica
Carsughi Flavio
Gobbi Luigi
Lucchetta Daniele Eugenio
Maccioni Elisabetta
Mariani Paolo
Marzocchini Renato
Pisani Michaela
Ponzi-Bossi
Rustichelli Franco

Università.di Ancona, Dipartimento di Scienze e dei Materiali della Terra , Sezione Chimica, Ancona

Bruni P.
Cingolani Francesca
Conti Carla
Iacussi Marco

Università.di Ancona, Dipartimento di Scienze e dei Materiali della Terra, sez. Fisica, e Istituto Nazionale per la Fisica della Materia, Ancona

Francescangeli Oriano

Università di Firenze, Dip. Scienze Fisiologiche, Firenze

Bagni Maria Angela
Cecchi Giovanni
Colombini Barbara
Linari Marco
Lombardi Vincenzo
Lucii Leonardo
Piazzesi Gabriella
Reconditi Massimo
Vannicelli Casoni M. Elisabetta

Università di Modena, Dip. di Fisica, Modena

Corni F.
Ottarini G.
Tonini R.

Università di Palermo, dipartimento di Chimica Fisica, Palermo

Crapanzano Laura
Di Giovanni C.
Donato Ines Dorina
Geppi Marco
LoCelso F.
Triolo Roberto

Università di Roma-La Sapienza, Dip. Di Chimica

De Nooy Arjan
La Mesa Camillo

Università di Trieste, Dip. Biochimica, Biofisica, Chimica delle Macromole (BBCM), Trieste

Delben F.
Gamini Amelia
Gianni Rita
Liut G.
Paoletti Sergio
Rizzo Roberto

Poland

A. Mickiewicz University , Department of Macromolecular Physics, Poznan

Maciej Kozak.

Polish Academy of Sciences, Institute of Metallurgy and Materials Science, Krakow

Bonarski Jan T.

Spain

IIQAB-CSIC, Dep. Tecnologia de Tensioactius, Barcelona

Caelles Jaime
Cocera Merce
Lopez O.
De la Maza
Pons Ramon

Sweden

University of Uppsala, Institute of Cell and Molecular Biology, Biomedical Centre for Structural Molecular Biology, Uppsala

Forstner Michael

Russia

Ivanovo State University, Ivanovo

Valkova Larissa

The Netherlands

FOM Institute for Atomic and Molecular Physics, Amsterdam

Kleppinger Ralf

United Kingdom

University Laboratory of Physiology, Oxford

Ashley Christopher C

Griffiths Peter J.

USA

University of California, Department of Chemistry, Berkeley, California

Gin D.

Smith R.

List of Performed Experiments

1999 (first half year):

Proposal	Proposer	Institution	Country	Title	Research Area
185	Rizzo Roberto	Università degli Studi di Trieste, Dip. Biochimica, Biofisica, Chim. Macromol.	Italy	Saxs Studies on new Polysaccharides Derivatives: Solution and Gels	Chemistry
188	Pabst Georg	Austrian Academy of Sciences, Inst. of Biophysics and X-Ray Structure Research, Graz	Austria	Realtime X-ray Diffraction Studies on the Trapping of Ordered Intermediates in Phospholipid Phase Transitions	Medical applications Biophysics
195	Resel Roland	Technische Universität Graz, Institut für Festkörperphysik	Austria	Nanostructured thin films on basis of Polymerised Lyotropic liquid Crystals-one possibility to obtain highly ordered Electroactive Molecules	Physics
197	La Mesa Camillo	Università di Roma "La Sapienza" - Dip. di Chimica	Italy	Fine Structure of Organised Solutions and Lytropic Mesophases	Physics Chemistry
207	Vitta Satish	Indian Institute of Technology, Dep. of Metallurgical Engineering and Materials Science, Bombay	India	Structural characterization of Langmuir-Blodgett multilayers and related nanostructures/composites using Synchrotron radiation	Material Science
208	Aswal Vinod K.	Bhabha Atomic Research Centre, Solid State Physics Division, Trombay, Mumbai	India	Study of the counterion distribution around gemini micelles in aqueous solutions	Physics
230	Saverstani Amir	Universität GHS Siegen	Germany	Measurements of System Performance of new one and two dimensional gaseous detectors	Technology/ Instrumen-tation
231	Kleppinger Ralf	FOM - Inst.for Atomic & Molecular Physics (AMOLF), Amsterdam	The Netherlands	The Competition between Long Range Order Formation and Physical Gelation in Triblock Copolymer Solutions	Physics
237	Agren Patrik	Åbo Akademi University, Department of Physical Chemistry, Materials Research Group, Turku	Finland	Kinetic studies of the MCM-synthesis under varying sample compositions and reaction, a continuation of proposal Nr.: 034/98	Chemistry
249	Mancini Giovanna	Centro C.N.R. di Studio di Meccanismi di Reazione, Dip. Chimica "La Sapienza", Roma	Italy	Chiral Recognition in Selfassemblies	Chemistry

263	Prassl Ruth	Austrian Academy of Sciences, Inst. of Biophysics and X-Ray Structure Research, Graz	Austria	In Situ 2D-SAXS Studies on the Crystallisation of Low Density Lipoprotein (LDL)	Life sciences
267	Kriechbaum Manfred	Austrian Academy of Sciences, Inst. of Biophysics and X-Ray Structure Research, Graz	Austria	Barotropic phase transitions of phospholids and admixtures studied by small-and wide-angle X-ray diffraction	Life sciences
274	Lombardi Vincenzo	Università di Firenze - Dip. di Scienze Fisiologiche	Italy	Combined mechanical and X-ray Diffraction study on the molecular motor in single muscle fibres	Life sciences
279	Paoletti Sergio	Università degli Studi di Trieste, Dip. Biochimica, Biofisica, Chim. Macromol.	Italy	Structural Investigations of Physical polymer networks	Biopolymeric poly-electrolytes
315	Rappolt Michael	Austrian Academy of Sciences, Inst. of Biophysics and X-Ray Structure Research, Graz	Austria	Time-Resolved Small Angle X-ray Scattering on the Response of the liquid Crystalline Phase of Lecithins to Rapidly Induced Osmotic Stress	Biophysics
319	Mariani Paolo	Università di Ancona - Istituto di Scienze Fisiche	Italy	Phase behaviour, molecular conformation and compressibility of the monoolein-water lytropic system	Biophysics
338	Pivac Branko	Ruder Boskovic Institute, Zagreb	Croatia	Crystalization of RTCVD deposited thin polycrystalline silicon films	Physics
Pilot	Dubcek Pavo	Sincrotrone Trieste S.C.p.A.	Italy	Grazing incidence small angle X-ray scattering investigation of annealed He implanted monocrystalline silicon	Physics
344	Fratzl Peter	Austrian Academy of Sciences - Erich Schmid Inst. für Festkörperphysik, Leoben	Austria	Interfaces and Mineralisation Defects in Connective Tissue	Physics Life sciences
349	Stelzer Franz	Technical University Graz - Institute for Chem. and Technology of Organic Materials	Austria	Investigation on the Formation of Superstructures in Optically Active Poly (Norbornene Derivatives)	Physics Chemistry
358	Amenitsch Heinz	Austrian Academy of Sciences, Inst. of Biophysics and X-Ray Structure Research, Graz	Austria	Scanning SAXS Study on the Proximal and Distal Threads from the Byssus of Mytillus Edulis	Life sciences
360	Zehetbauer Michael	Universität Wien - Institut für Materialphysik	Austria	Structural Investigation of Near Surface-Layers in Silicon Platelets for Solar Cells	Physics
361	Zehetbauer Michael	Universität Wien - Institut für Materialphysik	Austria	Time Resolved In-situ Bragg Peak Profile Analysis during Large Plastic Deformation of Cu	Physics

Pilot	Ollivon Michel	CNRS UMR 8612, University Paris-Sud, Paris	France	Simultaneous Differential Scanning Calometrie (DSC) and SAXS	Instrumen-tation
Pilot	SAXS-group	Austrian Academy of Sciences, Inst. of Biophysics and X-Ray Structure Research, Graz	Austria + Italy	Cool jumps down to -100 C	Instrumen-tation
Pilot	SAXS-group	Austrian Academy of Sciences, Inst. of Biophysics and X-Ray Structure Research, Graz, and Sincrotrone Trieste	Austria + Italy	Low resolution protein crystallography	Instrumen-tation
Pilot	SAXS-group	Austrian Academy of Sciences, Inst. of Biophysics and X-Ray Structure Research, Graz, and Sincrotrone Trieste	Austria + Italy	Is fiber diffraction on pubic hair a diagnostic tool for breast cancer ?	Medical Sciences
Pilot	Biermann	University Erlangen-Nürnberg, Institut für Werkstoffwissen-schaften	Germany	Microbeam X-ray diffraction diffraction of materia	

1999 (second half year):

Proposal	Proposer	Institution	Country	Title	Research Area
1999017	Pregetter Magdalena	Austrian Academy of Sciences, Inst. of Biophysics and X-Ray Structure Research, Graz	Austria	Time-resolved x-ray diffraction of shock-cooling of human Low Density Lipoprotein	Life Sciences
1999026	Triolo Alessandro	Heriot Watt University, Department of Chemistry, Riccarton Edinburgh	U.K.	iPP blends: phase diagram and crystallization kinetics via combined SAXS-WAXS techniques.	Chemistry
1999033	Cechi Giovanni	Università di Firenze - Dip. di Scienze Fisiologiche	Italy	Time-resolved mechanical and X-Ray diffraction studies on single frog muscle cells	Life Sciences
1999043	Baldrian Josef	Czech Acad. of Sciences, Inst. of Macromol. Chemistry, Praha	Czech Republic	Time-resolved SAXS/WAXS Studies on Macromolecular Materials: Cocrystallization in PEO/PEO Blends	Chemistry
1999058	Triolo Alessandro	Heriot Watt University, Department of Chemistry, Riccarton Edinburgh	U.K.	Aggregation processes of block copolymers in aqueous solution.	Chemistry
1999078	Farkas Rita	Austrian Academy of Sciences, Inst. of Biophysics and X-Ray Structure Research, Graz	Austria	Kinetics and mechanisms of apo A-I adsorption and insertion into phospholipid bilayers	Life Sciences
1999082	Pons	IIQAB-CSIC, Dep. Tecnologia de Tensioactius, Barcelona	Spain	Dynamics of non-equilibrium processes in surfactant systems.	Chemistry
1999083	Francesc-angeli Oriano	Università di Ancona - Dip. Scienze Mat. e Terra	Italy	X-ray Diffraction Study of the Structure of DNA-Liposome-Metal Complexes.	Life sciences
1999086	Dubcek Pavo	Sincrotrone Trieste S.C.p.A.	Italy	Grazing incidence small angle X-ray scattering investigation of annealed He implanted monocrystalline silicon	Physics
1999104	Pabst Georg	Austrian Academy of Sciences, Inst. of Biophysics and X-Ray Structure Research, Graz	Austria	The impact of chemical / mechanical membrane modulators to the L(alpha)-L(alpha*) phase transition.	Biophysics
1999105	Staudegger Erich	Austrian Academy of Sciences, Inst. of Biophysics and X-Ray Structure Research, Graz	Austria	Kinetics of Mebrane Perturbation and Disruption of Antimicrobial Peptides.	Biophysics

1999111	Chaudhari Suresh Manohar	Inter University Consortium for DAE Facilities, Indore	India	SAXS study to elucidate microstructural changes at the interface in amorphous multilayer structures.	Physics
1999127	Zehetbauer Michael	Universität Wien - Institut für Materialphysik	Austria	Microstructural Parameters during Plastic Deformation of fcc Metals as observed by In-situ Synchrotron Bragg Peak Profile Analysis.	Physics
1999129	Kriechbaum Manfred	Austrian Academy of Sciences, Inst. of Biophysics and X-Ray Structure Research, Graz	Austria	Simultaneous calorimetry and time-resolved SWAXS experiments on thermotropic phase transitions of lipids.	Life Sciences
1999130	Pivac Branko	Ruder Boskovic Institute	Croatia	Oxygen nucleation in Cz single crystal Si.	Physics
1999131	Rustichelli Franco	Università di Ancona - Istituto di Scienze Fisiche	Italy	The structural investigation of tBu substituted azaporphyrins Langmuir-Blodgett films""	Biophysics
1999134	Fratzl Peter	Austrian Academy of Sciences - Erich Schmid Inst. für Festkörperphysik, Leoben	Austria	Dynamical Structural Changes in Cross-Link Deficient Collagen.	Physics / Life Sciences
1999147	Rajewska	Università di Ancona - Dip. Scienze Mat. e Terra	Italy	Phase transition between isotropic phase and lamellar phase in ternary system CTAB/ hexanol/water.	Life sciences
1999155	Sarvestani Armir	Universität GHS Siegen	Germany	Advanced biological diffraction test measurements on novel gaseous detector systems	Technology/ Instrumen-tation
1999169	Amenitsch Heinz	Austrian Academy of Sciences, Inst. of Biophysics and X-Ray Structure Research, Graz	Austria	Time-resolved Langmuir-Blodgett (monolayer) studies on the interaction between Meletin and Phospholipids	Biophysics
1999182	Paoletti Sergio	Università degli Studi di Trieste - Dip. Biochimica, Biofisica, Chim. Macromol.	Italy	Structural investigations of polysaccharide mesophases.	Biochemistry
1999183	Milat Ognjen	University of Zagrab, Institute of Physics	Croatia	Interpretation of GISAXS spectra of nanostructure WC1-x films deposited by DC magnetron sputtering on mica substrate	Physics / Technology
Pilot	Amenitsch Heinz + Rappolt Michael	Austrian Academy of Sciences, Inst. of Biophysics and X-Ray Structure Research, Graz	Austria	Osmotic pressure jumps on model membrane systems	Biophysics

Pilot	Kriechbaum Manfred + Steinhart Milos	Austrian Academy of Sciences, Inst. of Biophysics and X-Ray Structure Research, Graz + Czech Acad. of Sciences, Inst. of Macromol. Chemistry, Praha	Austria + Czech Republic	Test of upgraded of high-pressure cell	Instrumen-tation
Pilot	Kriechbaum Manfred + Maciej Kozak	Austrian Academy of Sciences, Inst. of Biophysics and X-Ray Structure Research, Graz, + Department of Macromolecular Physics, A. Mickiewicz University, Poznan	Austria + Poland	Feasibility test of polymer measurements with CCD	Instrumen-tation

User Statistics

1. Number of submitted proposals and assigned shifts from 1995 until June 1999

The Austrian SAXS-beamline at ELETTRA opened to users in September 1996. Since then many experiments have been made on it related to the fields of life science, material science, physics, biophysics, chemistry, medical science, technology and instrumentation.

From September 96 on users gained access to the SAXS-beamline on the basis of the proposals received for the periods shown in Fig. 1. The assignment of beamtime at this beamline is done separately for the group of "General Users" (GU) and the "Collaborating Research Group" (CRG), i.e., the Research Team of the Austrian Partner. Beamtime was assigned to the proposals of each group in the order of the rating received by the Scientific Committee, and up to the maximum number of shifts available to each group according to the contract between "The Austrian Academy of Sciences" and the "Sincrotrone Trieste". Until December 1997 up to 55 % of the beamtime was given to CRG, up to 30 % to GU, and 15% was reserved for maintenance purposes. From January 98 on the quota for beamtime is 35 % for CRG and 50 % for GU.

Fig. 1 gives an overview of the numbers of received proposals, the numbers of requested and assigned shifts, as well as the percentage between assigned and requested shifts. Included in Fig.1 are also the same data for the period End 1995 - August 1996, during which some beamtime had been given already to users in order to perform first pilot- and test-experiments together with the beamline staff. These first experiments during the commissioning phase were not yet based on proposals, since the goal was mostly to evaluate and improve the performance of the beamline and the equipment of its experimental station. As can be seen in Fig.1, the request for beamtime at the SAXS-beamline increased continuously and strongly until the first half year of 1999 (also during the period Sept.-Dec. 1997, if one takes into account that this period was only 4 instead 6 month long, and that for this reason less proposals were submitted). Then, probably due to the high rejection rates, the number of submitted proposals decreased somewhat.

In 1999, in total 83 proposals (17 from CRG, and 66 from GU) were submitted. From these 27 proposals (2 from CRG, 25 from GU, corresponding to a total of 32.5 % (or 12 % CRG and 38 % GU, respectively) were submitted by "new" usergroups, i.e. groups which so far had never beamtime at the SAXS beamline. From these 19 proposals (2 CRG, 17 GU) were accepted, corresponding to 39 % (12 %, 39 %, respectively) of all accepted proposals.

Fig.1 (next page): The statistical information about the beamtime periods since end of 1995 are given for the groups "CRG", and "GU" separately, as well as for both together ("Total"). Shown are, for all beamtime periods:

(a) Number of received proposals
(b) Number of requested shifts
(c) Number of assigned shifts
(d) Relation between assigned and requested shifts

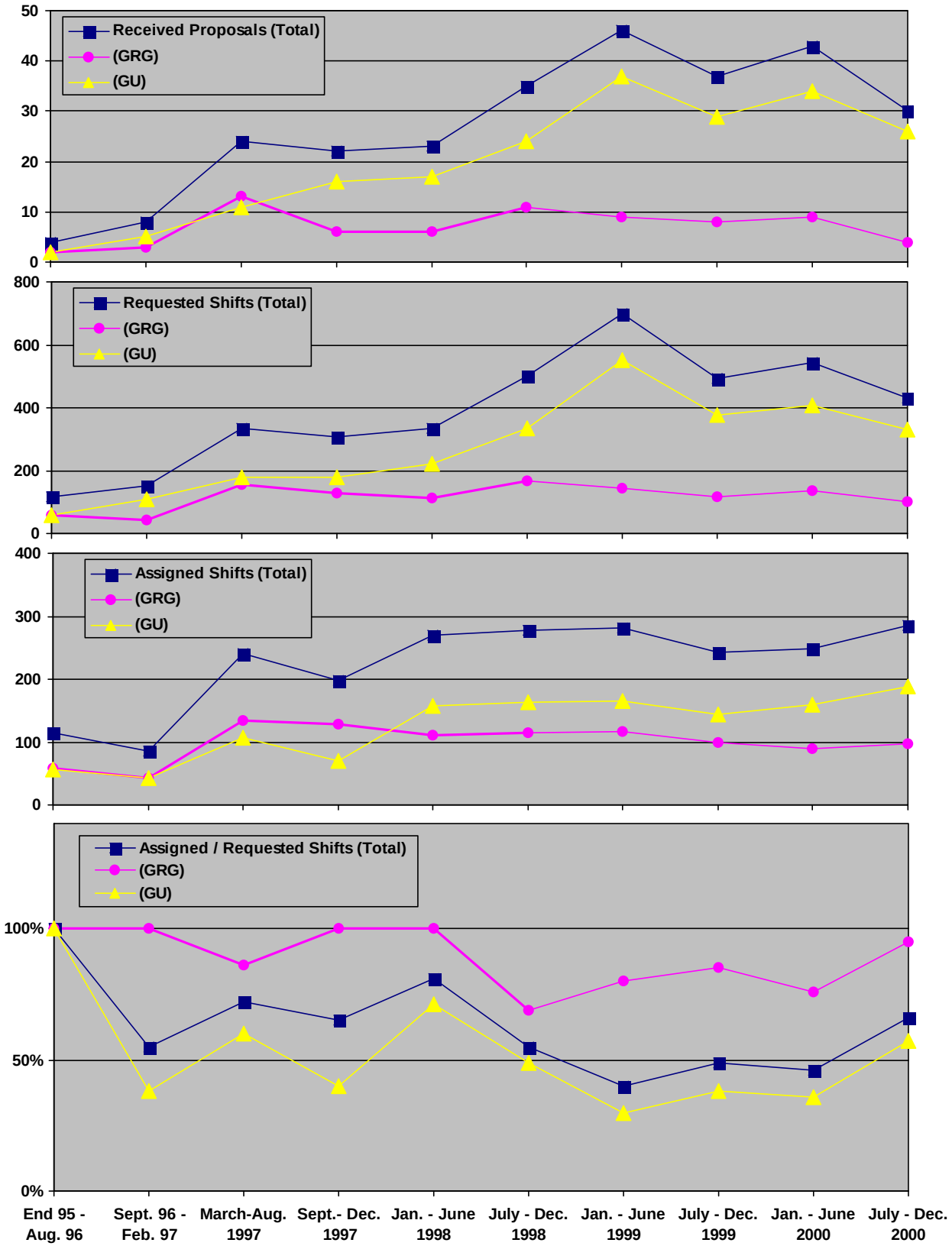
Received Proposals (Total)
(GRG)
(GU)
50
40
30
20
10
0
Requested Shifts (Total)
(GRG)
(GU)
800
600
400
200
0
Assigned Shifts (Total)
(GRG)
(GU)
400
300
200
100
0
Assigned / Requested Shifts (Total)
(GRG)
(GU)
100%
50%
0%
End 95 - Aug. 96
Sept. 96 - Feb. 97
March-Aug. 1997
Sept.- Dec. 1997
Jan. - June 1998
July - Dec. 1998
Jan. - June 1999
July - Dec. 1999
Jan. - June 2000
July - Dec. 2000

2. Provenience of Users

During 1999, 144 users from 47 institutes in 17 countries have performed experiments at the SAXS beamline. In Fig. 2 are shown both the provenience of these users, and of their respective institutes. Each user or institute was counted only once, even though many users performed experiments in both beamtime periods of 1999.

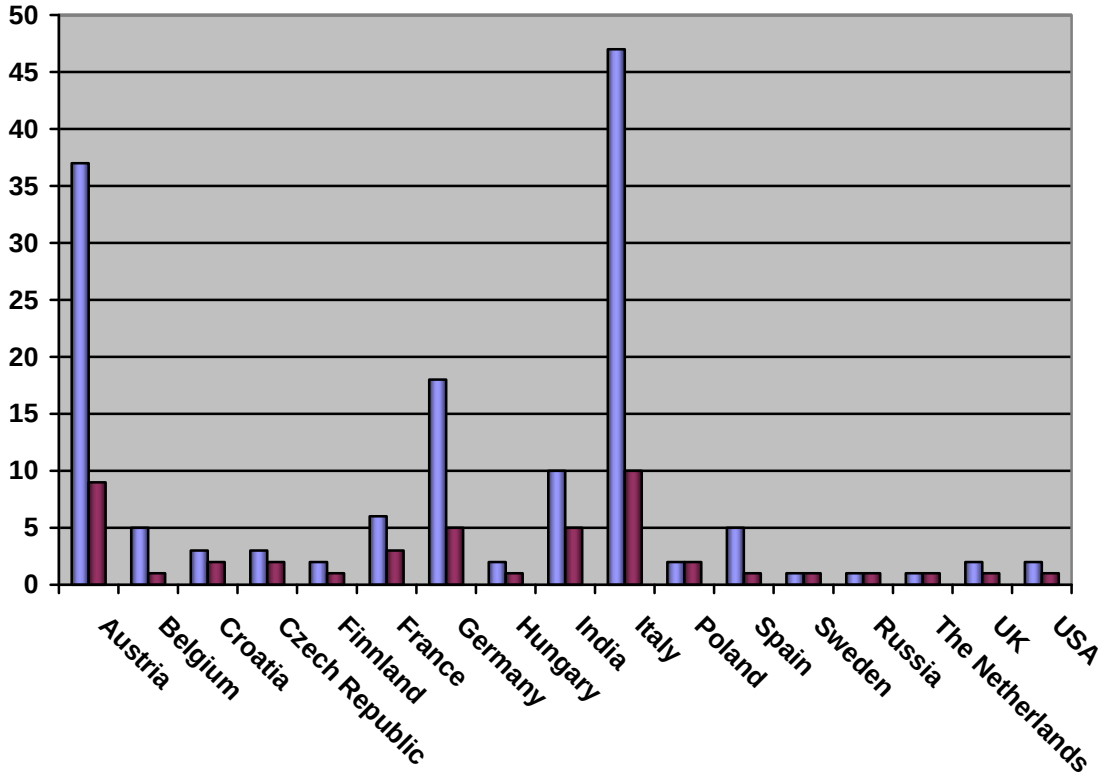

Fig. 2: Provenience of users (light grey) and of their corresponding institutes (dark grey).

3. Documentation of experimental results

As could be expected, with the start of user-operation at the SAXS-beamline the number of contributions to conferences started to increase strongly. With a delay of one year - the average time needed for paper publications - also the number of publications increased accordingly, as can be seen in Fig. 3 .

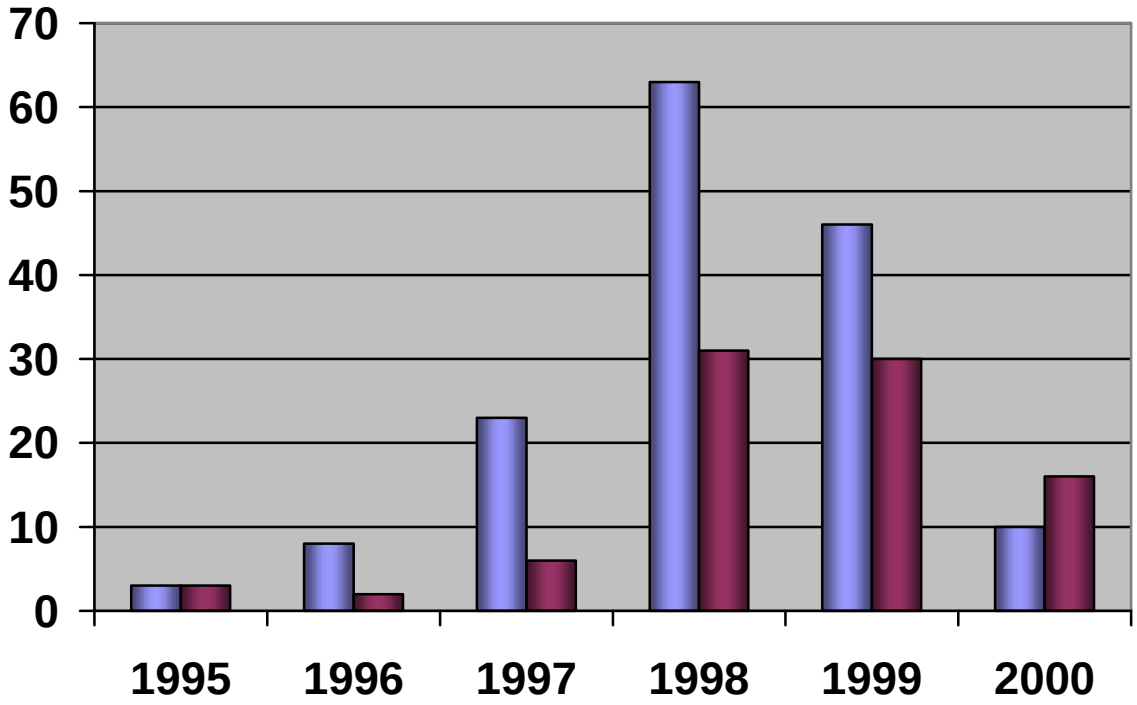

Fig. 3: Number of conference contributions (light grey) and of refereed paper publications (dark grey) for the years 1995-1999. Also refereed papers, which have been published in 2000, or were in press until 30.4.00, are included.

In addition, until December 1999, the following documentations based on instrumentation of the SAXS-beamline, or on data taken with it, have been produced.

Unrefereed publications:

Technical Reports on Instrumentation:	5
Contributions to Elettra Newsletters:	13
Contributions to Elettra Highlights:	7
PhD Thesis:	7
Diploma Thesis :	5

Experimental Possibilities at the SAXS-beamline

1. Installation of the Bio-Logic Stopped Flow Module (SMF)

The old 2 syringe SMF cell has been replaced by a new system, which consists of a 4 syringe cell with 3 mixer modules manufactured by Bio-Logic. In contrary to the conventional system the observation capillary and the last mixing stage are mounted separately from the syringe block. The connection is realised by a flexible thermostated tube system to allow the installation onto our movement stage. Each syringe is driven by an individual stepping-motor, which allows a high versatility of the mixing sequence. For example, injection sequences using one or up to 4 syringes, unequal filling of syringes, variable mixing ratio, reaction intermediate ageing in three- or four-syringe mode etc. With modern microprocessor techniques, stepping-motors can now operate more smoothly than any other fast driving technique; solution flow can be entirely software-controlled and can stop in a fraction of a millisecond. This great advance of computer-controlled stepping motors has broadened the capability of stopped-flow methods to many applications poorly served by first generation, pneumatically driven mixing devices:

- Vertical syringes driven by independent stepping motors
- Independent programming of each syringe (flow-rate, flow duration, sequential mixing)
- Free of over-pressure artefact
- Millisecond dead time
- Full computer control including variable ratio and sequential mixing

The motors are driven by four very efficient programmable current power supplies, four microprocessors to generate and control the movement of the motors and an additional microprocessor controlling the communications with the microcomputer. This unit is driven by a Windows software, which give fully access to the rapid mixing module. The software allows the set-up of the shot volumes of each of the 4 syringes in a certain time interval. Up to 20 mixing protocols can be programmed. Additionally macros for the repeated execution of individual frames can be defined. Furthermore, the input and output trigger accessible for user operation can be programmed. In the usual operation modus the start of rapid mixing sequence is triggered from our X-ray data-acquisition system (input trigger).

The observation cell: For experiments with Synchrotron Radiation the cell has been newly designed especially for us. A quartz capillary (1 mm) embedded in a stainless steal holder is separated from the main body by a 40 cm transfer-line, and thus, can be easily mounted on the sample stage for X-ray scattering experiments. In the observation cell the last mixer is installed to minimise the dead volume of the whole system. Both, the transferline and the observation cell are thermostated with a water bath, which can be used in the range from –40 to 60 °C. The main parameters of the system are:

- Temperature stability 0.1 °C
- Total sample wasted per mixing cycle:100 µl
- Maximum 2θ angle of 45°
- Dead volume 550 µl
- Speed: 0.045 – 6 ml/s
- Total Volume 8 ml
- Duration of flow 1 ms to 9999 ms/Phase
- Dead time: 1 ms

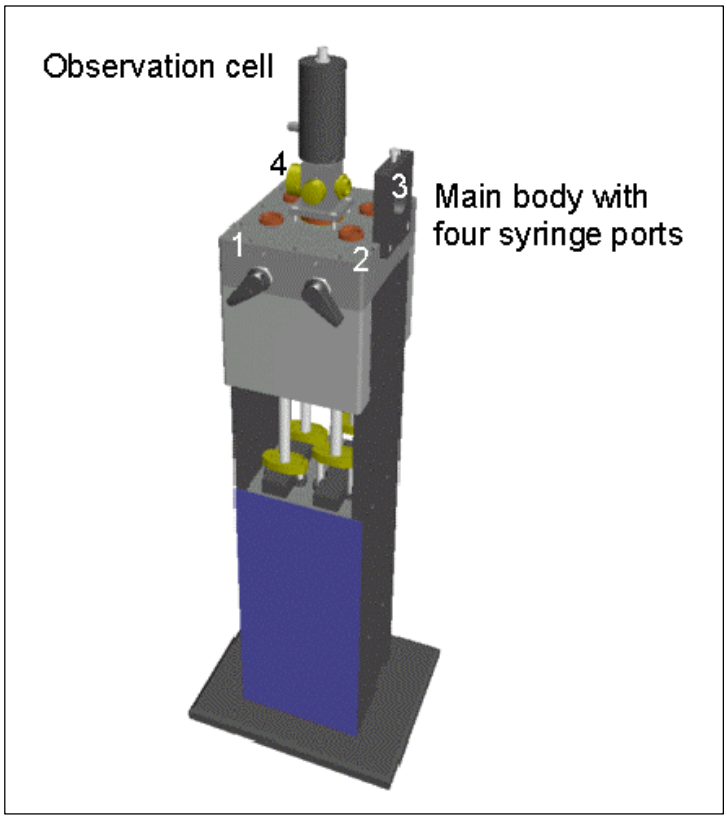

Fig. 1: Sketch of the Biologic Stop Flow Module.

Further information can be found in the homepage: http://www.bio-logic.fr/

2. Implementation of the Oxford Cryostream Cooler

Fig. 2: The Oxford Cryostream System.

The general working principle of the Oxford Cryostream system is the following: The liquid nitrogen is sucked out of an open Dewar, along a flexible transfer line into the Cryostream Coldhead where the liquid is evaporated to gas. The area inside the Coldhead is cooled to about -190 °C as the cold gas passes along one path of a heat exchanger. This means that Cryostream creates a cold environment only few centimeters from the sample position instead of at the bottom of a storage Dewar, which can be several meters away from the sample position. The cold nitrogen gas then passes out of the Cryostream Coldhead, through a diaphragm pump and a Three Term Programmable Temperature Controller, where the flow is regulated and monitored. Once the gas re-enters the Cryostream Coldhead, it is quickly re-cooled along the second path of the heat exchanger. The cold nitrogen gas will then enter the top of the Cryostream nozzle at about -190 °C. The temperature of the gas stream is controlled be an 'in stream' heater and thermo-sensor before it passes out over the sample.

The system has been especially developed for X-ray crystallography to perform diffraction experiments on shock frozen bio-crystals as applied for low angle X-ray diffraction on LDL (see contribution Schwarzenbacher et al., p. 66). However, the programmable temperature controller allows further implication for SAXS-experiments, e.g., rapid temperature drops in solvents. Summarising, the design of the Cryostream Cooler facilitates:

- nitrogen stream temperatures from -190 to 100 °C,
- a stability of 0.1 °C,
- a system that can be refilled without creating any disturbance of the temperature at the sample,
- temperature ramps can easily be carried out remotely controlled with scan rates up 6 °C/min
- individual temperature protocols can be cycled
- T-jumps in both directions can be performed by rapidly shooting the sample in a pre-cooled or -heated capillary using an fast syringe driver reaching a minimum temperature of -80 °C. Here, typical scan rates are about 15 °C/sec with a total process time in the order of 10 sec.

3. New multiple sample holder block for Anton Paar Standards

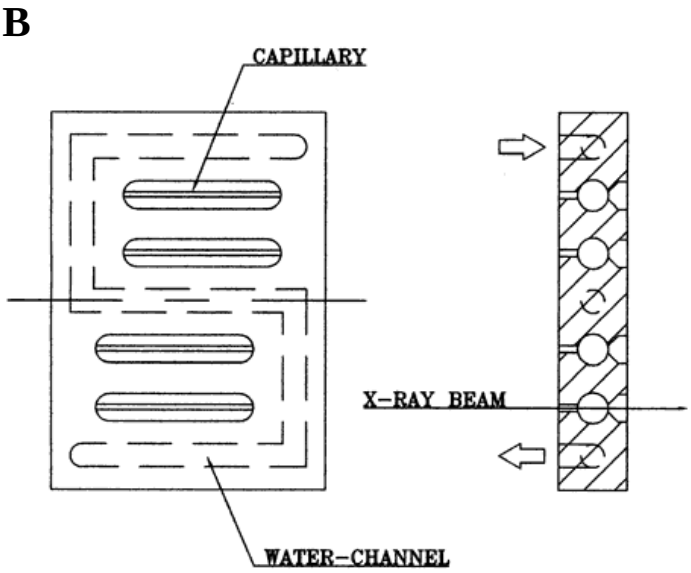

Fig. 3: (A) Photography of the sample holder block.
(B) Sketch of the Block: Up to four samples can be thermo-stated at the same time.

The multiple sample holder block is usually connected to a freely programmable water-bath, and thus, the sample temperature is easily controlled. The block can be loaded with up to 4 sample holders having the Anton Paar Standard. In comparison to the standard single-sample heating and cooling block the advantages are now the following:

- Faster experimental processing, since up to 4 samples can be handled
- Larger s-range, i.e., 45° exit aperture opens the window to the WAXS-regime
- Easy realisation of desired temperature protocol.

4. The 2D CCD-camera system

The CCD has a 115 mm diameter input phosphor screen made of a gadolinium oxysulphide polycrystalline layer. The screen is coupled by means of a fiber optic to the image intensifier. The image intensifier is coupled again with an additional taper to the CCD itself. The achieved spatial resolution of a pixel is 79 μm for the whole set-up.
The number of pixels is 1024 x 1024 and they can be pinned down to 2 x 2 and 4 x 4. The dynamic range of the CCD is 12 bit. The dark current of the CCD is in the order of 100 ADU (off-set) and the readout noise (read out speed: 10 MHz) is in the order of 6 ADU. (The CCD is cooled by multistage Peltier element for reducing the dark noise.) The intensifier gain is adjustable between 200 and 20000 photons full dynamic range. Typical readout times and exposure times are 150 ms and 100 ms, respectively. The readout times can be reduced down to 100 ms by using the pinning mode of the CCD. Between the frames additional wait times can be programmed e.g. for reducing the radiation damage in the sample or to extend the time for measuring long time processes.
For the external control a TTL trigger signal is provided (active low, when the CCD is accumulating an image), which is used to control the electromagnetic fast shutter of the beamline on one hand. On the other hand this signal can be used also to trigger processes as requested by the user.
The CCD is controlled by Image Pro+, which also includes non too sophisticated data treatment capabilities. The program is featuring a comprehensive set of functions, including:

- flat fielding/background corrections
- enhanced filters and FFT
- calibration utilities (spatial and intensity)
- segmentation and thresholding
- arithmetic logic operations
- various measurements, like surface, intensity, counts, profiles
- advanced macro management

The data are stored in 12 bit – TIFF format. At the present state up to 300 full images (1024 x 1024) can be recorded by the system, but a strict conservation of the timing sequence is maintained only for the first 15 - 17 frames until the RAM memory is full. Afterwards the images are stored in the virtual memory on the hard disk. At present a software development for the CCD readout system is under way to improve the stability of the readout cycles.
For the complete treatment of the 2D data Fit2D available from the ESRF is used, which is able to perform both interactive and "batch" data processing (homepage: http://www.esrf.fr/computing/expg/subgroups/data_analysis/FIT2D/index.html, programmed by Dr. Andy Hammersley) , which supports a complete spatial correction, flat field correction and background correction. Furthermore more elevated data-treatment can be performed within this software package, like circular integration, segment integration and similar.

5. Accessible SAXS and WAXS ranges

Simultaneous SAXS- and WAXS-measurements can be performed using a linear sensitive gas detector (Gabriel type, windows size 8 x 100 mm, active length 86.1 mm with a resolution of 0.135 mm/channel) for the WAXS-range, and either a second linear Gabriel type detector (windows size 10 x 150 mm, active length 134 mm with a resolution of 0.159 mm/channel), or the new 2D CCD-system for the SAXS-range. A specially designed vacuum chamber (SWAXS-nose, see Annual Report of 1996/97, p. 32) allows to use both scattering areas below (for SAXS) and above (for WAXS) the direct beam, respectively.

The available possible WAXS-ranges are summarised in Table 1. The overall length of the SWAXS-nose in the horizontal direction, measured from the sample position, is 512 mm and the fixed sample to WAXS-detector distance is 324 mm. At the shortest SAXS camera-length an overlap in the d-spacings covered by the SAXS- and WAXS-detectors, respectively, is possible: then, the common regime lies around 9 Å.

Range	**2q [deg]**	**d-spacing (Å)**		
		8 keV	**5.4 keV**	**16 keV**
1	9.4	*9.40*	14.03	4.27
	27.6	*3.23*	4.82	1.47
2	27.4	3.25	4.86	1.48
	45.6	1.99	2.97	0.90
3	45.4	2.00	2.98	0.91
	63.6	1.46	2.18	0.66
4	63.4	1.47	2.19	0.67
	81.6	1.18	1.76	0.54

Table 1: Possible d-spacing ranges in the WAXS-regime at the SAXS-beamline at ELETTRA. Since the WAXS-detector can be mounted at four different fixed positions on the SWAXS-nose (range 1-4), with the three possible energy choices (5.4, 8 and 16 keV) this results in 12 different d-spacing regimes. In italic the most common choice (8 keV, range 1) is highlighted. This range is suited for experiments, e.g., on lipid-systems and (bio)polymers.

Depending on the photon energy maximum SAXS resolutions of 2000 Å (5.4 keV) or 630 Å (16 keV) are available.

6. Available sample manipulations stages

1. General

Usually the sample is mounted onto the sample alignment stage which allows the user to place the sample into the beam with a precision of 5 µm (resolution: 1 µm). In fig. 3 the ranges for vertical and horizontal alignment as well as the maximum dimensions of the sample holders are given. The maximum weight on the sample stage is limited to 10 kg. In case the envelope dimensions of a sophisticated sample station provided by the users are slightly larger than those given in fig. 3, the user can ask the beamline responsible for a check up of his space requirements. If it does not fit at all to these specifications, user equipment can also be mounted directly onto the optical table, which allows much larger spatial dimensions.

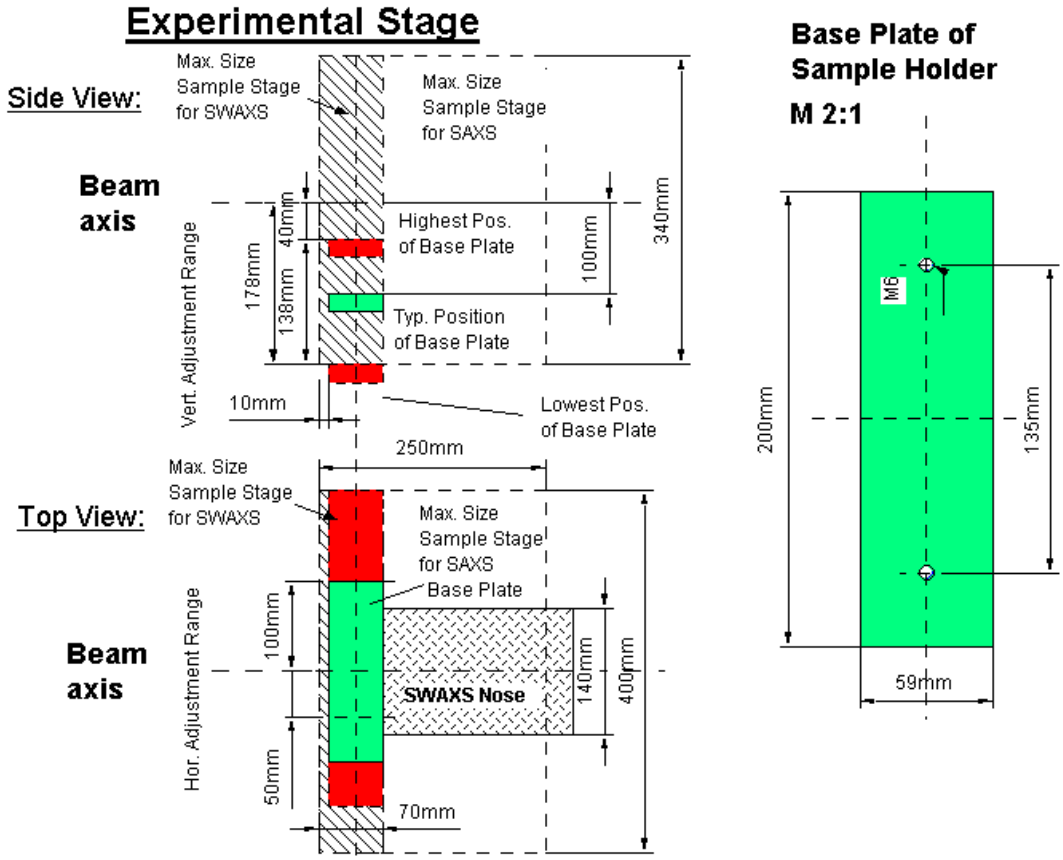

Fig. 4: Maximum dimensions and alignment range of the sample holder to be mounted via a base-plate onto the standard alignment stage (left), and dimensions of the base-plate (right).

2. Sample holders

As standard equipment for liquid samples Paar capillaries (diameter: 1 and 2 mm) are used thermostated with the KHR (electrical heating) or KPR (Peltier heating/cooling) sample holders (Anton Paar, Graz, Austria). For use in these sample holders flow through capillaries and Gel holders are standard equipment. Temperature scans can be performed with KHR and/or KPR in the range from 0 to 150 °C, typically the precision and the stability of this systems is < 0.1 °C. Additionally thermostats for temperature control or cooling proposes can

be used at the beamline (0-95 °C, at present). Helium and Nitrogen gas bottles are available at the beamline, for other gases please contact the beamline responsible.
Multiple-sample holders can be mounted onto the standard sample manipulator. At present a holder is available for measuring in automatic mode up to 30 solid samples at ambient temperature or up to 4 liquid samples in the temperature range 0 – 95 °C.

3. Magnet System

For studying magnetic effects in samples, capillaries or sample holders with suitable dimensions can be mounted inside an electromagnet. Up to now a sample holder for standard Paar capillaries (Anton Paar, Graz, Austria) is available for ambient temperature only. The alignment of the magnetic field is horizontal or vertical (transversal to the photon beam). For short times the maximum magnetic field can be up to 1.5 T, and 1.0 T for continues operation, respectively, assuming a pole gab of 10 mm for both.

4. Stopped Flow Apparatus

A commercial stopped flow apparatus (Unisoku Co., Ltd, Osaka, Japan) is presently available particularly designed for SAXS investigations of conformation changes of proteins, nucleic acids and macromolecules. The process is triggered by the rapid mixing of two solutions and typically the observation time is ranging from ms to minutes.
The main parameter of the system are:

- dead time: about 1 ms
- mixing ratio: 1:1 (at present)
- reservoir volume: 4 ml each
- syringe volume: 0.3 ml each
- shot volume: 0.1 ml - 0.25 ml each solution
- optical path length: 1 mm; X-ray windows: saphire 2 x 50 μm
- temperature range: by means of a thermostat water bath (0 - 60 °C)

Both solutions are filled in the reservoirs and the syringes are pulled up remote controlled. The syringes are pushed by a pneumatic system and consequently the liquids are rapidly mixed in a sphere mixer and filled into the rectangular observation cell within 1 ms. This process generates the trigger for starting the data acquisition system. The mixing can be repeated about 15 times before the reservoirs must be refilled. Depending on the diffraction power of the sample time resolutions of up to 10 ms can be obtained.

5. Grazing Incidence Small Angle X-ray Scattering

A special set-up has been designed to perform grazing incidence studies on solid samples, thin film samples or Langmuir-Blodget-films. The samples can be mounted onto a sample holder, which can be rotated around 2 axes transversal to the beam. Furthermore the sample can be aligned by translating it in both directions transversal to the beam. The precisions are 0.001 deg for the rotations and 5 μm for the translations. Usually the system is set to reflect the beam in the vertical direction. According to the required protocol and the

actual assembly of the rotation stages ω, θ, 2θ and φ scans can be performed. For further information see the experimental reports enclosed.

6. Temperature Gradient Cell

A temperature gradient cell for X-ray scattering investigations on the thermal behaviour of soft matter manybody-systems, such as in gels, dispersions and solutions, has been developed. Depending on the adjustment of the temperature gradient in the sample, on the focus size of the X-ray beam and on the translational scanning precision an averaged thermal resolution of a few thousands of a degree can be achieved.

7. IR-Laser T-Jump System for Time-Resolved X-ray Scattering on Aqueous Solutions and Dispersions.

The Erbium-Glass Laser available at the SAXS-beamline (Dr. Rapp Optoelektronik, Hamburg, Germany) delivers a maximum of 4 J per 2ms pulse with a wavelength of 1.54 μm onto the sample. The laser-beam is guided by one prism onto the sample, which is filled in a glass capillary (1 or 2 mm in diameter) and Peltier or electronically thermostated in a metal sample holder (A. Paar, Graz, Austria). With a laser spotsize of maximal 7 mm in diameter a sample-volume of maximal 5.5 μl or 22 μl, respectively, is exposed to the laser-radiation. In a water-solutions/dispersions with an absorption coefficient of A = 6.5 cm^{-1} T-jumps up to 20 °C are possible.

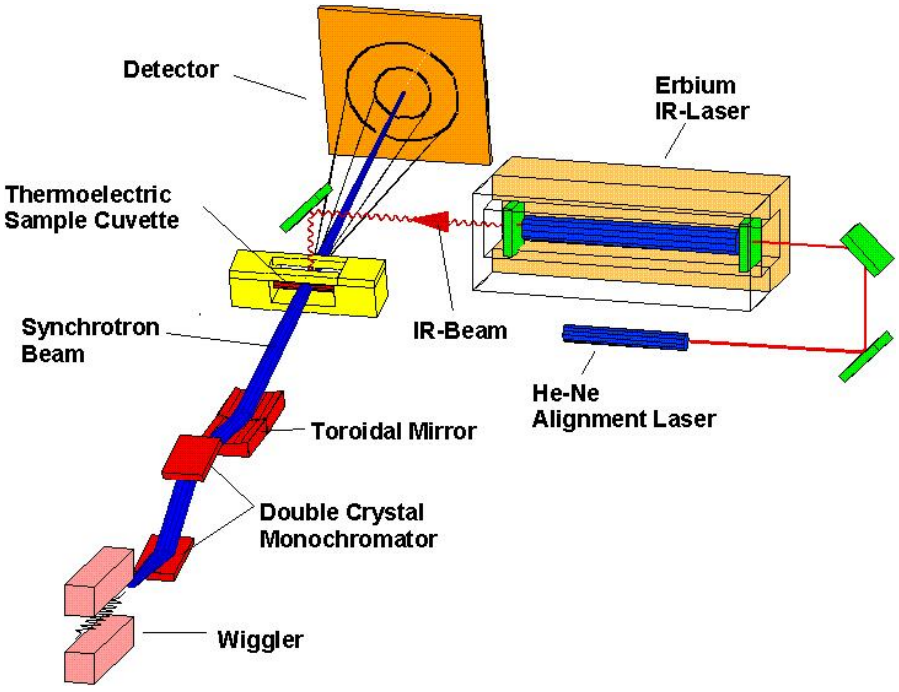

Fig. 5: Sketch of the T-jump set-up.

8. High-Pressure Cell for Static and Time-Resolved SAXS-Experiments

A compact X-ray sample cell allows to measure diffraction patterns at hydrostatic pressures up to 3 kbar. Both the entrance and the exit-window for the X-rays are made of 1.5 mm thick Be-discs (3.5 mm diameter), coated with 5µm polyimide with a total transmission of 55% for X-rays at a wavelength of 1.54 Å. The sample thickness can be 1.5 mm with a volume of approximately 1 mm^3 completely irradiated by pin-hole collimated (1.0 mm diameter) X-rays. Optional diamond windows with a thickness of 0.75 mm can be used, resulting in a total transmission of about 10%. However, the background at small angles is much more reduced as compared to the Be-windows, which have a maximum resolution limit of about 200 Å. The sample thickness with diamond windows is 3 mm. The cone-shaped exit window allows detection of scattered X-rays from the sample within a maximal angular range of 30°. The hydrostatic pressure is generated by using water as the pressure transmitting liquid, directly connected via a high-pressure control network with the cell interior. The temperature in the pressure cell can be regulated in the range from 0°C to 80°C.

The large accessible angular range in the reciprocal space makes the cell well suited for scattering/diffraction measurements in the small- (SAXS) and wide-angle (WAXS) region of samples like solid polymers, liquid-crystalline probes and biological model-membrane systems. Static measurements of lipid samples at different pressures show an excellent signal/noise ratio of the diffraction patterns at exposure times of 10 s. Alternatively, this system can be used for time-resolved measurements of dynamic processes (pressure-jump relaxation experiments) with a time resolution of the diffraction patterns in the millisecond range and with jump amplitudes up to 3kbar (1 kbar/10 ms) in both directions (pressurizing and depressurizing jumps). Diffraction patterns of p-jump induced barotropic phase-transitions of lipid samples could be measured with 5 ms time-resolution.

User Contributions

1. Materials Science

MEASUREMENTS OF LOCAL LATTICE PARAMETER CHANGES IN NI-BASE SUPERALLOYS WITH HIGH LATERAL RESOLUTION

H. Biermann, F. Pyczak and H. Mughrabi

Institut für Werkstoffwissenschaften, Lehrstuhl I, Universität Erlangen-Nürnberg, Martensstr. 5, D-91058 Erlangen, Fed. Rep. Germany

Ni-base superalloys have been widely used materials for high-temperature applications in the last 50 years. The properties of the alloys have been improved further and further by different measures like casting the alloys as a single-crystal material or increasing the amount of gamma'-phase. Modern commercial Ni-base superalloys consist of a so called gamma matrix phase and coherently embedded gamma' particles with a cuboidal shape. The mechanical properties of the alloy are recognizably enhanced due to this two-phase composition. As the lattice parameters in gamma- and gamma'-phase are slightly different, a lattice mismatch exists at the interface between the two phases, resulting in X-ray peaks which consist of two superimposed sub-peaks, belonging to the gamma- and the gamma'-phase, respectively. These lattice mismatches cause internal stresses in both phases. Under external mechanical loading, these internal stresses superimpose on the external stresses and influence in this way the development of the gamma' structure from a cuboidal initial structure to a coarsened plate-like, so-called rafted structure after long-time service at high temperatures.

The mechanical properties of the Ni-base superalloys are strongly influenced by this change in precipitate shape, which is driven by the internal stresses due to lattice misfit under the action of the external applied stress. Hence, lattice misfits in Ni-base superalloys were thoroughly investigated during the last three decades and remain an important topic of research in present day Ni-base superalloys. The lattice parameters of the two phases vary due to the actual non-stoichiometric chemical composition of the phases. In recent years, further improvements of the mechanical properties were achieved by the alloying of refractory elements like tungsten or rhenium. These alloying elements affect the lattice mismatch more or less depending on their distribution between the gamma- and gamma'-phases. Tungsten which distributes nearly equally between the two phases has much weaker effects on the lattice mismatch than rhenium which is strongly enriched in the gamma matrix phase. Rhenium also tends to segregate in the dendritic cores. Hence, rhenium additions in Ni-base superalloys affect the lattice misfit differently in dendritic cores and interdendritic regions. This inhomogeneous distribution of rhenium leads to inhomogeneous internal stresses and affects the microstructural features such as shape and size of gamma'-precipitates, when comparing dendritic cores with secondary dendrite arms and interdendritic regions.

The aim of our measurements at the SAXS-beamline of the ELETTRA synchrotron was the investigation of local changes of the lattice parameter and lattice misfit between dendritic cores, secondary dendrite arms and interdendritic regions in different Ni-base superalloys. As the typical dimension of a dendrite core in Ni-base superalloys is about 50 microns and that of dendrite arm spacings about 100 microns, small beam sizes were necessary to achieve the necessary lateral resolution to measure lattice parameters solely in a certain region of a dendrite. The small beam sizes were achieved by the use of a slit-shaped diaphragm: the high intensity of the synchrotron beam allows to perform measurements and obtain sufficient intensity even if a large portion of the beam diameter is blocked by the diaphragm. The specimens were sections cut parallel to {001}-planes which are parallel to the solidification direction of the directionally solidified alloys. Samples of standard heat-treated and aged materials were measured to investigate also the effects of homogenizing the segregated

alloying elements during extended heat treatments. The series of measurements were accomplished by shifting the measurement position several microns perpendicular to the solidification direction of the alloy for each measurement. Thus, dendritic cores, secondary dendrite arms and interdendritic regions are scanned succesively.

At a first session at the synchrotron in November 1999, the applicability of these concepts to samples of Ni-base superalloys was tested. Due to problems with intensity diffracted at the diaphragm and illuminating also areas beside the region of interest, it is uncertain whether the requested lateral resolution which is necessary for the kind of measurements we wished to perform was achieved. At the next session in Triest, we plan to avoid this kind of problems by the use of appropriately mounted beam stops near the specimen in order to block all radiation scattered by the diaphragms.

The measurements obtained in the first session show no clearly detectable changes in the lattice parameters on a length scale between 100 to 200 microns. Variations of the lattice parameters on this length scale would be expected, if the changes in lattice parameters were caused by the dendritic structure of the material. The only measurable effect was a reduction of the changes in lattice parameters depending on the measurement position in the aged states of some alloys. This effect could be explained with the homogenization of some alloying elements after extended heat treatment. During the next measurement session in Triest, it should be possible to resolve also the lattice parameter changes caused by the dendritic structure, after having overcome the problems with intensity diffracted at the diaphragm.

STRUCTURAL CHARACTERISATION OF LANGMUIR BLODGETT MULTILAYERS AND RELATED NANOSTRUCTURE/COMPOSITES USING SYNCHROTRON RADIATION

S.Vitta[1], N.P. Kumar[2] and S.S. Major[2]

1.) Department of Metallurgical Engineering and Materials Science, Indian Institute of Technology, Bombay. Mumbai 400 076.
2.) Department of Physics, Indian Institute of Technology, Bombay. Mumbai 400 076.

(a) Zn-arachidate multilayers: The molecular packing and their orientation in a series of divalent metal fatty acid salts is predicted to be dependent on the electronegativity of the metal ion. An exception to this behaviour has been observed in the case of Zn-arachidate multilayers. The molecular packing was found to depend strongly on the pH of the subphase from which the monolayers are transferred. The molecular tilt was found to depend on the subphase pH and also the multilayers were found to exist in different polymorphic states, different angular tilts of the molecules, even in multilayers deposited from a single subphase pH. Hence the structural development in theses multilayers as a function of subphase pH was investigated. The diffraction scan results from multilayers deposited at different subphase pH show that the molecular arrangement in the plane of the layers changes with changing pH. The molecules are found to be organised into hexagonal and/or orthorhombic arrangement depending on the subphase pH. The different polymorphs are found to have different in plane molecular packing.

(b) Semiconducting CdS and ZnS nano-aggregates in LB matrix: One of the important applications of LB multilayers has been their use as precursors for the growth of semiconducting chalcogenide nano-aggregates distributed in an insulating fatty acid matrix. The main advantage of using these LB multilayers as precursors is the high degree of molecular order present in them, which can facilitate better control over the size, shape and spatial distribution of the nano-aggregates.
In the present work the formation of CdS and ZnS from Cd-arachidate and Zn-arachidate precursor multilayers was investigated as a function of time of exposure of the precursor multilayers to H_2S gas. The precursor Cd-arachidate multilayers have an orthorhombic in-plane molecular arrangement and this structure changes when exposed for 15 minutes. The structure however reverts back to the precursor arrangement when exposed to long durations of the order of 5 hours.
The structural development due to the formation of ZnS from Zn-arachidate precursor multilayers is also found to be a function of duration of the exposure to H_2S gas. The structure in the plane of the multilayers changes when exposed to 2 hours and 40 hours as compared to the unexposed multilayers. These structural changes are associated with the formation and growth of sulfide, CdS and ZnS, nano-aggregates in the LB matrix, arachidedic acid.

(c) Polyaniline (PANI) and Cd-arachidate composite LB multilayers: The poor processability of the polymeric materials such as polyaniline (PANI) was overcome in the present work by co-depositing them together with LB amphiphilic molecules. The PANI-CdA composite multilayers were deposited using the LB technique and their structure was studied using grazing incidence X-ray scattering. The molecular arrangement in the plane of the multilayers is found to remain unchanged even after incorporating PANI. These results show that PANI occupies spaces within the CdA molecular network without disturbing the overall structure.

(d) Ni-Nb/C inorganic multilayers: The development of reflection mirrors using multilayers for soft X-rays is of significant technological importance for the application ranging from biology to advanced micro-devices. The realisation of such mirrors specifically for the 2.2 nm to 4.4 nm wavelength X-ray region is of crucial importance to biology and it is limited by various material behaviour limited problems. One of this is the structural stability, both temporal and thermal. In the present work the stability of Ni-Nb/C multilayers with a nominal period of 2.4 nm was studied. The diffraction scan shown in figure (a) below clearly indicates that the multilayers are temporally stable for long periods of time, after 2.5 years of deposition, at room temperature as it shows an identical scattering behaviour as was observed after deposition. However when the multilayers were exposed to elevated temperature, 200 C, the individual layers in the multilayer crystallise into different phases. The vertical layering however is found to be highly stable even after exposure to 200 C as shown in the figure (b) above.

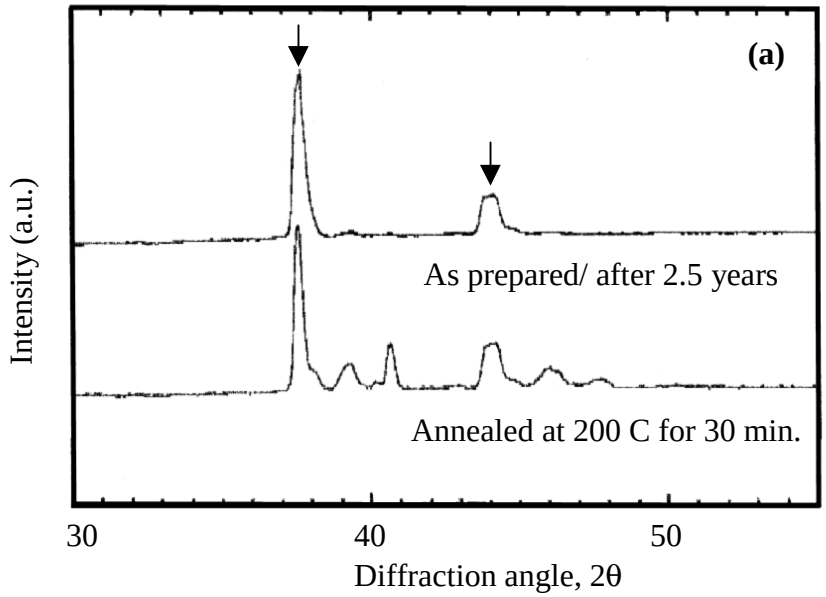

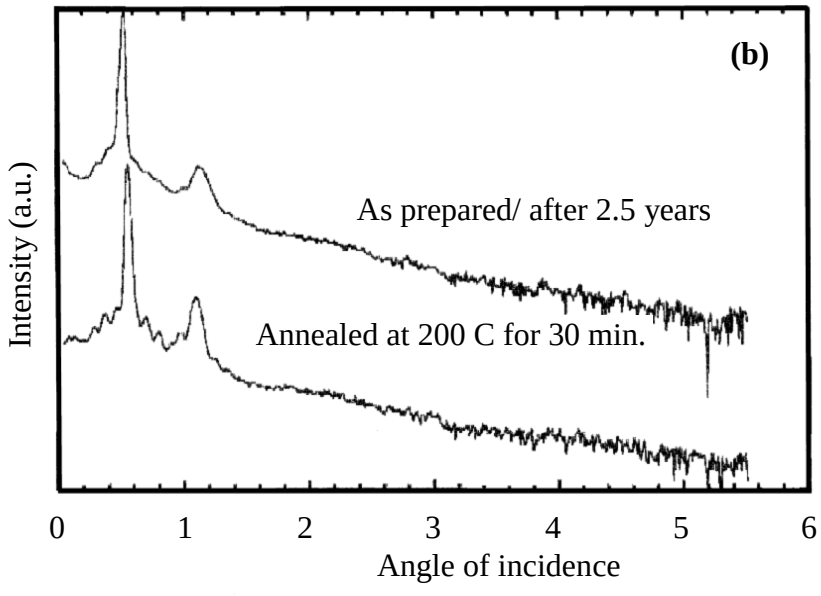

2. Life Sciences

NO CORRELATION BETWEEN BREAST CANCER AND HAIR STRUCTURE

H. Amenitsch[1], M. Rappolt[1], P. Laggner[1], S. Bernstorff[2], R. Moslinger[3], E. Fleischmann[3], T. Wagner[3], P. Lax[4] and L. Dalla Palma[5]

1.) Institute of Biophysics and X-ray Structure Research, Austrian Academy of Sciences, Graz, Austria
2.) Sincrotrone Trieste, Basovizza, Italy
3.) Abteilung für Spezielle Gynäkologie, AKH Wien, Vienna, Austria
4.) Institute of Pathology, University of Graz, Graz, Austria
5.) Institute of Radiology, University of Trieste, Trieste, Italy

Introduction: In an article by James et al. [1] it was stated, that "hair from breast-cancer patients has a different intermolecular structure to hair from healthy subjects." Such a dramatic claim demanded verification, which was immediately initiated by us and world wide by at least 4 other groups.

Experimental: Our work bases on three different sources. First, hair from families with a history of BRCA-1 and/or -2 mutations (gynaecology group of Dr Wagner), second, hair from breast tumor patients in Trieste (radiology group of Prof. Dalla Palma) and last, normal healthy male and female hair (samples by courtesy of Drs Petru and Hudabiunigg, Graz). For minimizing the risk of spoiled hair samples, we used throughout all experiments only pubic hairs of each individual. To avoid any kind of pre-justice all samples from clinically tested patients were coded and their records given to us solely after completion of our hair analysis.

X-ray diffraction pattern from bundles of four hairs each were taken at the Austrian SAXS beamline at Trieste [2] using a CCD-detector (Photonic Science, Millham, U.K.). The hairs were mounted on a flat support with a central hole with adhesive tape and gently stretched to allow for parallel and non-twisted alignment. Except an air gap of 1 cm the whole diffraction path was evacuated. The total exposure time for each sample was averaged over 100 frames each with typical integration times of 2-5 s. The raw data was corrected for the detector efficiency and the background scattering.

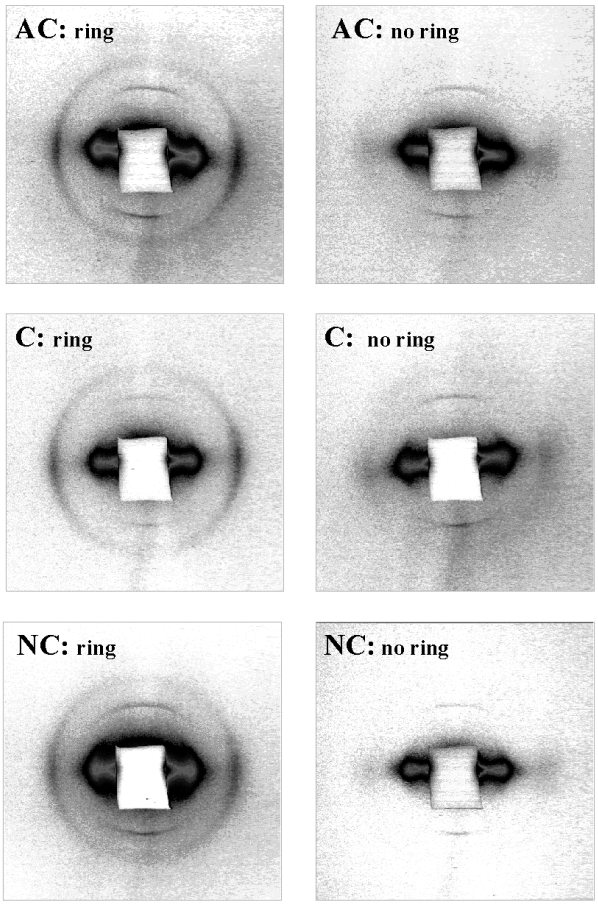

Figure 1. Six representative dif-fraction pattern showing “changed” structures on the left and “normal” ones at the right hand side, respectively (for the abbreviations AC, C and NC, see text).

All data was classified into two groups according to the appearance or non-appearance of the diffuse 4.4 nm ring [1], “which places it directly in the position of the equatorial arc representing the plasma membrane in the normal hair” [1,3]. Unfortunately, also after personnel communication with Dr James the characterization of this ring remained very sparse, so that its

appearance was valued by eye according to “strong significance” (weight 1), “significance” (weight 0.6) and “no significance” (weight 0). This way each diffraction pattern was evaluated independently by four researchers. Only in a few ambiguous cases it was necessary to decide the class of the hair by determining a mean weighting factor in order to state whether it accounted for a “normal” or a ”changed” hair diffraction pattern.

Results: In all cases from families with a history of BRCA-1 and/or -2 mutations, i.e., in carriers of a BRCA mutation with breast and/or ovary cancer (AC = active carrier), in those who have one of the mutation without cancer (C = carrier) and in negative controls without BRCA mutations and without cancer (NC = non-carrier), we found both types of X-ray diffraction patterns: with and without the 4.4 nm ring (Fig. 1). Most surprisingly, there is no prevalence of patterns with this ring in any of these three groups (Fig. 2A). To the contrary, the AC-subgroup, which according to the work by James et al. [1] was expected to show only the ring-type pattern, showed in our examination in fact the smallest proportion of it. We do not attribute any statistical significance to the fact that the proportion of ring-patterns was found highest in the C-subgroup, but it is important to stress that it was always below 50%. The non-carriers (NC) served as an internal control within this familially related population, and showed the average proportion of about 30 % ring patterns. Moreover, also a small set of breast-tumor patients from Trieste was screened. But also here, no correlation between patients with benign tumors with “normal” hair pattern or those with breast cancer and “changed” pattern, respectively, could be found. Furthermore, even healthy hair from male donors show a similar distribution and like healthy females (Fig. 2B), with a possibility that the ring pattern might occur more frequently with hair samples from males.

In view of these results [4], which differ most strongly from those presented by James et al. [1], the expectation that x-ray diffraction from hair samples might provide a diagnostic tool for breast cancer, cannot be further upheld.

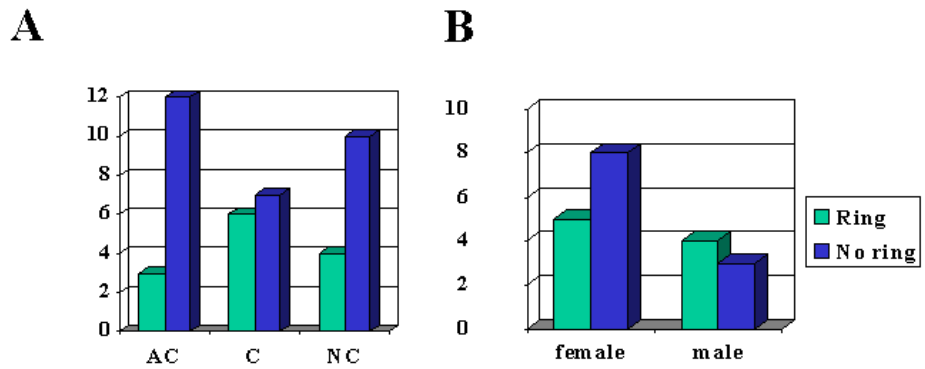

Figure 2. A. Distribution of “normal” and “changed” hair pattern within the sub-groups AC, C and NC (cf. Fig. 1). B. Distribution of “normal” and “changed” hair pattern among healthy women and men, respectively.

References:

[1] James, J., Kearsley, J., Irving, T., Amemiya, Y. and Cookson, D. (1999): *Nature* **398**, 33.
[2] Amenitsch, H., Rappolt, M., Kriechbaum, M., Mio, H., Laggner, P. and Bernstorff, S. (1998): *J. Synchrotron Rad.* **5**, 506.
[3] Wilk, K.E., James, J. and Amemiya, Y. (1995): *Biochim. Biophys. Acta* **1245**, 392.
[4] Amenitsch, H. et al.(1999): *Synchrotron Radiation News* **12 (5)**, 32-34.

X-RAY DIFFRACTION STUDY OF THE STRUCTURE OF DNA-LIPOSOME-METAL COMPLEXES

O. Francescangeli[1], P. Bruni[1], F. Cingolani[1], C. Conti[1], M. Iacussi[1], D. E. Lucchetta[1], R. Marzocchini[1], S. Bernstorff[2] and H. Amenitsch[3]

1.) Dipartimento di Scienze dei Materiali e della Terra, Universita' di Ancona, Via Brecce Bianche, 60131 Ancona, Italy
2.) Sincrotrone Trieste, Basovizza (TS), Italy
3.) Institute for Biophysics, Austrian Academy of Sciences, Graz, Austria

Within the general scope of providing new biological materials for gene delivery systems we are carrying on a systematic study of the interactions among DNA, liposomes (L) and metal cations (M) in triple DNA-L-M complexes. In fact, the introduction of a metal cation leads to the formation of complexes that, in principle, are more stable and less toxic as compared with those with cationic liposomes (CL) [1,2]. The structural characterization of these complexes is an essential feature to be investigated in order to understand the role played by the metal cations in stabilizing the DNA-liposome interactions and then in the formation of supramolecular aggregates. In this contribution we report the results of X-ray diffraction (XRD) studies performed on complexes of DNA, DOPC (dioleilphosphatidilcholine) and different metal ions (Mn^{++}, Mg^{++}, Co^{++}, Cr^{+++}, Fe^{++}, Fe^{+++}) at different concentrations of the metal and different temperatures. The results show the presence of two diffraction peaks in the small (scattering) angle region of the spectrum, corresponding to spacings of ≈ 61.0 Å and ≈ 73 Å, respectively (Figure 1). The former periodicity, which is also present in the XRD spectrum of the DOPC solutions in buffer (HEPES) at pH=7.2, corresponds to the 1D periodic lamellar structure of the liposomes, whereas the latter one indicates the presence of a 1D periodic superstructure where the DNA and the metal cations are intercalated between the liposome layers. However, only in the case of Mn^{++} we obtained enough intense and stable diffraction peaks due to the formation of stable triple DNA-L-M complex.

The periodicity measured at ≈73 Å is in agreement with a high ordered multilamellar structure where both DNA and metal cations are „sandwiched“ between liposome layers, similar to the model proposed in refs [1,2] for DNA-CL complexes. The presence of the two periodicities in the triple complexes indicates the coexistence at equilibrium of the two layered structures. Our XRD experiments indicate that: *(i))* the peak at 72.7 Å is completely absent when the molar ratio of the three components DNA-L-M is 4-3-1; *(ii)* on increasing the concentration of Mn^{++}, it becomes apparent and its intensity increases consequently (figure 2). Finally, we have studied the kinetic of the formation of the triple complex at 27 °C by the stopped-flow measurement technique (figure 1). In particular, the peak at 72.7 Å is observed to form after 12 s, to increase for some tenths of seconds and remain stable up to 10 minutes from mixing of the three components.

The effect of the temperature on the DNA-MLV-Mn^{++} complex is shown in figure 3. It can be seen that either after 4 min. or after 10 min. from mixing, the intensity of the peak of the triple complex increase with increasing the temperature. These experimental evidences, in connection with EPR measurements that we performed at 27, 37 and 47^0C and which gave stability constants (K_{stab}) of 9.5, 15.0 and 15.2 x 10^4 M^{-1}, indicate the existence of an endothermic equilibrium in the formation of the triple complex.

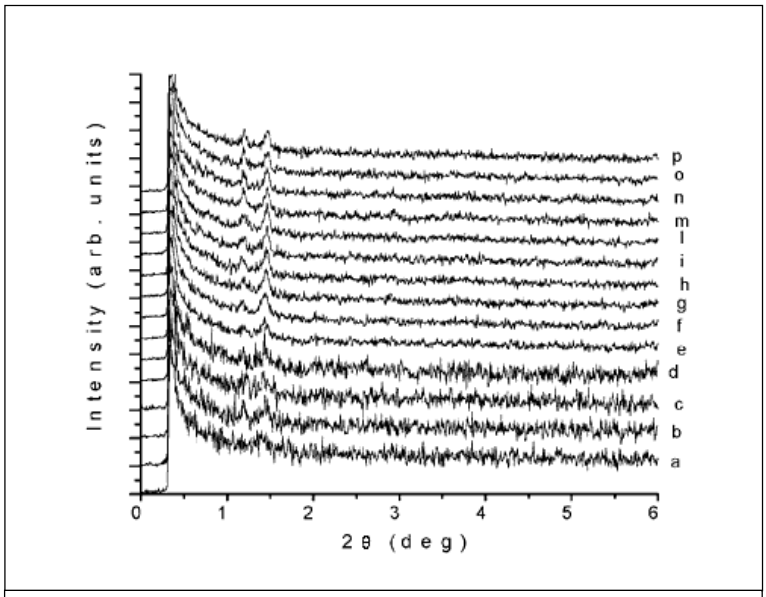

Figure 1. Time evolution of the XRD pattern of the DNA-L-Mn^{++} complex (4:3:24) at 27 °C: (a)-(d) every six seconds; (e)-(p) every thirty seconds.

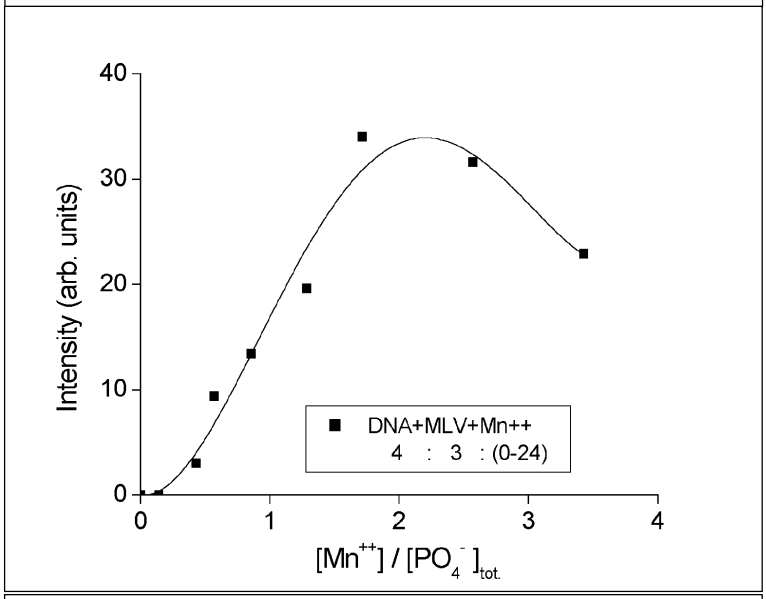

Figure 2. Intensity of the peak at ≈ 73 Å vs. the ratio of concentration of Mn^{++} and total PO_4^-.

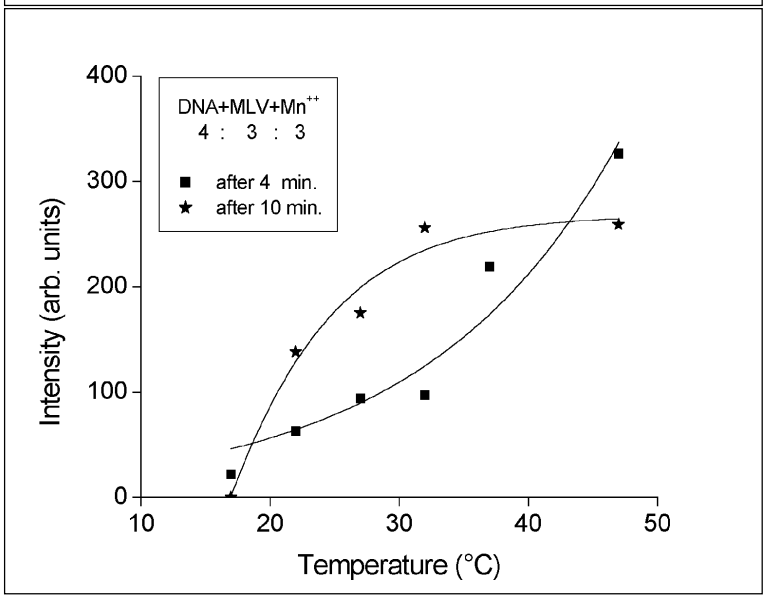

Figure 3. Intensity of the peak at ≈ 73 Å vs. temperature recorder after 4 and 10 minutes.

References:

[1] Lasic, D. et al. (1997): The Structure of DNA-Liposome Complexes. *J. Am. Chem. Soc.* **119**, 832-833.

[2] Rädler, J.O. et al. (1997): Structure of DNA-Cationic Liposome Complexes: DNA Intercalation in Multilamellar Membranes in Distinct Interhelical Packing Regimes. *Science* **275**, 810-814.

SAXS STUDY ON THERMO-REVERSIBLE κ-CARRAGEENAN GELS BY SYNCHROTRON RADIATION

A. Gamini[1], S. Paoletti[1], K. Bongaerts[2], E. Theunissen[2], G. Evmenenko[2], H. Rheynaers[2], H. Amenitsch[3] and S. Bernstorff [4]

1.) Department of Biochemistry, Biophysics and Macromolecular Chemistry, University of Trieste, Via L. Giorgieri 1, I-34127, Trieste, Italy.
2.) Laboratory of Macromolecular Structural Chemistry, University of Leuven, Celestijnenlaan 200F, B-3030, Heverlee, Belgium.
3.) Institute of Biophysics and X-ray Structure Research, Austrian Academy of Science, Steyrerg. 17, A-8010 Graz, Austria.
4.) Sincrotrone Trieste S.C.p.a., Area Science Park, Strada Statale 14, Km 163.5, I-34012, Basovizza, Trieste, Italy.

κ-carrageenan is a sulphated poly-galactose extracted from red algae which is known to undergo thermoreversible salt induced conformational transition. The transition is generally described as disorder-to-order transition and may eventually lead to gel formation depending on type and concentration of the added salt. However, despite the extensive studies until now performed a clear picture of the κ-carrageenan gel state as well as an unambiguous understanding of the involved gelling mechanism has not yet been achieved. As in most gelling system either synthetic or natural a qualitative representation of the gelling mechanism should include the formation of an ordered secondary structure for a sufficient length of the main chain followed by aggregation in bundles of ordered segments belonging to different chains, with the result of having a three-dimensional network formed. Being the secondary κ-carrageenan ordered structure still a debated matter in as much as single, double or multiple chains may represent the fundamental ordered state from which gel formation takes place, we performed SAXS measurements as a function of temperature. Two different aqueous 0.1M salt solutions has been chosen as solvent media for κ-carrageenan chains: a non gelling solvent as NaI and a typical gelling solvent as KCl. Indeed, in the former medium it has been shown that the low temperature ordered conformation be fairly described by a single polymer chain of relatively high stiffness while a firm gel is obtained at room temperature when κ-carrageenan is dissolved in the presence of the latter simple electrolyte. The intensity of the radiation scattered by the polysaccharide-electrolyte solution was measured at several, constant T values after a suitable time (i.e.30 min) was given to the system to reach its thermal equilibrium. The temperature ranged from 20 to 70°C.

Considering the scattering vector as a magnifying lens, at sufficiently large q values the intensity of the scattered radiation should be independent of the concentration as well of the polymer molar mass and should depend only from the chain statistics. Moreover, for q^{-1} smaller than the length of the statistical segment the chain should behave as a rigid rod. At large q values for a rod of length L and molar mass M the intensity I (q) becomes a linear function of q^{-1} which slope is proportional to the inverse of the mass per unit length [1, 2]:

$$c\,\mathrm{I}(q)^{-1} = A\left[\frac{q\,\mathrm{L}}{\pi\,\mathrm{M}} + \frac{2}{\pi^2\,\mathrm{M}}\right] \qquad (1)$$

In eq. 1) c is the polymer concentration expressed as mass per unit volume and A, cluster of parameters including the scattering volume and the "contrast factor", is constant for a given polymer-solvent system. According to eq. 1), the quantity $q\mathrm{I}(q)/c$ at sufficiently large q should reach a constant plateau value of magnitude $q\mathrm{I}(q)/c \sim \pi \mathrm{M_L}$ with $\mathrm{M_L}$=M/L [3] the mass per unit length of the rod. In Figures 1 and 2 the intensity measured at different T is reported as $q\mathrm{I}(q)$

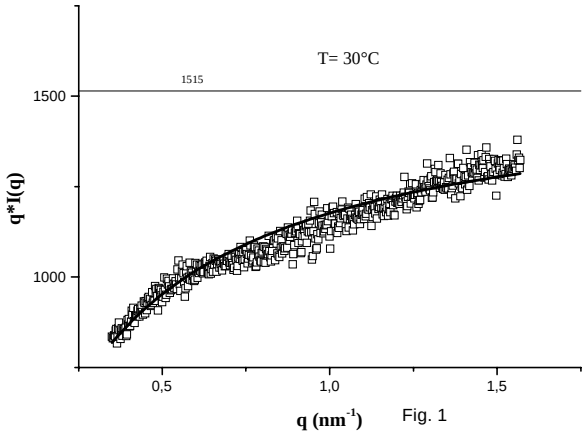

Fig. 1

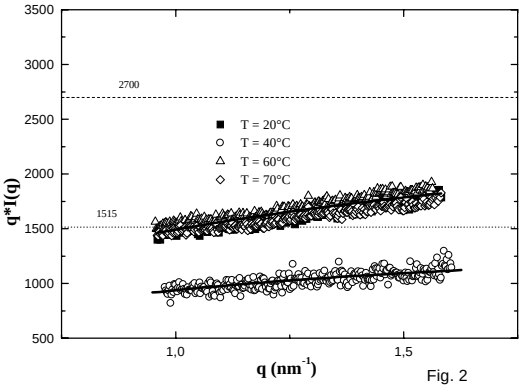

Fig. 2

vs *q* for κ-carrageenan in NaI and KCl, respectively. The horizontal lines represent the calculated asymptotic,~ πM_L values. Being identical the polymer concentration in the two solvent media, the mass per unit length of the polysaccharide chain in KCl, relatively to that in NaI salt solution may be then deduced on a length scale of the order of few repeating units. In other words, known the molecularity of the chain in the non-gelling solvent, the molecularity of the aggregated state can be readily obtained. The calculated relative mass per unit length, reported as function of temperature in Fig. 3, show that in KCl single chains pair to an extent of ~ 97% at low temperature to melt at about 40°C to a single strand. Beyond this temperature the re-newed high M_L can be reasonably interpreted considering the overimposition of the partial melting of, until then not visible, big chain clusters containing at a temperature as high as 70°C still a considerable amount of associated chains [4].

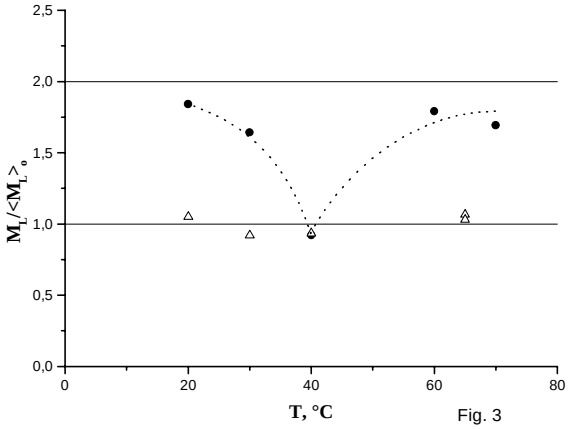

Fig. 3

References:

[1] Holtzer, A.M.(1955): *J. of Polymer Sci*., **17**,432.

[2] Casassa, E.F. & H. Eisenberg, H. (1964): *Adv. Protein Chem.*, **30**, 287.

[3] Higgins, J.S. & Benoit, H.(1994): In "*Polymers and Neutron Scattering*", Clarendon Press-Oxford.

[4] Gamini, A., Paoletti, S., Bongaerts, K., Theunissen, E., Evmenenko, Rheynaers, G.H., Amenitsch, H., Bernstorff, S. (1998): *SAXS Annual Report*.

EFFECTS OF TEMPERATURE ON 14.5 nm MERIDIONAL REFLECTION INTENSITY DURING SINUSOIDAL LENGTH CHANGES IN FROG MUSCLE FIBRES.

P.J. Griffiths[1], H. Amenitsch[2], C.C. Ashley[!], M.A. Bagni[3], S. Bernstorff[4], B. Colombini[3], G. Cecchi[3].

1.) University Laboratory of Physiology, Oxford U.K.
2.) Institute for Biophysics and X-ray Structure Research, Austrian Academy of Sciences, Graz Austria.
3.) Dipartimento di Scienze Fsiologiche, Università di Firenze, Firenze, Italy.
4.) Sincrotrone Trieste, Basovizza, Italy.

It has been shown that sinusoidal fast length oscillations (3 kHz frequency) in activated fibres produce changes in 14.5 nm meridional reflection intensity (IM3) which are sinusoidal in shape and in opposition of phase respect to length changes [1, 2]. However at lower frequency (100-400 Hz) the intensity changes are not sinusoidal [3] but show a strong distortion with the formation of a double peak during the release phase of the sinusoids. Both of these results can be explained by a model in which myosin heads (the crossbridges) are elastic and the IM3 changes are caused by a synchronized tilting of the myosin heads due to both the force applied and to the quick recovery mechanism [3, 4]. To explain the sinusoidal shape of the intensity changes the mean position of the heads during the oscillations at 3 kHz should be few nm away from the position which gives the maximum intensity. During the release phase the heads would approach the optimal orientation and the intensity would increase. The opposite would occur during stretch. Using this model the double peak seen at low frequency is caused by the relatively greater head tilting which during the release phase produces first an increases as the heads approach the optimum, and than a decrease as the heads go beyond the maximum. On this base the presence of the double peak allows to calculate the mean position of the myosin heads during the oscillations. This is an important information since the mean position could be related to the force developed by the preparation. Frog muscle fibres develop higher tension as the temperature increases above 0-2 °C. It is though that this increase is due to an increase of crossbridge extension rather than an increase of crossbridge number. If this is true the mean position of myosin heads should change with the temperature and it should be possible to detect this change through the analysis of the intensity data during oscillations at low frequency.

Experiments were made in single or small bundles of frog muscle fibres at 4, 14 and 24 °C. Sinusoidal oscillations at 1 kHz frequency and about 4-6nm/half sarcomere peak to peak amplitude were applied to the preparation during isometric contractions. IM3 was measured using the SAXS beam line at Elettra. The beam dimension at the preparation were 4 x 0.3 mm which gave a flux of 10^{12} photons^{-1} at wavelength of 0.15 nm. The meridional x-ray diffraction spectra was collected using an one dimensional delay line detector driven by a PC based data collection system by which force, sarcomere length and fibre length could be simultaneously sampled. The preparation was mounted between a capacitance force transducer and a moving coil motor by means of aluminum foil clips. The mean sarcomere length of a fibre region of about 200 μm located in the segment illuminated by the x-ray beam, was measured by means of a laser light diffractometer. Oscillations were imposed for a period of 0.5 s during a sequence of up to 40 tetani given at 3 min intervals. Spectra were then summed over a sequence of tetani and within an individual tetanus to obtain 20 averaged spectra covering one period of the imposed length oscillation. At the temperature of 4 and 14 °C IM3 showed periodic fluctuation in opposition of phase respect to force and length change. Peak to peak force oscillations was in the range of 0.6-0.1 the tetanic tension and IM3 change was around 0.25 the mean intensity. IM3 was characterized by a strong distortion during the

release phase of the sinusoidal length change. At 24 °C IM3 changes were in the opposite direction: intensity increased during stretch and decreased during the release. This result suggests that at higher temperature the mean position of the myosin heads could be significantly different respect to lower temperature. However, several other aspects for example the effect of quick recovery at high temperature, need to be further investigated before to reach a firm conclusion.

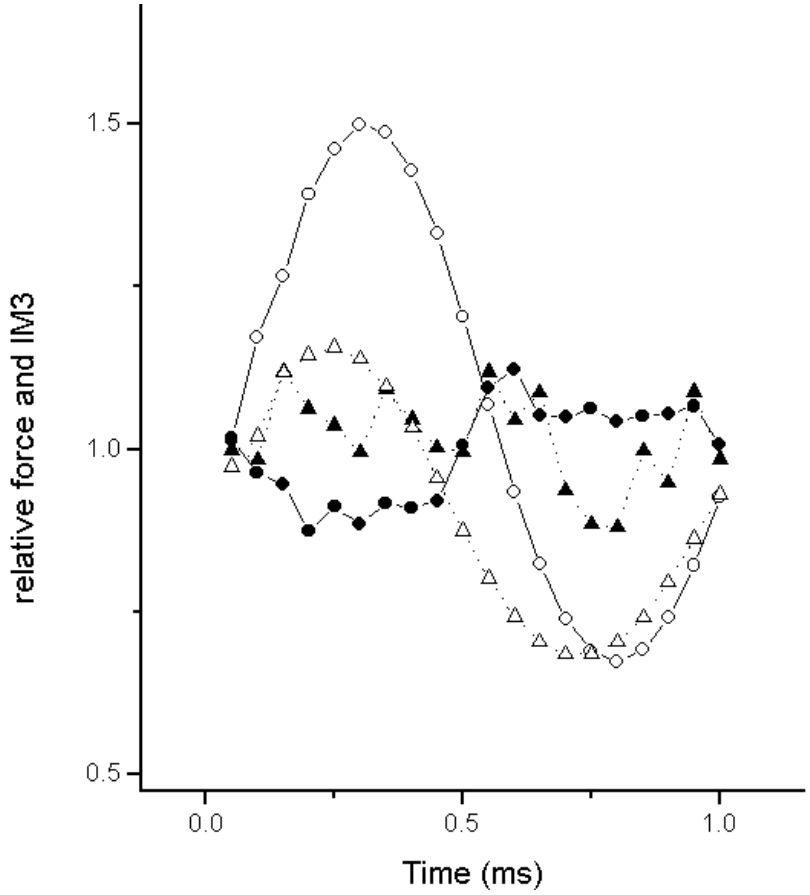

Figure 1. Force and IM3 changes in activated small bundles of frog skeletal muscle fibres during sinusoidal length oscillations at 1 kHz. Empty symbols: Force at 4 °C (circles) and, in a different bundle, at 24 °C (triangles). Filled symbols: IM3 changes at 4 °C (circles) and 24 °C (triangles). Force and IM3 values are expressed relatively to the respective mean values. Note that: 1) IM3 changes at 4 and 24 °C are not sinusoidal and 2) increasing the temperature from 4 to 24 °C inverted the IM3 changes.

References:

[1] Dobbie, I., Linari, M., Piazzesi, G., Reconditi, M., Koubassova, N., Ferenczi, M.A., Lombardi, V. & Irving, M. (1998) Elastic bending and active tilting of myosin heads during muscle contraction. *Nature*, **396 (6709)**, 383-387.

[2] Amenitsch H., Ashley, C.C., Bagni, M.A., Bernstorff, S., Cecchi, G., Colombini B. & Griffiths, P.J. (1999): 16 μs time resolution X-ray diffraction measurements in living skeletal muscle cells of the frog. *Austrian SAXS - Beamline at Elettra, Annual report 1998*, 44-45.

[3] Bagni, M.A., Cecchi, G., Colombini, B., Amenitsch, H., Bernstorff, S., Rapp, G., Ashley, C.C. & Griffiths, P.J. (2000): 14.5 nm meridional X-ray diffraction intensity changes associated with the myosin head elasticity and the quick recovery phase. *Biophysical Journal*, **78 (1)**, A227.

[4] Piazzesi, G., Lombardi, V., Ferenczi, M.A., Thirlwell, H., Dobbie, I. & Irving, M. (1995): Changes in the x-ray diffraction pattern from single, intact muscle fibers produced by rapid shortening. *Biophysical Journal* **68(4)**, 2S-96S.

KINETIC STUDIES OF PRESSURE-JUMP INDUCED PHASE-TRANSITIONS OF PHOSPHOLIPIDS BY TIME-RESOLVED SMALL-ANGLE X-RAY SCATTERING

M. Kriechbaum[1], M. Steinhart[2], P. Laggner[1], H. Amenitsch[1] and S. Bernstorff[3]

1.) Institute of Biophysics and X-Ray Structure Research, Austrian Academy of Sciences, A-8010 Graz, Austria.
2.) Institute of Macromolecular Chemistry, Academy of Sciences of the Czech Republic, Prague, Czech Rep.
3.) Sincrotrone Trieste, Basovizza, Italy.

We have performed kinetic studies on pressure-jump induced phase transitions of phospholipids monitored by time-resolved X-ray scattering with milli-second time-resolution in the SAXS (10-200 Å) and WAXS (3-6 Å) region, simultaneously, using the setup as described in the previous Annual Report 97/98 with the technical details published in [1]. In these studies we have focused on the kinetics of barotropic phase transitions of the phosphatidylethanolamine (PE) lipids DOPE and SOPE, respectively, by applying pressure-jump amplitudes up to 1.7 kbar (0.17 GPa) in both directions (compression and decompression) at different temperatures. Using an optimized setup, SAXS and WAXS diffraction data with good statistics could be obtained with 5 ms time-resolution in a single-shot experiment. It was shown that the time constants for a completion of a phase transition depend strongly on the magnitude of the depth of the quench into the new phase.

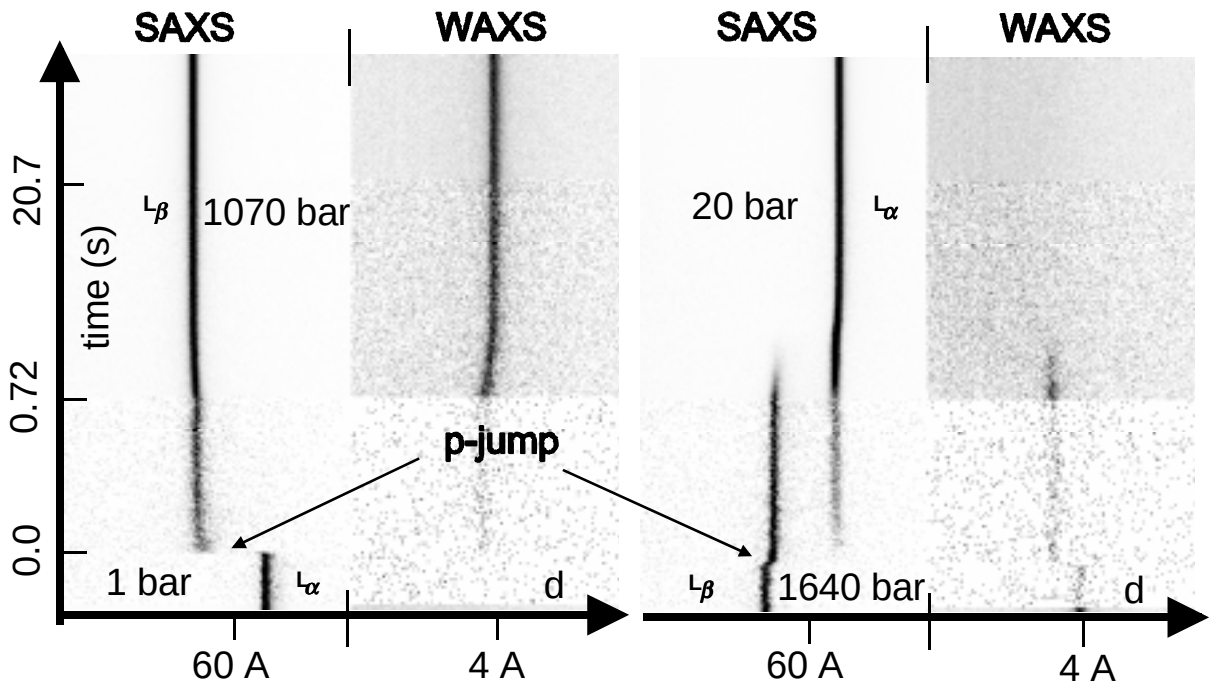

Figure 1. Time-resolved p-jump experiments of SOPE (T=40°C) with p-jump amplitudes as indicated in the plots with a maximum time-resolution of 5 ms. P-jumps (completed within 10 ms) from the lamellar-fluid to the lamellar-gel phase (left; compression) and vice versa (right; decompression) are shown in the SAXS region (lamellar lattice-spacing d) and the WAXS region (lateral (short-range order) lattice-spacing d within the lipid bilayer). Each image shows 512 frames of a single-shot experiment with decreasing time-resolution (5/50/500ms) from the bottom to the top (time-normalized, unsmoothed intensity-data displayed in a linear gray-scale).

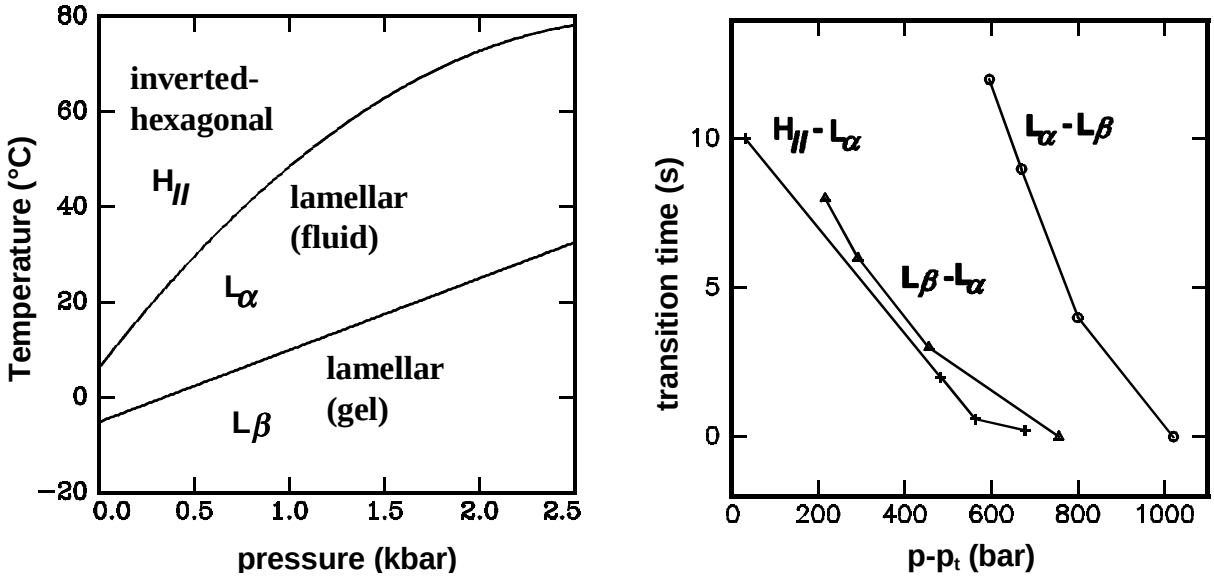

Figure 2. Pressure-temperature phase diagram of DOPE in excess water (left), consisting of two lamellar phases, L_β (gel) and L_α (fluid), respectively, and an inverted hexagonal phase H_{II}. The figure to the right shows for three different barotropic phase-transitions the dependency of the transition time of the respective phase undergoing a p-jump induced transition as a function of the applied p-jump amplitude p-p_t, where p is the final pressure after the jump and p_t the transition pressure in p-T equilibrium phase diagram. The phase transformation proceeds the faster the higher the jump amplitude (quench into the new phase as being indicative for the driving force) is chosen.

References:

[1] Steinhart, M., Kriechbaum, M., Pressl, K., Amenitsch, H., Laggner, P. & Bernstorff, S. (1999): High-Pressure Instrument for Small- and Wide-Angle X-Ray Scattering. II. Time-Resolved Experiments. *Rev.Sci.Instrum.* **70**, 1540-1545.

THE MECHANISM OF STRETCH POTENTIATION IN MUSCLE: STRUCTURAL MODIFICATIONS OF THE MYOSIN CROSS-BRIDGES DURING AND AFTER STEADY LENGTHENING

M. Linari[1], M.E. Vannicelli Casoni[1], L. Lucii[1], M. Reconditi[1], H. Amenitsch[2], S. Bernstorff[3], G. Piazzesi[1] and V. Lombardi[1]

1.) Università di Firenze, 50134 Firenze, Italy.
2.) Austrian Academy of Sciences, 8010 Graz, Austria.
3.) Sincrotrone Trieste, 34012 Basovizza, Trieste, Italy.

The first part of the allocated time was used to improve the statistics of the data collected during the previous visit (see report on experiments 104/98) on the changes in the intensity and spacing of the third order myosin-based meridional reflection at 14.5 nm (M3, sensitive to the axial movements of the myosin cross-bridges) during potentiation of contraction elicited by stretching tetanized single muscle fibres.

Single muscle fibres, freshly dissected from the tibialis anterior muscle of Rana temporaria, were mounted between the lever arms of a force transducer and a servo-controlled loudspeaker motor (Lombardi and Piazzesi, *J. Physiol.* **431**, 141-171, 1990 and references therein) and placed vertical at the beamline. The linear gas-filled detector was placed at 2.2 m from the sample, parallel to the fibre axis in order to collect reflections along the meridian. In some experiments the detector was rotated by 90° and shifted vertically to the level of the third myosin-based layer line, in order to collect the changes in the dispersion of the M3 reflection across the meridian (*W*) and correct for the change in lattice sampled by the reflection due to change of filament coherence in different physiological conditions. Tetanic contraction was induced at 4°C and 2.2 μm sarcomere length by electrical stimulation at the frequency of 15-30 Hz. The intensity of the M3 reflection was recorded with 250 ms frames at rest, during the isometric tetanus when force had attained a plateau value (T_0), during the steady state force response (1.6 T_0) to lengthening of 60 nm per hs, at the velocity of 200 nm s^{-1} per hs and during the force enhancement after stretch (starting 50 ms after the end of the lengthening). Data obtained from a total of 18 fibres (including 10 fibres from previous visit) were analysed by means of Sigmaplot and Peakfit (Jandel Scientific) software.

Spacing of M3 reflection, *S*(M3), increased by 1.49 ± 0.03 % during the transition from rest to isometric tetanus plateau. During force response to steady lengthening there was a further increase of *S*(M3) of 0.14 ± 0.05 %, not fully explained by the filament compliance (Wakabayashi et al. *Biophys. J.* **67**, 2422-2435, 1994; Huxley et al. *Biophys. J.* **67**, 2411-2421, 1994; Dobbie et al. *Nature* **396**, 383-387, 1998). The intensity of M3 reflection, *I*(M3), decreased to 0.48 ± 0.02 $I(M3)_0$ (the isometric plateau value) during steady lengthening and partially recovered during the after stretch potentiation (0.65 ± 0.03 $I(M3)_0$). After the correction for the change in lattice sampled by the reflection (estimated from the change in *W* and for the influence of the beam size, *I*(M3) reduced to 0.67 ± 0.04 $I(M3)_0$) during steady lengthening and recovered to 0.86 ± 0.05 $I(M3)_0$ during force enhancement after stretch (Table 1).

Reduction of intensity during steady lengthening is explained according to Huxley and Simmons theory (*Nature* **233**, 533-538, 1971, see also Piazzesi et al. *J. Physiol.* **445**, 659-711, 1992) by both myosin head tilting away from the perpendicular to the filament axis and increase of dispersion of head conformations; intensity recovery soon after the stretch end supports the idea of a rapid detachment/reattachment process which involves specifically the more strained cross-bridges (Colomo et al. *J. Physiol.* **415**, 130P, 1989). These results solve the question of the contribution of the cross-bridges to after-stretch potentiation, that cannot consist in potential energy stored in a long-lived state of cross-bridges (Cavagna et al. *J.*

Physiol. **481**, 689-708, 1994) but rather in the increase in number of attached cross-bridges, recruited during the previous lengthening.
Increase of *S*(M3) under strain indicates a compliance of the thick filament (0.23 % T_0^{-1}) about twice the value expected from the instantaneous compliance (0.12 % T_0^{-1}, Dobbie et al. 1998) suggesting a more complex modification in the arrangement of myosin monomers along the filament. The nature of this spacing change was investigated during the second part of the visit, by means of a protocol which allowed to determine the time course of the change in *S*(M3) when the strain is abruptly increased above the isometric level. Stretch and shortening steps were imposed 100 times during each tetanus so that the X-ray signals could be summed and the time resolution increased to 500 μs per frame. A stretch of ~0.5% the fibre length was followed after 4 ms by a release of the same size, then after 16 ms the cycle was repeated. With this protocol each stretch starts from the isometric force level (Lombardi et al., *Nature*, 374, 553-555, 1995).
Data collected during this visit (Fig.1) had the necessary signal to noise ratio only for the *I*(M3) signal, describing with the adequate time resolution the changes occurring both during the elastic response and the quick tension recovery. As regards the *S*(M3) signal, the results seem to show that the quick force recovery following the stretch is accompanied by further increase in spacing, a result opposite to that expected on the basis of the instantaneous compliance in the thick filament, but more data must be collected to attain the adequate signal to noise ratio.

Table 1. Mean values ± SE of spacing and intensity of M3 reflection in the different physiological conditions. *I*(M3) is normalised by the value at the isometric tetanus plateau ($I(M3)_0$).

	rest	**plateau**	**stretch**	**after stretch**
spacing (nm)	14.340 ± 0.003	14.554 ± 0.004	14.575 ± 0.006	14.572 ± 0.003
$I(M3)/I(M3)_0$	1.19 ± 0.03	1.00	0.48 ± 0.02	0.65 ± 0.03
corrected $I(M3)/I(M3)_0$	0.58 ± 0.02	1.00	0.67 ± 0.04	0.86 ± 0.05

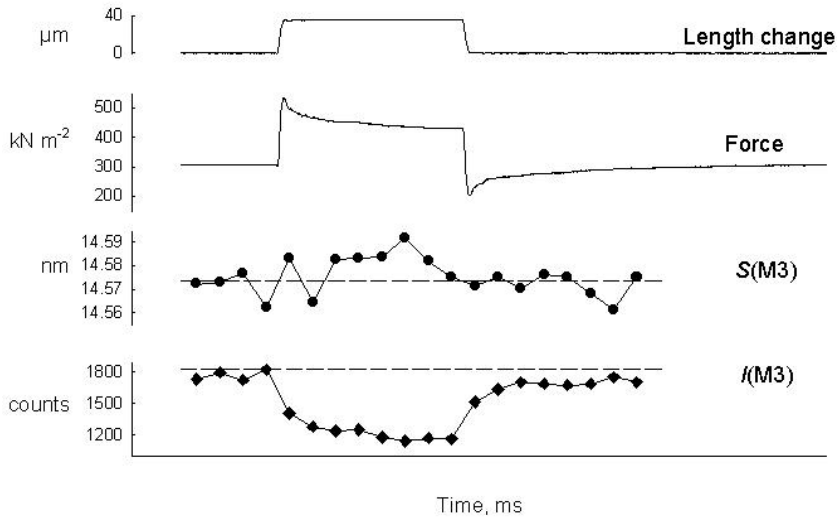

Figure 1. Changes in force, spacing (circles) and intensity (diamonds) of M3 reflection produced by a ~0.5% step stretch followed by 4 ms by a step release of the same size, with the cycle repeated every 20 ms for 100 times during a tetanus of 2.2 s. X-ray data from 110 tetani from 2 fibres; total exposure for each 500 μs frame, 5.5 s. Temperature 4 °C. The dashed lines show the spacing and the intensity in tetani without imposed steps.

PRESSURE EFFECTS ON MONOOLEIN HYDRATED SYSTEM

P. Mariani[1], M. Pisani[1], S. Bernstorff[2] and C. Ferrero[3]

1.) Istituto di Scienze Fisiche and INFM, Università di Ancona, Via Ranieri 65, I-60131 Ancona, Italy
2.) Sincrotrone Trieste S.C.p.A., Strada Statale 14, km 163.5, I-34016 Basovizza (Trieste), Italy
3.) European Synchrotron Radiation Facility, POB 220, F-38043 Grenoble Cedex, France

The effects of hydrostatic pressure on monoolein hydrated system have been investigated by means of synchrotron X-ray diffraction [1]. At atmospheric pressure, the monoolein presents several mesophases as a function of water concentration, including a lamellar structure, an inverted hexagonal phase and two bicontinuous inverted cubic phases (*Ia3d -Pn3m*) [2]. It should be noticed that the structure of bicontinuos cubic phases has been described in terms of Infinitely Periodic Minimal Surfaces (IPMS).
We have studied the polymorphism of the monoolein at very high hydration condition (c_{wat} running between 0.35 and 0.4 w/w, i.e. in the region where the *Pn3m* cubic phase exits at ambient pressure) under hydrostatic pressure up to 2 kbar. The experiments revealed a different pressure dependent phase behaviour for the less hydrated samples and for a sample prepared in excess water (c=0.4, at ambient pressure).
For the fully hydrated monoolein sample, pressure induces the transition from the cubic *Pn3m* phase to a lamellar phase with a lattice spacing of about 49 Å. As no extra peaks were observed in the wide-angle region, the lamellar phase was identified as a liquid-crystalline L_α phase. Remarkably, the *Pn3m*-L_α phase transition occurs over about 400 bar. Instead, the samples prepared in less hydrated conditions exhibit a cubic-to-cubic phase transition. During compression at about 1000 bar and within a relatively narrow pressure range, two series of Bragg reflections, which can be properly indexed considering the *Pn3m* and *Ia3d* cubic lattices, occur (see figure1).

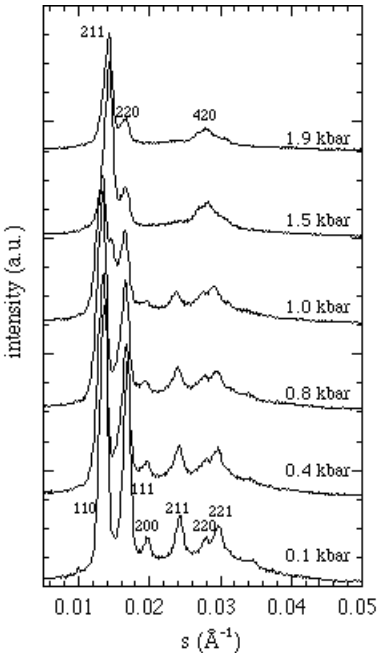

Figure 1. Low-angle X-ray diffraction profiles at different pressure from monoolein sample at 39wt.%.

It should be noticed that scattering data obtained at the intermediate pressures indicate that the two cubic phases coexist in a thermodynamic equilibrium.
From a structural point of view, noticeable is the fact that during compression the unit cell of the different phases increases. This fact has been related to a continuous change in shape of the monoolein molecule, due to an increase of the chain order parameter induced by pressure. In the less hydrated conditions, both *Pn3m* and *Ia3d* unit cell shows a linear increase as a function of pressure. A linear fit to the data has been then used to determine the pressure dependence *da/dP* (see figure2).

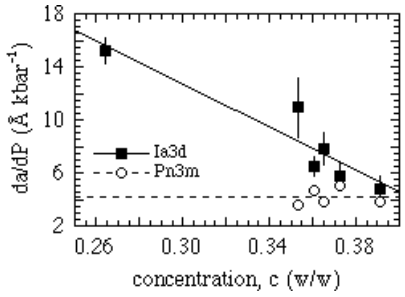

Figure 2. Cubic lattice parameter variation per unit pressure versus monoolein sample concentration.

The increase of the cell size corresponds to a reduction of the principal curvatures, thus a tentative analysis of the pressure effects on the energetics of the two bicontinuous cubic phases has been exploited. A simple theoretical model based on curvature elastic contributions [3] has been used to calculate the free energy of the two cubic phases both as a function of concentration and pressure (see the examples in figure 3). In particular, the calculations show that pressure reduces the spontaneous curvature H_0 of the monoolein layer and determines a sign inversion of the Gaussian curvature modulus K_G. As a negative value of K_G favors the *Pn3m* cubic phase, the transition to the *Ia3d* cubic appears dictated by changes in the spontaneous curvature. As a conclusion, our results show that pressure can be also used as a suitable thermodynamic variable to obtain information on the energetics and stability of lipid phases.

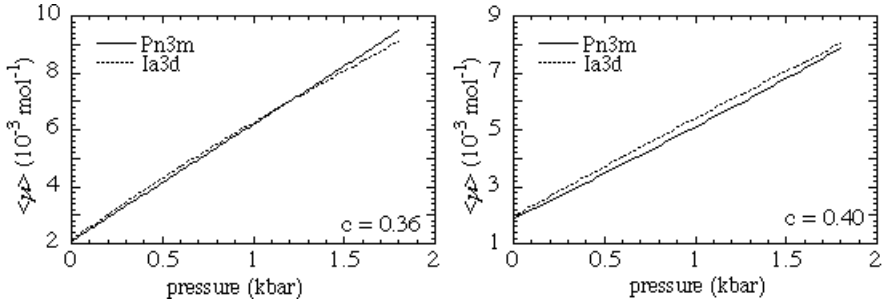

Figure 3. Scaled curvature elastic free energy for the Pn3m and Ia3d cubic phases at two different concentration as a function of pressure.

References:

[1] Pisani, M., Bernstorff, S., Ferrero, C. & Mariani, P., submitted.
[2] Hyde, S.T., Andersson, S., Ericsson, B.& Larsson, K. (1984): *Z. Kristallogr.* **168**:213-219.
[3] Templer, R.H., Turner, D.C., Harper, P. & Seddon, J.M. (1995): *J. Phys. II (France)* **5**:1053-1065.

MCG, OR THE STRUCTURE OF UNORIENTED FLUID PHOSPHOLIPID BILAYERS AT FULL HYDRATION

G. Pabst[1], M. Rappolt[1], H. Amenitsch[1], S. Bernstorff[2] and P. Laggner[1]

1.) Institute of Biophysics and X-ray Structure Research, Austrian Academy of Sciences, Steyrergasse 17, A-8010 Graz, Austria.
2.) Synchrotron Trieste (ELETTRA), SS 14, Km 163.5, I-34012 Basovizza (TS), Italy.

A novel X-ray analysis method (MCG) has been developed [1] and tested on various phospholipid dispersions. MCG, which is an indirect Fourier method, combines a modified Caillé theory (the "M" and the "C" of MCG) structure factor [2] with a Gaussian (the "G" of MCG) model representation of the bilayer electron density profile and is thus capable of fitting the full q-range, i.e., both Bragg peaks plus diffuse scattering. Hence, meaningful structural information can be derived from the powder diffraction patterns of fully hydrated phospholipid bilayer stacks, exhibiting usually only 2 – 3 diffraction peaks in the L_α-phase. The details of the method are described in [1].

As an example we present the structure of POPC (1-palmitoyl-2-oleoyl-*sn*-glycero-3-phosphocholine) 20% w/w in a temperature range of 10°C to 70°C. Figure 1 shows the diffraction pattern of POPC at 50°C, exhibiting only two orders of diffraction. A simple integration of the Bragg peaks results in the rude electron density profile depicted in the insert of Fig. 1 (dashed line). The MCG model (solid line) gives a good fit to the diffraction data in the full q-range and a clearly refined structure of the electron density profile.

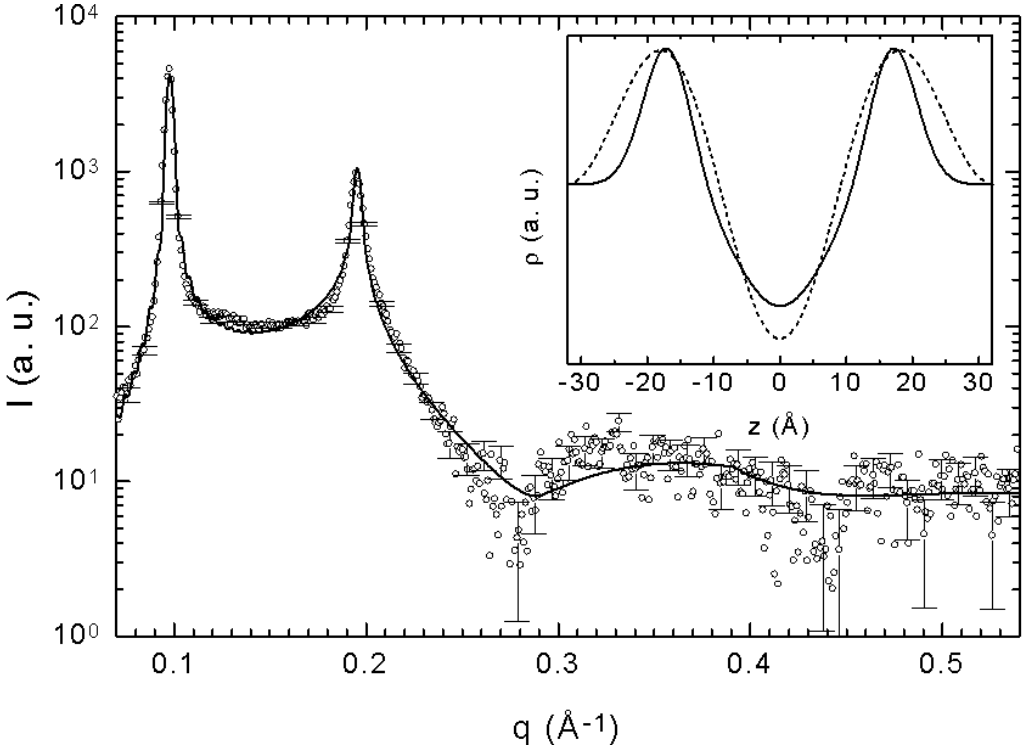

Figure 1. The best fit of the MCG model (solid line) to the diffraction pattern of POPC at 50°C. The insert gives the electron density profile obtained by a Fourier synthesis (dashed line), using Lorentzians to fit the Bragg peaks, and the profile refined with MCG (solid line).

Figure 2 depicts the MCG results for d-spacing, the membrane thickness, d_B, the water layer thickness, d_W, and the area per lipid, A, for POPC in the temperature range of 10°C to 70°C. The lamellar repeat decreases as the temperature is raised up to 30°C down to a value of d = 63.6 ± 0.1 Å. Above 30°C, the bilayer-water system swells again and finally exhibits a larger lattice parameter at 70°C than at 10°C. The decomposition of the d-spacings into bilayer and interbilayer water thickness reveals that this is caused by an uptake of water, as the membrane thickness continuously decreases with increasing temperature, but the bilayer separates more and more, such that the sum of both gives the observed re-increase in d-spacing. The area per lipid is found to increase, as the temperature is augmented. This is the result of increased molecular motions and hydrocarbon chain melting such that the individual lipid molecules require laterally more space.

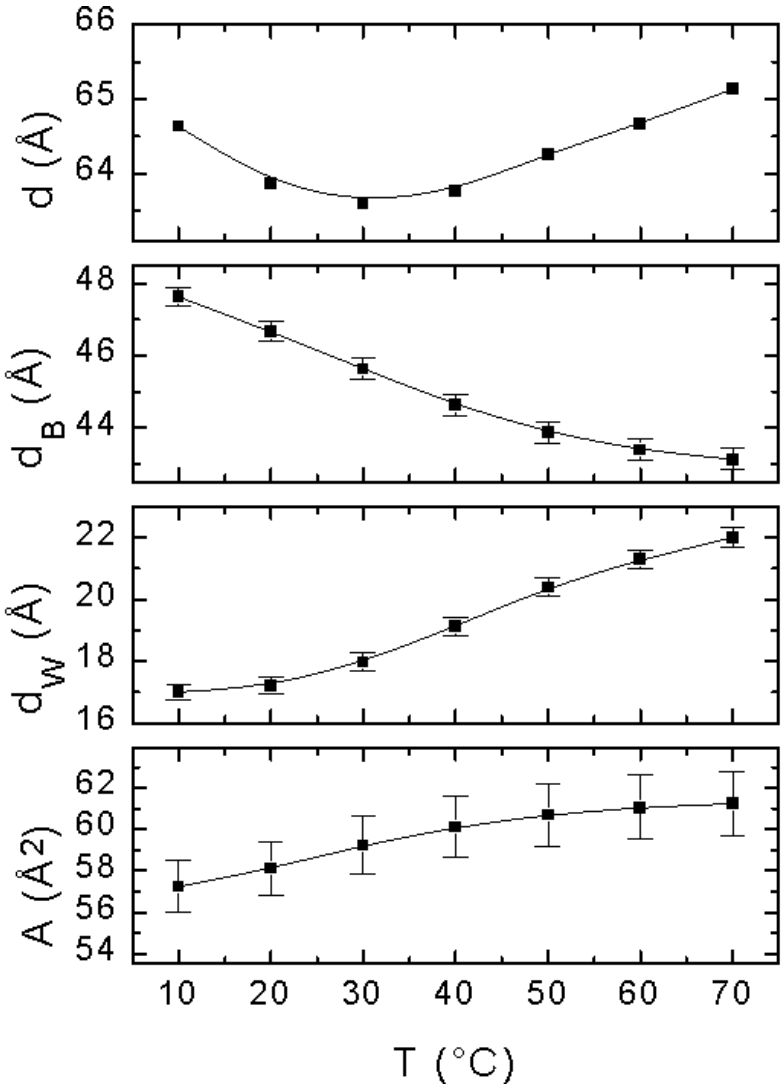

Figure 2. The equilibrium structure of POPC bilayers in the L_α-phase at different temperatures. The changes on d-spacing, membrane thickness and interbilayer water thickness are depicted. The observed re-increase in lamellar repeat distance is due to a uptake of water which increases the bilayer separation, whereas the membrane itself gets thinner with temperature and exhibits an asymptotic behavior above 50°C. Data published in [3].

References:

[1] Pabst, G., Rappolt, M., Amenitsch, H., & Laggner, P : Structural information from multilamellar liposomes at full hydration: full q-range fitting with high quality X-ray data. *Phys. Rev. E*, submitted.

[2] Zhang, R., Suter, R.M. & Nagle, J.F. (1994): Theory of the structure factor of lipid bilayers. *Phys. Rev. E* **50**, 5047-5060.

[3] Pabst, G., Rappolt, M., Amenitsch, H., Bernstorff, S. & Laggner, P : X-ray kinematography of temperature-jump relaxation probes the elastic properties of fluid bilayers. *Langmuir*, submitted.

STRUCTURE OF THE INTERMEDIATE L_{α^*}

G. Pabst[1], M. Rappolt[1], H. Amenitsch[1], S. Bernstorff[2] and P. Laggner[1]

1.) Institute of Biophysics and X-ray Structure Research, Austrian Academy of Sciences, Steyrergasse 17, A-8010 Graz, Austria.
2.) Synchrotron Trieste (ELETTRA), SS 14, Km 163.5, I-34012 Basovizza (TS), Italy.

Fast temperature-jumps (T-jumps), induced by an infrared laser (amplitudes: ~ 10 °C/ms) [1], within the L_α-phase of phospholipid model membranes have revealed an ordered intermediate structure, denoted as L_{α^*}, which displays an anomalously thin lattice constant [2]. In order to find an answer to the question, whether the anomalously thin d-spacing is the result of an anomalously thinning of the lipid bilayer, the water layer, or both, the diffraction pattern of L_{α^*} was analyzed in terms of the MCG method [3, 4] (see also the previous report).

For these experiments the sample (POPC 20% w/w) was equilibrated at a temperature of 20°C and the T-jump amplitude was set to 10°C. The time resolved X-ray diffraction experiments were repeated 12 times, and the single diffraction patterns were added up to reduce statistic noise. We further summed up the first four 5 ms time resolved diffraction patterns after the laser pulse, again to improve the statistics of the L_{α^*} diffraction pattern. Thus, the L_{α^*} diffraction pattern, which was analyzed in terms of MCG, corresponds to a total integration time of 20 ms. Table 1 lists the results for the intermediate structure and compares them to the equilibrium structure at 20°C and at 30°C.

Table 1. The structure of the L_{α^*} intermediate structure (20 ms time resolution), induced by a 10°C T-jump. The structural parameters of the intermediate are compared to the equilibrium structure at 20°C, and at 30°C.

parameter	**POPC @ 20°C**	**POPC @ 30°C**	**POPC* @ 30°C**
d [Å]	63.9 ± 0.1	63.6 ± 0.1	62.1 ± 0.5
d_B [Å]	46.6 ± 0.3	45.6 ± 0.3	45 ± 2
d_W [Å]	17.3 ± 0.3	18.0 ± 0.3	17 ± 2
A [Å^2]	58 ± 1	59 ± 2	60 ± 6
n_W	17 ± 1	18 ± 1	17 ± 3

d.....d-spacing
d_B...membrane thickness
d_W...water layer thickness
A...area per lipid
n_W...number of free water molecules (not bound to headgroup)

According to the results listed in Tab. 1 it can be assumed within the limits of measurement error that the bilayer remains within equilibrium values. In other words, it is the water layer, which is too thin to be in equilibrium. This can be explained by considering that the heating time of 2 ms is too short for water to diffuse into the interbilayer region. The T-jump induced decrease in membrane thickness is accompanied by a lateral expansion of the bilayer (Tab. 1). As there is no water exchange with the excess aqueous phase directly after the laser shot, the interbilayer water will follow the lateral bilayer expansion which gives the observed thin layer. The transient water deficit can also explain the observed sharp Bragg peaks of the L_{α^*}-phase [2], as more layers can contribute coherently to Bragg diffraction, similarly to phosphatidylethanolamine multilayers, which incorporate less than half the amount of water

compared to phosphatidylcholine multilayers, and which exhibit sharper Bragg peaks than phosphatidylcholines in the L_α-phase [5]. Figure 1 shows a cartoon of the T-jump induced structural transformation.

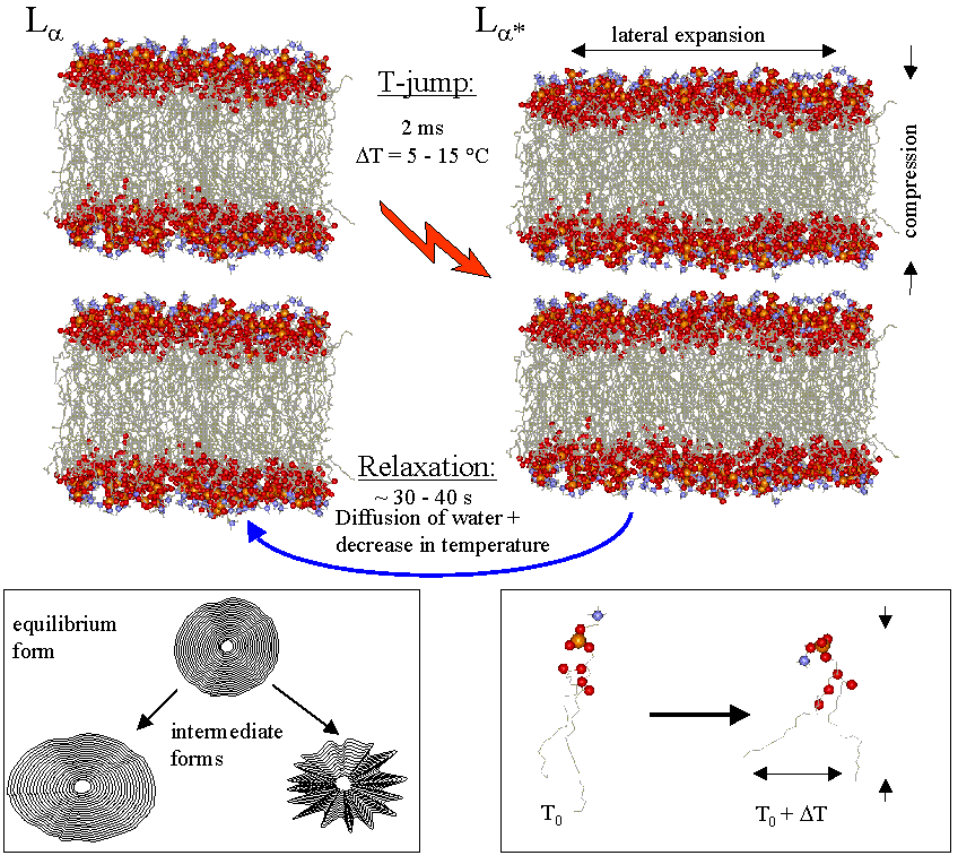

Figure 1. Cartoon of the T-jump induced structural chances on fluid bilayers (using PDB-files by Heller et al. [6]). An increase in temperature induces *trans-gauche* transitions in the fatty acid tails and an increase in lateral area per each single phospholipid molecule (bottom right insert). This leads in the compound of the membrane to a compression normal to the bilayer surface and a lateral bilayer expansion. Since water cannot diffuse fast enough from the excess phase into the interbilayer water region the water layer thickness reduces to an anomalous thin value. The bottom left insert depicts the possible intermediate forms of the liposomes.

References:

[1] Rapp, G. & Goody, R.S. (1991): Light as a trigger for time-resolved structural experiments on muscle, lipids, p21 and bacteriorhodopsin. *J. Appl. Cryst.* **24**, 857-865.

[2] Laggner, P., Amenitsch, H., Kriechbaum, M., Pabst, G. & Rappolt, M. (1998): Trapping of ordered intermediates in phospholipid phase transitions: The L_{α^*} phase. *Faraday Discuss* **111**, 31-40.

[3] Pabst, G., Rappolt, M., Amenitsch, H., & Laggner, P : Structural information from multilamellar liposomes at full hydration: full q-range fitting with high quality X-ray data. *Phys. Rev. E*, submitted.

[4] Pabst, G., Rappolt, M., Amenitsch, H., Bernstorff, S. & Laggner, P : X-ray kinematography of temperature-jump relaxation probes the elastic properties of fluid bilayers. *Langmuir*, submitted.

[5] McIntosh, T.J. & Simon, S.A. (1986): Area per molecule and distribution of water in fully hydrated dilauroylphosphatidylethanolamine bilayers. *Biochemistry* **25**, 4948-4952.

[6] Heller, H., Schaefer, M. & Schulten, K. (1993): Molecular dynamics simulation of a bilayer of 200 lipids in the gel and in the liquid-crystal phases. *J. Phys. Chem.* **97**, 8343-8360.

PROBING ELASTICITY CHANGES DUE TO CHOLESTEROL CONTENT IN PHOSPHOLIPID BILAYERS BY USING A TEMPERATURE-JUMP TECHNIQUE

M. Rappolt[1], G. Pabst[1], H. Amenitsch[1], S. Bernstorff[2] and P. Laggner[1]

1.) Institute of Biophysics and X-ray Structure Research, Austrian Academy of Sciences, Steyrergasse 17, A-8010 Graz, Austria.
2.) Synchrotron Trieste (ELETTRA), SS 14, Km 163.5, I-34012 Basovizza (TS), Italy.

To gain insight into the qualitative relaxation parameters of phospholipid bilayer in the crystalline phase after a T-jump perturbation the relaxation behaviour of the lattice parameter d was studied as a function of starting temperature (T_0), and temperature jump amplitude (ΔT), respectively. Therefore, in a series of experiments liposomal dispersions of POPC were equilibrated at temperatures between 10 and 70 °C. At each temperature a T-jump experiment with a jump amplitude of ΔT = 10 °C was performed. The relaxation kinetics of the d-spacings were analysed in terms of the double exponential decay model [1,2]. Figure 1 shows the results for the most important parameters, i.e., the change in repeat distance Δd, the square of oscillation frequency ω^2_0 , the damping factor δ, the zero velocity v_0 and the zero acceleration a_0. As T_0 is augmented, the absolute value of Δd decreases linearly up to a temperature of 50 °C. The results demonstrate that below 50 °C, the transmitted thermal energy can be directed into a membrane thinning. Mechanically, this regime corresponds to a linear relationship between applied tension and deformation, i.e., Hooke's law.

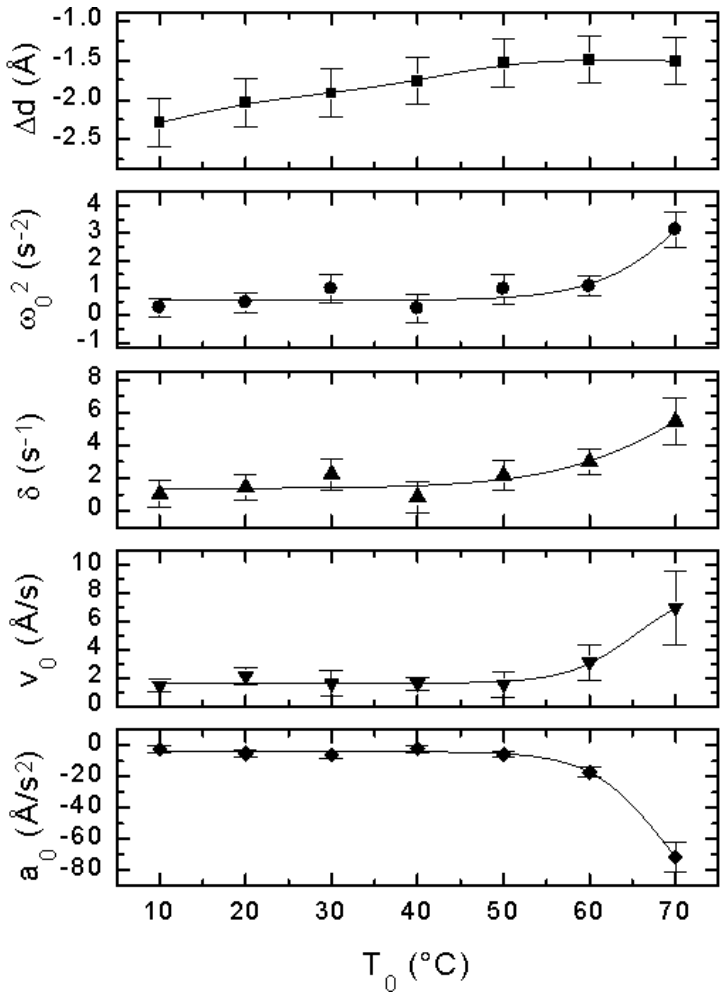

Figure 1. The relaxation parameters of POPC liposomes as a function of initial temperature T_0. The T-jump amplitude was set to 10°C at each temperature.

Finally, the impact of cholesterol to the elastic membranes was studied with the T-jump technique. Figure 2 depicts the results in terms of change in lattice parameter for POPC bilayers containing 0, 3, 5, 10 and 25 mol% cholesterol (data to be published). For these experiments the T-jump amplitude was set to 5 °C and the samples were equilibrated at 10 °C. The resulting $|\Delta d| = d_{eq}$-value increases first with cholesterol concentration and exhibits a maximum at a cholesterol content of 5 mol%; for higher cholesterol concentrations Δd decreases again. Since the T-jump induced lattice change is directly related to the compressability of the bilayer system, the results indicate that the membrane is softest at 5 mol% cholesterol content. This is in complete agreement with published data, from which it was concluded that low cholesterol contents promote a softening of the lipid bilayers, whereas high cholesterol contents induce a rigidification [3]. Moreover, these experiments give a further proof that the T-jump technique indeed probes the elastic properties of model membranes.

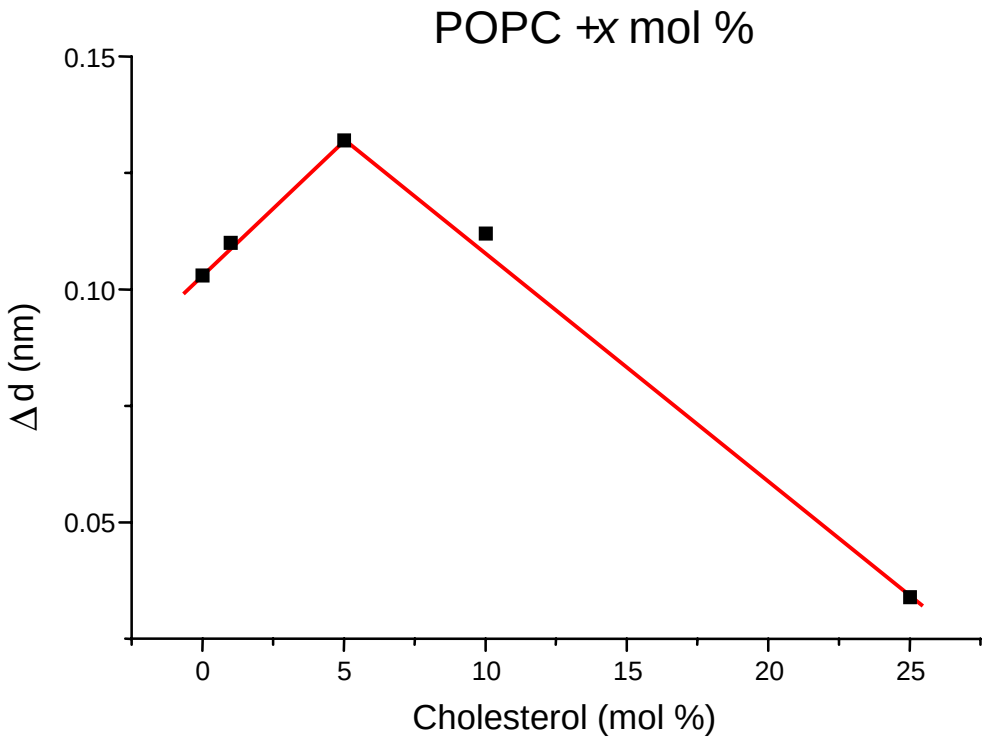

Figure 2. T-jumps of 5 °C were carried out @ T_0 = 10 °C. The structural response of the lipid systems to the rapid perturbation displays the rigidity of the bilayer: up to a concentration of 5 % cholesterol the membrane gets more fluid and thereafter at higher cholesterol concentration stiffer.

References:

[1] Pabst, G., Rappolt, M., Amenitsch, H., Bernstorff, S. & Laggner, P : X-ray kinematography of temperature-jump relaxation probes the elastic properties of fluid bilayers. *Langmuir*, submitted.

[2] Laggner, P., Amenitsch, H., Kriechbaum, M., Pabst, G. & Rappolt, M. (1998) Trapping of Short-Lived Intermediates in Phospholipid Phase Transitions: The L_{α^*}- Phase. *Faraday Discuss* **111**, 31-40.

[3] Lemmich, J., Mortensen, K., Ipsen, J. H., Hønger, T., Bauer, R. & Mouritsen, O. G. (1997)The effect of cholesterol in small amounts on lipid-bilayer softness in the region of the main phase transition. *Eur. Biophys. J.* **25**, 293-304.

THE STRUCTURAL INVESTIGATION OF tBu SUBSTITUTED AZAPORPHYRINS LANGMUIR-BLODGETT FILMS

F. Rustichelli[1], L. Valkova[1], M. Pisani [1], F. Carsughi[1] , E. Maccioni [1] and S. Bernstorff [2]

1). Istituto di Scienze Fisiche Universita di Ancona, Via Ranieri,65, 60131,Ancona, Italy
2). Sincrotrone Trieste, Basovizza, 34012 Trieste, Italy

To develop sensors for organic pollutants, p-rich semiconductors, in particular azaporphyrines, are considered to be promising materials [1-4]. The opportunity to design azaporphyrine sensors discriminating between analytes of different polarity is confirmed by our comparative study of tetra-tert-butyl-substituted copper phthalocyanine and porphyrazine. In fact, the benzene/hexane selectivity of the porphyrazine LB film is twice higher than selectivity of the phthalocyanine one. Unlike the formers, porphyrazine LB film sensitivity is strongly influenced by the crystal packing.

Therefore, structural investigation of LB films formed of non-substituted and substituted copper porphyrazines and copper phthalocyanines was undertaken. The superlatices 1A2B and 1A1B (A- PctBu4, B-Stearic Acid) were studied also.

Langmuir layers have been transferred onto hydrophobised silicon plates by horizontal lift technique at different surface pressures (from 2 mN/m to 50 mN/m). Number of transferred layers has been varied from 10 to 50.

X-ray diffraction patterns of LB film of oligomer non-substituted copper porphyrazine at room temperature show a system of equidistant reflections on the curves. Calculated value of the layer packing period is 38.4 Å. At 60^{o} C the film structure suffers destruction reversible by cooling (Figure1). It is noteworthy that for LB films of monomer copper porphyrazine only one wide reflection with packing period about 14 Å on X-ray patterns is registered, their molecular layers being poorly packed.

The X-ray diffartion pattern of LB film of 1A2B superlatice (A- PctBu4, B-Stearic Acid) at room temperature is shown at Figure 2a. Calculated layer packing period is 71 Å.

The pattern registrated after heating the sample (t=80^{o}C) is conformed to the layer packing with d = 44 Å. The corresponding curve is shown at Figure 2b.

So the temperature dependent structural rearrangements in the LB films of oligomer non-substituted copper porphyrazine and of LB film of 1A2B superlatice (A- PctBu4, B-Stearic Acid) were detected.

We are developing a physical model based on the formation of layers with controlled molecular orientation on a surface in order to monitor the interaction between sensible molecules and analytes. From our preliminary results, it appears that porphyrazine oligomer could form suitable systems for biosensor technology.

References:

[1] Schierbaum, K.-D., Zhou, R., Knecht, S., Dieing, R., Hanack, M.& Goepel, W., (1995): *Sensors and Actuators B*, 24-25, 69-71.

[2] Oeztuerk, Z. Z., Zhou, R., Weimar, U., Ahsen, V., Bekaroglu, Oe.& Goepel, W., (1995): *Sensors and Actuators B*, 26-27, 208-212.

[3] Valkova L., Pisani M., Ciuchi F.& Rustichelly F. Abst.INFMeeting (III-1). (june 25-30.1998) Rimini, Italy.

[4] Valkova, L.A., Shabyshev, L.S., Borovkov, N.Yu., Feigin, L.A. & Rustichelli,F. (1999): Supramolecular Assembly Formation in Monolayers of tert-Butyl Substituted Copper Phthalocyanine and Tetrabenztriazaporphine. *J.Inclusion Phenomena* **V.35(1/2),** 243-249.

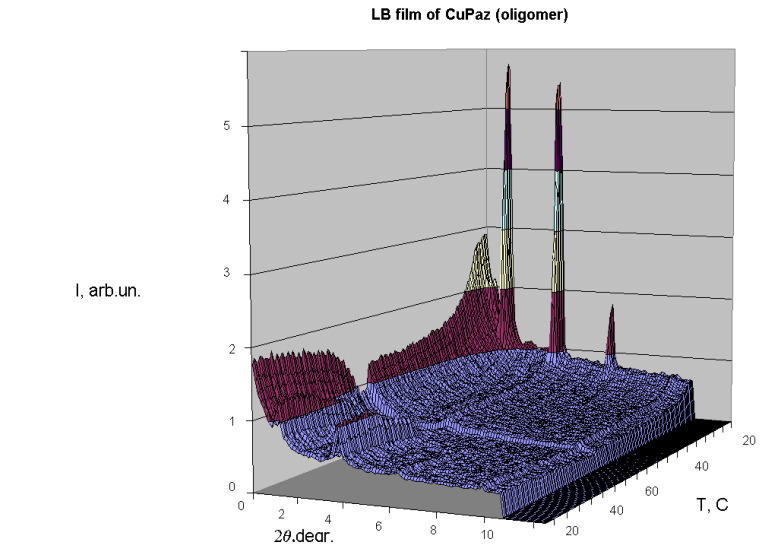

Figure 1. X-ray scattering patterns of LB film of oligomer non-substituted copper porphyrazine at different temperatures.

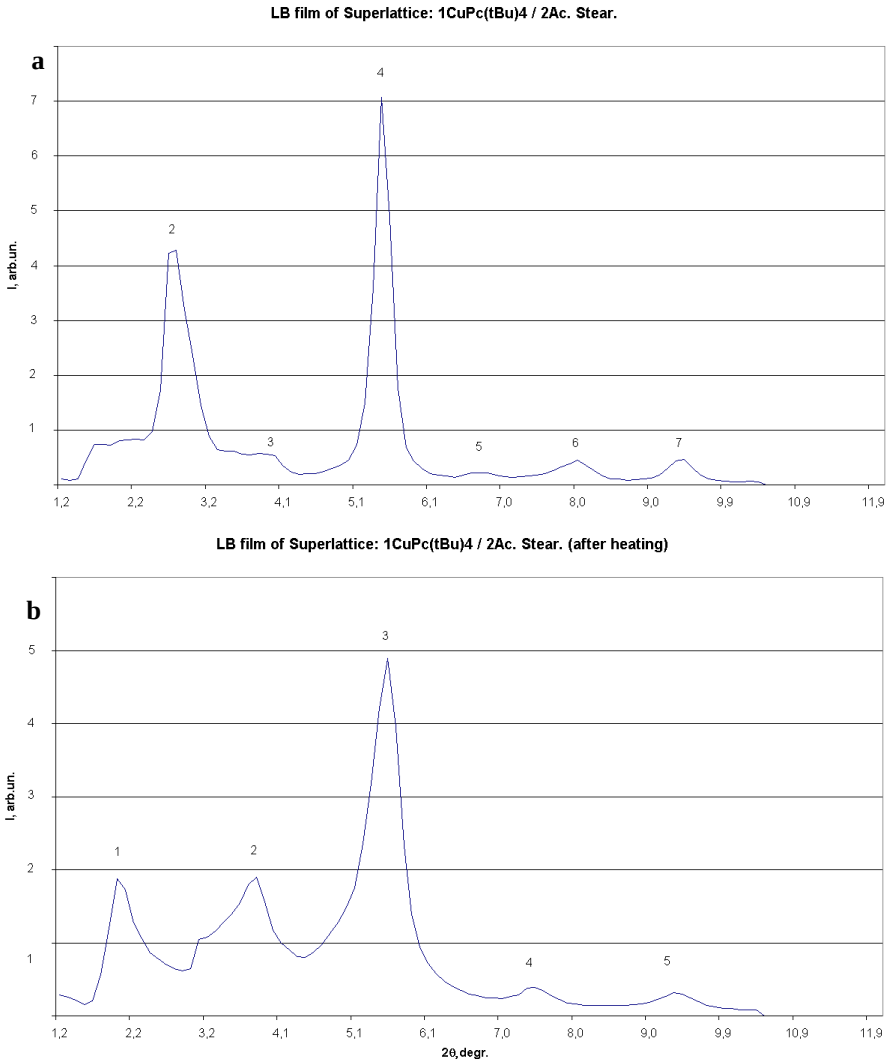

Figure 2. X-ray scattering patterns of LB film of 1A2B superlattice (A- PctBu4, B-Stearic Acid) at different temperatures (a- t=20^{o}C; b- t=80^{o}C).

LOW RESOLUTION CRYSTALLOGRAPHY ON HUMAN PLASMA LOW DENSITY LIPOPROTEIN (LDL)

R.Schwarzenbacher[1], H.Amenitsch[1], F.Nigon[2], M.J.Chapman[2], S.Bernstorff[3], P.Laggner[1] and R. Prassl[1]

1.) Institute of Biophysics and X-ray Structure Research, Austrian Academy of Science, Steyrergasse 17, 8010 Graz, Austria
2.) INSERM Unite 321, F-75651 Paris, France
3.) Sincrotrone Trieste, SS14, Km163.5, Basovizza, Italy

Human plasma low density lipoproteins (LDL, Mw = 2.6×10^6 Da) are the main carrier of cholesterol in the blood stream and hence of central biomedical interest for cardiovascular research and premature development of atherosclerotic disease [1-3]. The long term goal of the present project is the analysis of the 3-dimensional structure of apo-B100 (4536 amino acid residues and a molecular mass of about 550 kDa) in intact LDL, i.e. associated with various lipids, mainly phospholipids and cholesteryl esters. The knowledge of the detailed structure of apo-B100 would lead to an understanding of receptor-mediated pathways and structure-function relationship of the LDL-particle.

Crystals with dimensions of approx. 400x200x100 microns are obtained from highly homogenous LDL subspecies [4]. X-Ray diffraction data show a strongly anisotropic behavior and are limited to a resolution of a = 15Å, b =c = 28Å.

Patterns like the one shown in Fig.1 indicate a colloidal type of crystal form, with one dimensional long range ordering along the a-axis, showing reflections up to the 12^{th} order (15Å), with a prominent 5^{th} order at 35Å, corresponding to the length of a cholesterylester molecule.

The aim of the present experiment is to obtain the global arrangement of protein, lipid and cholesterol within the particle, which requires accurate measurements of all the low resolution reflections in the range of 400-20Å.

To achieve this we used a 0.2 x 0.2mm beam profile and a sample to detector distance of 750mm, equipped with an evacuated beam path and a beam stop mounted in vacuum close to the CCD-camera. The CCD-camera is equipped with a fast read out electronic (typical readout times of 150 ms) and has 1024x1024 pixels with an optical active area of ~ 80 x 80mm.

The crystal was measured under cryogenic conditions (100K) using a delta-phi of 10 degrees and exposure-times of 10 sec/frame (corresponding to rotation speed of 1deg/s). 40 frames of each angular slice were summed for the final images (Fig.2).

A structural model based on a combination of X-ray diffraction data, solution scattering data and cryo-electronmicroscopic images [5], which indicate an elliptical particle shape and a well-defined internal layer-structure with a periodicity of about 1/35 $Å^{-1}$ shall be constructed.

References:

[1] Brown,M.S. and Goldstein,J.L. (1986) A receptor-mediated pathway for cholesterol homeostasis. *Science* **232**, 34-47.

[2] Chapman,M.J., Laplaud,P.M., Luc,G., Forgez,P., Bruckert,E., Goulinet,S., and Lagrange,D. (1988) Further resolution of the low density lipoprotein spectrum in normal human plasma: physicochemical characteristics of discrete subspecies separated by density gradient ultracentrifugation. *J.Lipid Res.* **29**, 442-458.

[3] Schuster,B., Prassl,R., Nigon,F., Chapman,M.J., and Laggner,P. (1995) Core lipid structure is a major determinant of the oxidative resistance of low density lipoprotein. *Proc.Natl.Acad.Sci.USA* **92**, 2509-2513.

[4] Prassl,R., Chapman,J.M., Nigon,F., Sara,M., Eschenburg,S., Betzel,C., Saxena,A., and Laggner,P. (1996) Crystallization and preliminary X-ray analysis of a low density lipoprotein from human plasma. .*Biol.Chem.* **271**, 28731-28733.

[5] Orlova,E.V., Sherman,M.B., Chiu,W., Mowri,H., Smith,L.C., and Gotto,A.M. (1999) Three-dimensional structure of low density lipoproteins by electron cryomicroscopy. *PROC.NAT.ACAD.SCI.USA* **96**, 8420-8425.

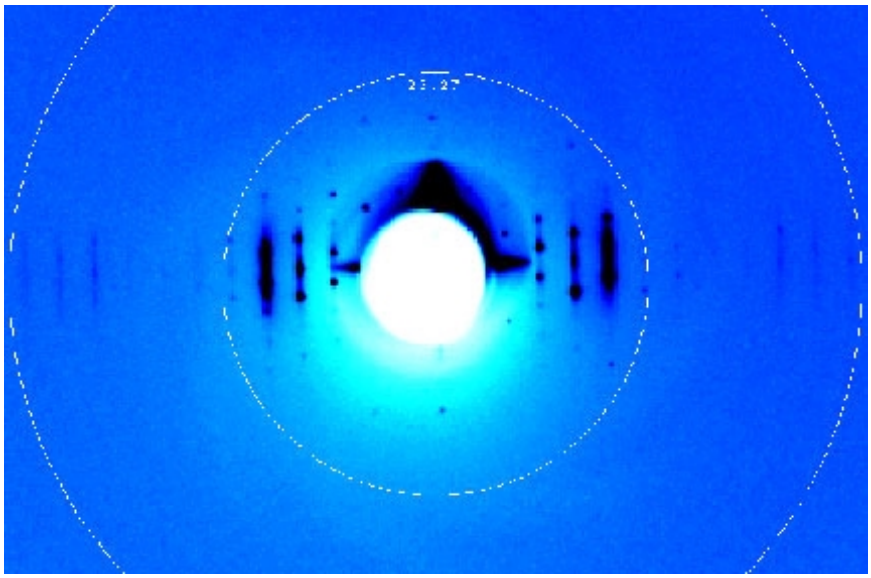

Figure 1: Diffraction pattern of a LDL crystal showing the dimensional long range ordering along the a-axis, and reflections up to the 12th order (15Å), with a prominent 5th order at 35 Å, corresponding to the length of a cholesterylester molecules.

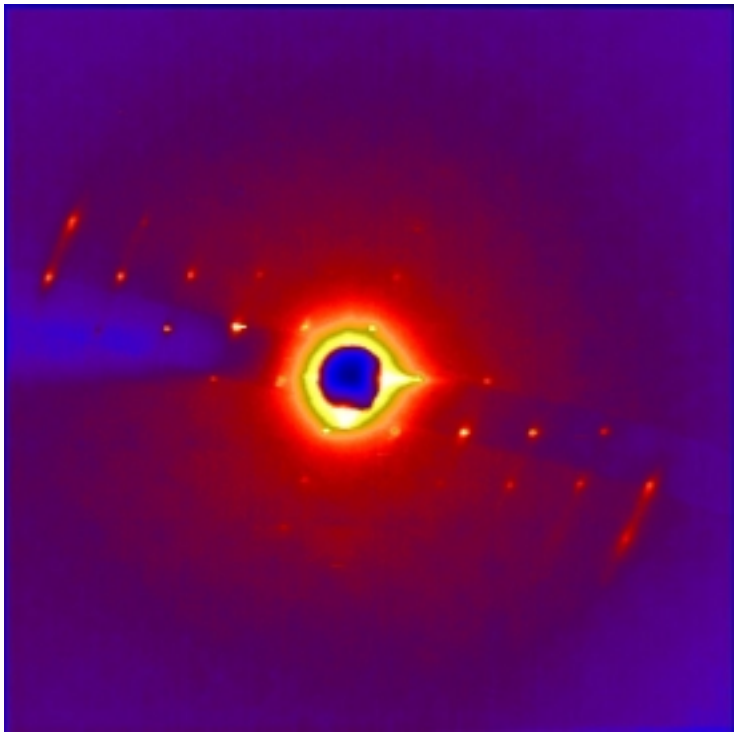

Figure 2. Example for a LDL single crystal diffraction image of a 180 deg phi-rotation with an angular slicing of 10 deg/frame. Each frame has been sampled 40 times. Rotation speed was 1 deg/s.

INTERACTION OF ANTIMICROBIAL PEPTIDES WITH MICROBIAL LIPID EXTRACTS: EVIDENCE FOR CUBIC PHASE FORMATION

E. Staudegger, H. Amenitsch and K. Lohner

Institute of Biophysics and X-ray Structure Research, Austrian Academy of Sciences, Steyrergasse 17, A-8010 Graz, Austria.

Cubic lipid structures are found in the plasma membrane of thermoacidophilic archaebacteriae as infoldings of the respective lipid membranes [1,2] and further in subcellular structures of eucaryotic cells like the endoplasmatic reticulum, nucleus, or mitochondria [3]. By now little is known about the possible functional relevance of these topological changes in the membrane structures, which seem to play an important role in dynamic processes.

Total lipid extracts of *Escherichia coli* are rich of non-lamellar forming lipids and form inverse bicontinuous cubic phases of the space group Pn3m at elevated temperatures. These cubic phases, exhibiting periodic minimal surfaces, consist of curved membranes that fill up space in a regular pattern, forming a complicated network of interconnected water tubes. This study aimed to gain information on the effect of membrane-active compounds like antimicrobial amphipathic peptides on the formation of the inverse bicontinuous cubic phases.

Mixtures of *E. coli* lipid extracts and membrane-active peptides (lipid-to-peptide molar ratio of 25:1) were measured at 25°C using rotating capillaries. The Synchrotron small-angle X-ray scattering experiments clearly showed the formation of cubic phases, predominantly of space group Pn3m. In the presence of gramicidin S, a cyclic decapeptide from *Bacillus braevis* (Figure 1), the lattice spacing was reduced from 14.9 to 13.4 nm (Figure 2) as compared to the pure lipid, whereas the other membrane-active peptides studied, i.e. GS14 (the 14-mer analogous peptide of gramicidin S), the frog skin peptide, PGLa, and PG-1 from porcine leukocytes, lead to a significant increase of the cubic lattice (16.7 nm, GS14; 17.4 nm, PGLa; 17.2 nm, PG-1). Further, the hkl-reflections corresponding to a cubic phase of space group Pn3m were much less resolved for mixtures containing PGLa (α-helical structure) or PG-1 (β-sheet conformation). This observation may indicate a lower preference of the non-cyclic peptides for promotion of cubic lipid phases. This work will be the basis for future experiments, where the influence of temperature, ionic strength and in particular lipid composition on the formation/promotion of inverse biconinuous cubic lipid phases will be studied in more detail.

References:

[1] Landh, T. (1995): *FEBS Lett.* **369**, 13–17.
[2] Luzatti, V. (1997): *Curr. Opinion Struct. Biol.* **7**, 661–668.
[3] Deng, Y., Marko, M., Buttle, K. F., Leith, A.-D., Mieczkowski, M. & Mannella, C. A. (1999): *J. Struct. Biol.* **127**, 231–239.

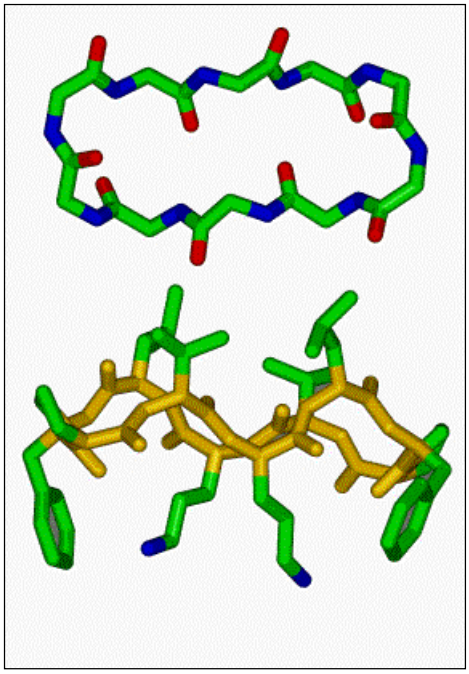

Figure 1. Structure and conformation of gramicidin S.

Upper panel: view perpendicular to the plane of the ring, illustrating the peptide backbone structure. The antiparallel β-sheet region is stabilized by hydrogen bonds.

Lower panel: side-view, indicating the disposition in space of the hydrophobic Val and Leu residues (top) and the basic Orn (bottom) relative to the peptide ring.

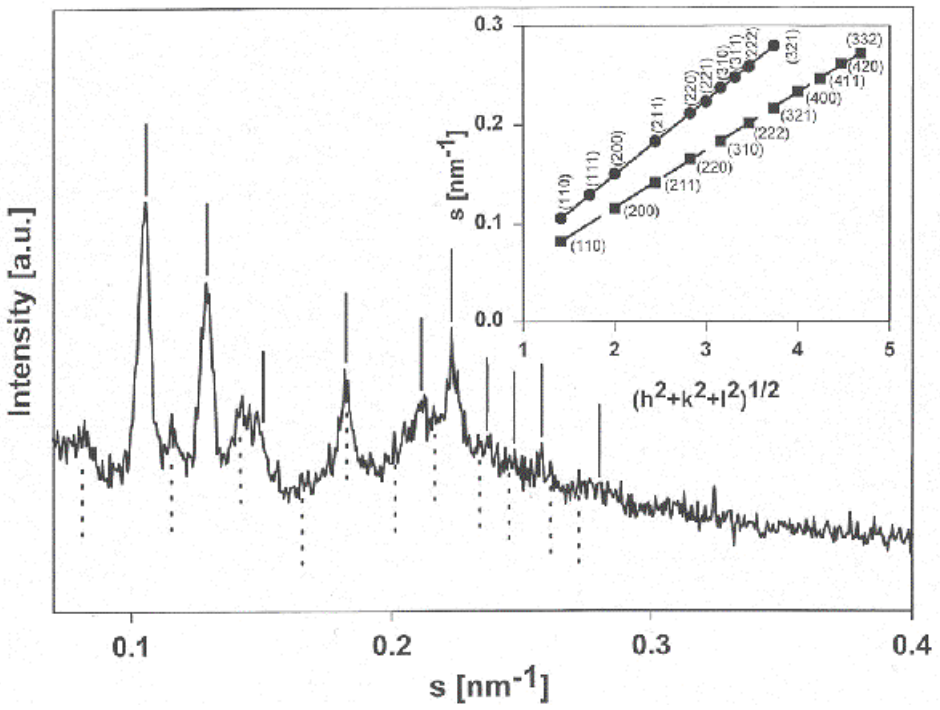

Figure 2. Small-angle X-ray diffractogram of a mixture of *E. coli* membrane total lipid extract and gramicidin S (lipid-to-peptide molar ratio of 25:1) recorded at 25°C. Position of the hkl-reflections corresponding to a cubic phase of space group Pn3m (solid line) and Im3m (dotted line) are indicated. Insert: Indexing of the two cubic lattices from the plot s vs. $(h^2 + k^2 + l^2)^{1/2}$.

INTERFACES AND MINERALIZATION DEFECTS IN CONNECTIVE TISSUE

I. Zizak [1], O. Paris [1], P. Roschger [2], W. Tesch [1,2], B. Grabner [2], S. Bernstorff [3], H. Amenitsch [4] and P. Fratzl [1]

1.) Erich Schmid Institute of Materials Science, Austrian Academy of Sciences, and Metals Physics Institute, University of Leoben, Jahnstraße 12, A-8700 Leoben, Austria.
2.) Ludwig Boltzmann Institute of Osteology, 4th Medical Department, Hanusch Hospital, Heinrich Collinstr. 30, A-1140 Vienna, Austria.
3.) Sincrotrone Trieste, Area Science Park, I-34012 Trieste, Italy.
4.) Institute of Biophysics and X-Ray Structure Research, Austrian Academy of Sciences, Steyrerg. 17, A-8010 Graz, Austria.

Many biological materials (e.g. wood and bone) but also some artificial materials are hierarchically structured. Human bone for example exhibits a foam-like structure (trabecular bone), which is surrounded by a compact outer layer (cortical bone). The trabeculae (typical thickness: 200 μm) consist of lamellae, every lamella being a fiber reinforced composite. This composite is built of collagen fibrils (typical diameter: 200 nm) reinforced with particles (calcium-phosphate crystallites) with a thickness of only a few nanometer. It is well documented for bone [1], that all these hierarchical levels contribute to the macroscopic (in particular mechanical) properties. It is, therefore, necessary to characterize these materials on different length scales.

Small-Angle X-ray Scattering (SAXS) is a commonly used tool for studying the size, shape and orientation of particles in the nanometer-range. Performing SAXS measurements using a microbeam, and scanning the sample through the beam, it is possible to map changes in size, shape and orientation of the nanometer-sized particles on a micrometer scale. In recent experiments at ELLETRA we have developed an experimental set-up for scanning-SAXS with a spatial resolution of 20 micrometer and used it for the investigation of human bone samples [2,3,4].

As a continuation of these experiments on bone, we studied different samples of medical interest. Human bone sections containing a bone-cartilage interface were investigated to determine the position- and age-dependence of the mineral particles in bone and adjacent mineralized cartilage. This interface had a similar structure for human femur head, knee patella, and vertebra sections. For all three types of tissue there was a change of the preferred orientation of the mineral particles at the bone-cartilage interface as already reported in [3] for a special case. While the orientation of the particles follows the orientation of the trabeculae in bone, in cartilage they are oriented perpendicular to the local bone-cartilage interface. The differences in size and shape between the two tissues are rather small. Studying bone-cartilage interfaces from patients of different age, we could confirm the increase of particle size in bone with age [5]. In cartilage, the particle size and their degree of orientation show a very similar age dependence as bone.

Additionally, we studied the microstructure of the bone tissue in osteons. Osteons are regions of compact bone around blood vessels and are particularly interesting due to the high degree of bone remodeling in this regions. By scanning areas of about 0.3 x 0.3 mm^2, we could map the structural parameters of the mineral crystals in cancellous (lammellar) bone. Figure 1 shows an example of the orientation mapping in the neighborhood of an osteon. In all of the four investigated osteons from healthy patients, the orientation of the mineral particles followed the direction of the lamellae winding around the hole. Further data evaluation is still in progress. The complete evaluation includes the determination of the thickness of the

mineral particles from the scanning SAXS experiments, and the density distribution of the mineral from backscattered electron images collected from the same specimens. Furthermore, these parameters will be compared with data achieved from other experimental techniques, like e.g., the Calcium-Phosphorus ratio determination by EDX.

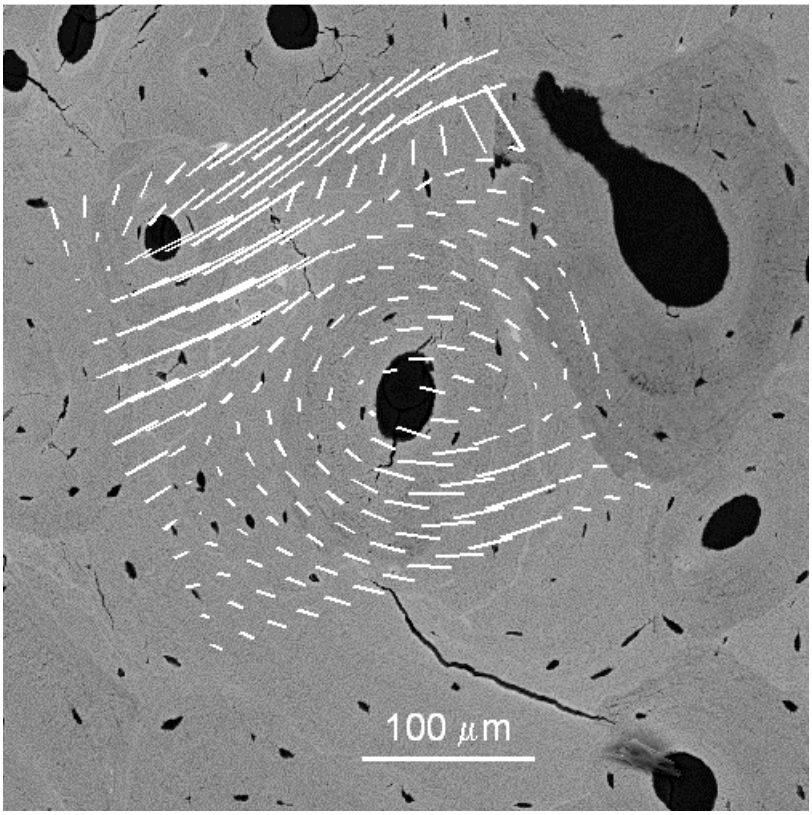

Figure 1. Mapping of the orientation of the mineral particles in an osteon. The back-scattered electron image in the background shows the mineral density (proportional to the brightness of the grayscale). Black stains are holes (blood vessels) surrounded by osteons. The overlaying array of white stripes describes the orientation and the degree of orientation of the mineral particles at the actual positions. The longest line stays for the largest degree of orientation (40% of mineral particles are oriented). It is easily seen that the mineral particles are arranged in a onion-skin structure around the hole.

References:

[1] S. Weiner and H.D. Wagner; *Ann. Rev. Mater. Sci.* **28** (1998) 271.

[2] I. Zizak, O. Paris, P. Roschger, S. Bernstorff, H. Amenitsch, K. Klaushofer, P. Fratzl, *ELETTRA NEWS* (1999) **31: (**http://www.elettra.trieste.it/science/news/volume36/EN60.html).

[3] I. Zizak, O. Paris, P. Roschger, S. Bernstorff, H. Amenitsch, K. Klaushofer, P. Fratzl; *J. Appl. Cryst.* (2000) in press.

[4] I. Zizak et al., *Annual Report 1998,* Austrian SAXS beamline at ELETTRA

[5] P. Fratzl, et al., *Calcif. Tissue Int.* **48** (1991) 407.

3. Physics

STUDY OF THE COUNTERION DISTRIBUTION AROUND GEMINI MICELLES IN AQUEOUS SOLUTIONS

V.K. Aswal[1], P.S. Goyal[2], S. De[3], S. Bhattacharya[3], H. Amenitsch[4] and S. Bernstorff [5]

1.) Condensed Matter Physics Division, Bhabha Atomic Research Centre, Mumbai 400 085
2.) IUC-DAEF, Mumbai Centre, Bhabha Atomic Research Centre, Mumbai 400 085
3.) Department of Organic Chemistry, Indian Institute of Science, Bangalore 560 012
4.) Institute of Biophysics and X-ray Structure Research, Austrian Academy of Sciences, Graz, Austria
5.) Synchrotrone ELETTRA, Trieste, Italy

Surfactant molecule (e.g. cetyltrimethylammonium bromide (CTAB)) consists of a hydrophilic head group and a hydrophobic tail. These molecules above critical micelle concentration (CMC) in aqueous solutions aggregate and are called micelles. The micelles formed are of various types such as spherical, ellipsoidal or cylindrical. The hydrophobic tails of the surfactant molecules constitute the central core of the micelle and thereby avoid contact with water. The hydrophilic head groups reside on the outer surface of the micelle [1].

Surfactant molecule such as CTAB ionizes in aqueous solution and the micelle largely consists of CTA^+ ions. The micelle is charged and is called ionic micelle. The Br^- ions, referred to as counterions, tend to stay near the surface of the micelle. The shape and size of the micelle and the inter-micelle interaction depend on the distribution of these counterions. The shapes and sizes of the micelles are studied using SANS [2,3]. In general, neutrons see the core of the micelle. The neutron scattering intensity from the counterion distribution is negligible in comparison to that from the core. On the other hand, X-rays will be largely scattered by counterions, especially if the counterion has large atomic number [4]. Thus a combined study of SANS and SAXS can be used for determining the counterion distribution around the micelles [5,6]. We have carried out SAXS experiments to the study of the counterion distribution in aqueous solutions of recently developed gemini surfactants.

Gemini or dimeric surfactants consist of two hydrophobic tails and two hydrophilic head groups covalently connected by a hydrocarbon spacer [7-9]. We have earlier reported micellar structures of bis-cationic $C_{16}H_{33}N(CH_3)_2$-$(CH_2)_m$-$N(CH_3)_2C_{16}H_{33}$, $2Br^-$ gemini surfactants, referred to as 16-m-16, $2Br^-$, using SANS for different lengths of hydrocarbon spacer [10]. The shape and size of the micelles depend on the spacer length. For example, micelles are disc-like for m = 3, rod-like for m = 4 and ellipsoidal for m = 12. We have now carried out SAXS measurements at the synchrotron source ELETTRA, for the study of counterion distribution around gemini micelles. The measurements were performed for the above gemini surfactants with different spacer lengths at different temperatures and concentrations. It may be mentioned that scattering from counterions is usually very week and such experiments with the conventional X-ray sources are not possible.

Fig. 1

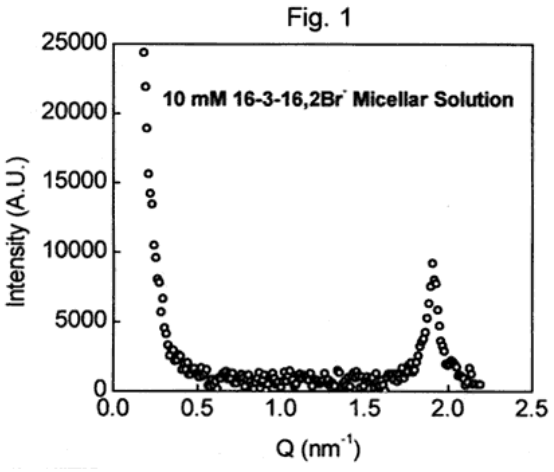

The SAXS distribution from 10 mM 16-3-16, $2Br^-$ is shown in **Fig. 1**. The distribution shows a Bragg peak at Q ~ 0.19 nm^{-1}. The peak is an indication of the presence of the lamellar structure in this micellar solution.

Fig. 2

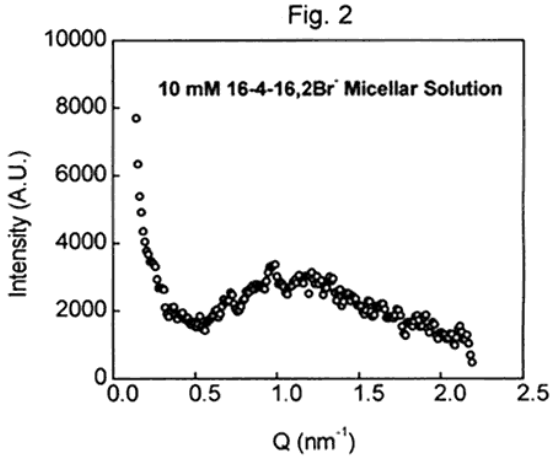

Fig. 3(a)

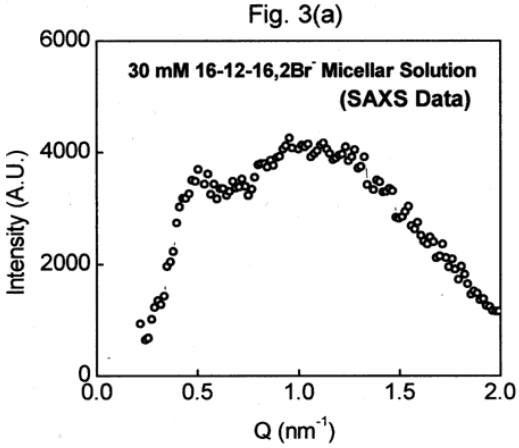

Fig. 3(b)

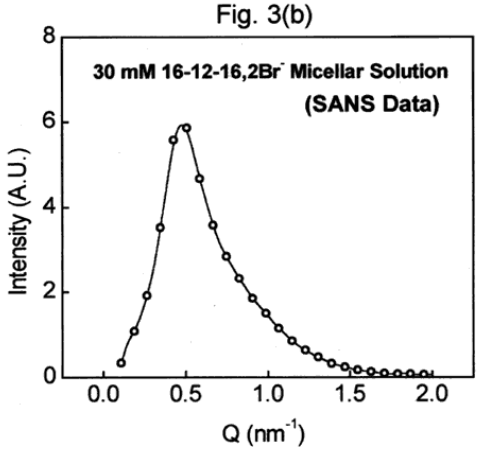

Fig. 2 shows the SAXS distribution for spacer length m = 4. The system consists of rod-like micelles [10]. The broad peak in Fig.2 at Q ~ 0.11 nm^{-1} is due to the scattering from counterion distribution. These results are similar to the earlier observation of counterion distribution of Cs^+ ions around the cylindrical micelles [5].

The SAXS distribution from 30 mM 16-12-16, $2Br^-$ micellar solution is shown in **Fig. 3(a)**. The SANS distribution for the same micellar solution is shown in **Fig. 3(b)**. It is seen that there are significant differences in the two distributions. This is because of the fact that while neutrons see the core of the micelle, X-rays are mainly scattered from the outer shell of the counterions. In particular, the peak at Q ~ 0.11 nm^{-1} in SAXS distribution arises from the intraparticle structure factor P(Q) of the shell-like structure of the counterions. The peak at Q ~ 0.5 nm^{-1}, which appears both in SAXS and SANS distributions, arises because of interparticle structure factor S(Q). A detailed analysis to determine the counterion distribution around the micelles is in progress.

References:

[1] Chevalier, Y. & Zemb, T. (1990): *Rep. Prog. Phys.* **53**, 279.
[2] Chen, S.H. (1986): *Annu. Rev. Phys. Chem.* **37**, 351.
[3] Goyal, P.S. (1994): *Phase Transitions* **50**, 143.
[4] Zemb, T. & Chaprin, P. (1985): *J. Physique* **46**, 249.
[5] Wu, C.F., Chen, S.H., Shih, L.B. & Lin, J.S.(1988): *Phys. Rev. Lett.* **61**, 645.
[6] Sumaru, K., Matsuoka, H., Yamaoka, H. & Wignall, G.D. (1996): *Phys. Rev.* **E 53**, 1744.
[7] Menger, F.M. & Littau, C. (1991): *J. Am. Chem. Soc.* **113**, 1451.
[8] Zana, R., Benrraou, M. & Rueff, R. (1991): *Langmuir* **7**, 1072.
[9] De, S.,Aswal, V.K., Goyal, P.S. & Bhattacharya, S. (1996): *J. Phys.Chem.* **100**, 11664.
[10] Aswal, V.K., De, S., Goyal, P.S., Bhattacharya, S. & Heenan, R.K. (1998): *Phys. Rev.* **E 57**, 776.

SAXS STUDY OF NB/SI AND GE/C MULTILAYER STRUCTURES

S.M. Chaudhari[1], D.M. Phase[1], A. Gupta[1], B.A. Dasannacharya[1], S. Bernstorff[2], P. Dubcek[2] and H. Amenitsch[3]

1.) Inter University Consortium for DAE facilities, University Campus, Khandwa Road, Indore-452 017INDIA
2.) Sincrotrone Trieste, in Area Science Park, 34012 Basovizza / Trieste, ITALY
3.) Institute of Biophysics and X-ray Structure Research, Austrian Academy of Sciences, Steyergasse 17, 8010 Graz, Austria

Small angle X-ray scattering measurements of Nb/Si and Ge/C multilayer structures were carried out using SAXS beamline at Elettra [1,2]. Nb/Si structures having 15 bilayers and periodicity of 70 Å were deposited using e-beam evaporation techniques under UHV conditions in our laboratory. [Nb (35Å)/Si (35Å)], [Nb (40Å)/Si(30Å)] and [Nb (30Å)/Si (40Å)] multilayer structures were prepared on Si(100) substrates. Similar periodicity and layer thickness were also deposited in case of Ge/C multilayers. These multilayers were characterised using laboratory grazing incidence x-ray reflectivity set-up.

The SAXS beamline is normally used in transmission geometry but could also be employed for our experiments in reflection geometry. For that the sample is mounted on a cradle with z-translation table, so that the samples could be aligned by the usual procedure and desired angle of incidence could be selected. One dimensional PSD was used to record the spectra. For all measurements presented here 8 keV monochromatised X-ray beam was used.

SAXS spectra corresponding to Nb-Si multilayers having interlayer thicknesses of [Nb(40Å):Si(30Å)], [Nb(35Å):Si(35Å)] and [Nb(30Å):Si(40Å)] recorded at grazing incidence angle of 0.8^o are shown in Fig.1(a), (b) and (c) respectively. The specularly reflected peak at $2\theta=1.6^o$ in between the 1^{st} and 2^{nd} order Bragg sheets is the highest intense peak observed in all the three samples. The intensity of this peak goes on decreasing from spectrum (a) to spectrum (c). Peaks corresponding to $1^{st,}$ 2^{nd}, 3^{rd} and 4^{th} bragg sheets are clearly observed in sample (a) and (b) and marked by vertical lines. It is clear from the spectra that Bragg sheets are well defined in spectrum (a) and (b) however in spectrum (c) they are not well resolved. This indicates the poor quality of [Nb(30Å):Si(40Å)] multilayer structure. From the observed Bragg sheets one can calculate the period of the multilayer structure. By plotting the graph of $\sin^2\vartheta$ Vs n^2 and the slope one can determine the period of the multilayer structure. It turned out to be 86Å, 82 Å and 76Å in sample (a), (b) and (c) respectively. Besides periodicity, the height-height self-correlation of one rough interface, and the correlation's between different interfaces are also of interest in a multilayer structure. These are called as height-height cross correlation's. If a static interface fluctuation (roughness) of lateral wavelength 'r' is copied throughout the multilayer stack or at least over a certain number N of interfaces, then the non-specular scattering at parallel momentum $q_{\uparrow\uparrow} = \pi/r$ will be modulated along $q_z = 2\pi/d$ (the Bragg sheets) (Fig.1c). In this case Bragg peak width is determined by the number of correlated interfaces [3]. By measuring the half width of second Bragg peak one can calculate q value and from $q_z = 2\pi/D$, one gets the total thickness of the multilayer structure. In case of [Nb(40Å):Si(30Å)] multilayer structure, the second Bragg peak width is 0.083^o and corresponding total thickness of multilayer structure comes out to be 1100Å , indicating all the interfaces are correlated including the interface at the substrate; since the total deposited thickness of this multilayer is 1070 Å. Similarly for [Nb(35Å):Si(35Å)] and [Nb(30Å):Si(40Å)] multilayer structures, the calculated thickness from 2^{nd} bragg peak widths are 700 Å and 250 Å respectively. Even considering the deposited thickness of 1070 Å in each structure one can conclude that correlated interfaces in sample (b) and and (c) are 20 Å and 8 Å respectively.

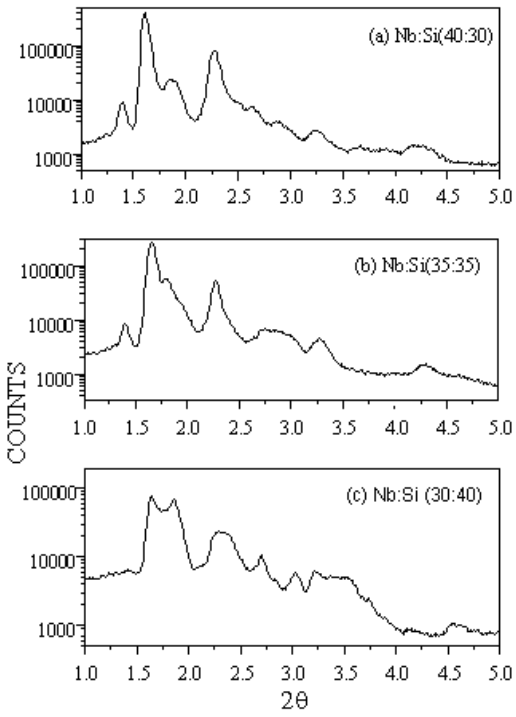

Figure 1. SAXS spectra of Nb-Si multilayers at same grazing angle (0.8°)

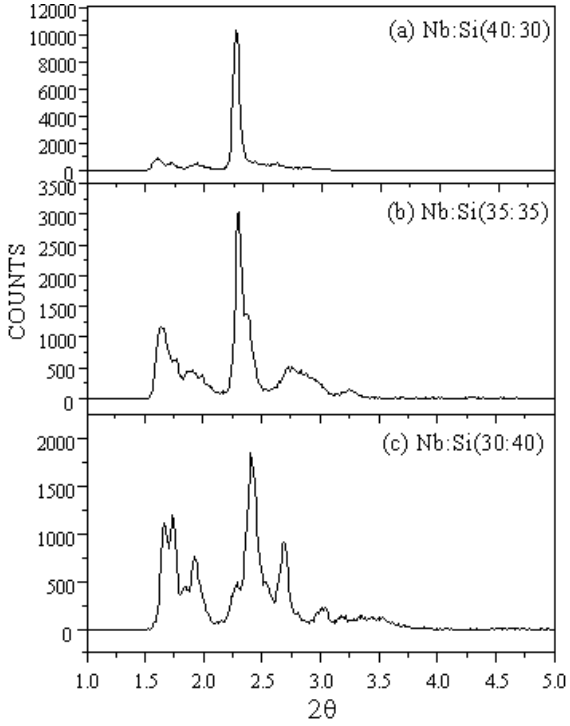

Figure 2. SAXS spectra of Nb-Si multilayers at grazing angle kept at 2nd Bragg peak

The SAXS spectra for all the three samples recorded at incidence angle equal to 2nd Bragg peak position (Fig.2 (a),(b) and(c) for samples [Nb(40):Si(30)], [Nb(35):Si(35)] and [(Nb(30):Si(40)] respectively. For [Nb(40):Si(30)] multilayer structure mainly intense 2nd order bragg peak is observed. However the SAXS spectrum corresponding to [Nb(35):Si(35)] shows broad peaks having appreciable amount of intensity at other 2θ value. In this case also 2nd Bragg peak with reduced intensity is observed. The SAXS spectrum corresponding to [Nb(30Å):Si(40Å)] sample (Fig.2(c)) shows many sharp peaks around 2nd Bragg peak. In this case intensity of 2nd Bragg peak is substantially reduced. This again confirms our conclusion that [Nb(40Å):Si(30Å)] multilayer structure is superior than [Nb(35Å)Si(35Å)] and [Nb(30Å):Si(40Å)] multilayer structure. Only difference in three multilayer samples is that individual thickness variation from 30 Å to 40Å of Nb and Si. One can attribute this difference in observed SAXS spectra to the different growth and morphology of Nb and Si layer with thickness variation.

Similar exercise was carried out on the Ge:C multilayer structures. In-situ annealing study of [Nb(35Å)Si(35Å)] and [Ge(35Å):C(35Å)] multilayer structure were carried out at 100°C. Each measurement in this case contains variation of incidence angle from $\theta_I = 0.85^o$ to 1.35^o in order to record the variation of 2nd order Bragg peak intensity with annealing time. From this one can get the information about the dynamical changes across the interface in the multilayer structure. Analysis of data is in progress.

Acknowledgements:

The work carried out in this project is under the INDO-ITALIAN collaborative programme of Department of Science & Technology (DST), India. SMC & DMP are thankful to DST, India for Travel support and Italian Government for local hospitality.

References:

[1] Amenitsch, H., Bernstorff, S. & Laggner, P.(1995): *Rev. Sci. Instru.* **66(2)**, 1624.
[2] Amenitsch, H. et al. (1997): *J. Appl. Cryst.* **30**, 872.
[3] Phang, Y.H. et al. (1993): *J. Appl. Phys.* **74**, 3181 and references therein.

GRAZING INCIDENCE SMALL ANGLE X-RAY SCATTERING STUDY OF DISORDERED TUNGSTEN-CARBON ALLOYS PRODUCED BY REACTIVE MAGNETRON SPUTTERING

P. Dubcek[1,2], N. Radic[2], B. Pivac[2], O. Milat[3] and S. Bernstorff [1]

1.) Sincrotrone Trieste, SS 14 km 163,5, 34012 Basovizza (TS), Italy
2.) Ruder Boskovic Institute, Bijenicka 54, 10000 Zagreb, Croatia
3.) Institute for Physics, Bijenicka 46, 10000 Zagreb, Croatia

Wolfram carbide as a material has a variety of applications, mainly because of its mechanical properties. Here we report investigation of W-C films that have been prepared by reactive magnetron sputtering using benzene C_6H_6 as a carbon percusor. The film structure is strongly disordered, presumably due to the incorporation of the unbound carbon.

Tungsten-carbon thin films were deposited onto monocrystalline silicon substrates by reactive sputtering in a two-source device. The magnetron discharges operated in argon + benzene gas mixture at 2 Pa total pressure. The current density was 6 mA/cm^2 in both magnetrons, while discharge voltage increased with the C_6H_6 partial pressure and varied in the 330-450 V range. Deposition rate was 0.2-0.3 nm/s and the final film thickness was about 1 μm. The benzene partial pressure was 1.25%, 2.5% or 5% of total pressure, respectively. The substrate temperature was varied in steps of 200^{o}C, while substrate potential was floating or biased -70 V with respect to discharge plasma.

The films deposited at room temperature exhibit structure resembling a strongly disordered W_2C or WC_{1-x} carbides, while WC_{1-x} microcrystalline structure with very small grains formed on substrates held at 400^{O}C during deposition. In the case of 2.5% and 5% C_6H_6 partial pressure, the films with strongly disordered WC_{1-x} structure are generally formed.

The grazing incidence SAXS spectra of the films are shown in figure 1. The samples with lower unbound carbon content (low benzene partial pressure and low substrate temperature) can be successfully interpreted according to distorted wave Born approximation (DWBA). An example of the DWBA fit is shown in Figure 2. The main characteristics of these films in the light of DWBA, are poor substrate to film surface correlation, as well as short lateral correlation length (along the surface of the film: in the order of few 100 Å).

In the case of higher carbon content, grains of amorphous WC are formed, while the carbon is probably concentrated in the grain boundaries region. This results in an additional strong contribution to the scattering, revealing the sizes of the grains (on the surface of the film) to be in the order of 7-16 nm.

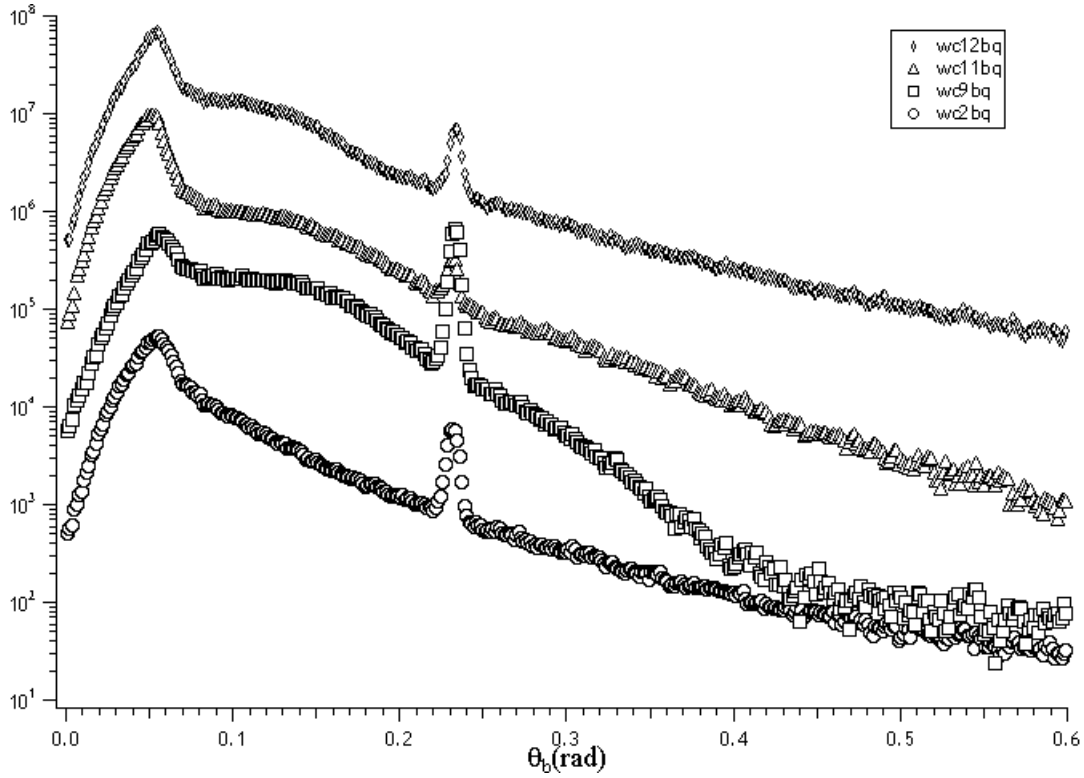

Figure 1. The GISAXS from WC amorphous films vs. angle to the sample surface.

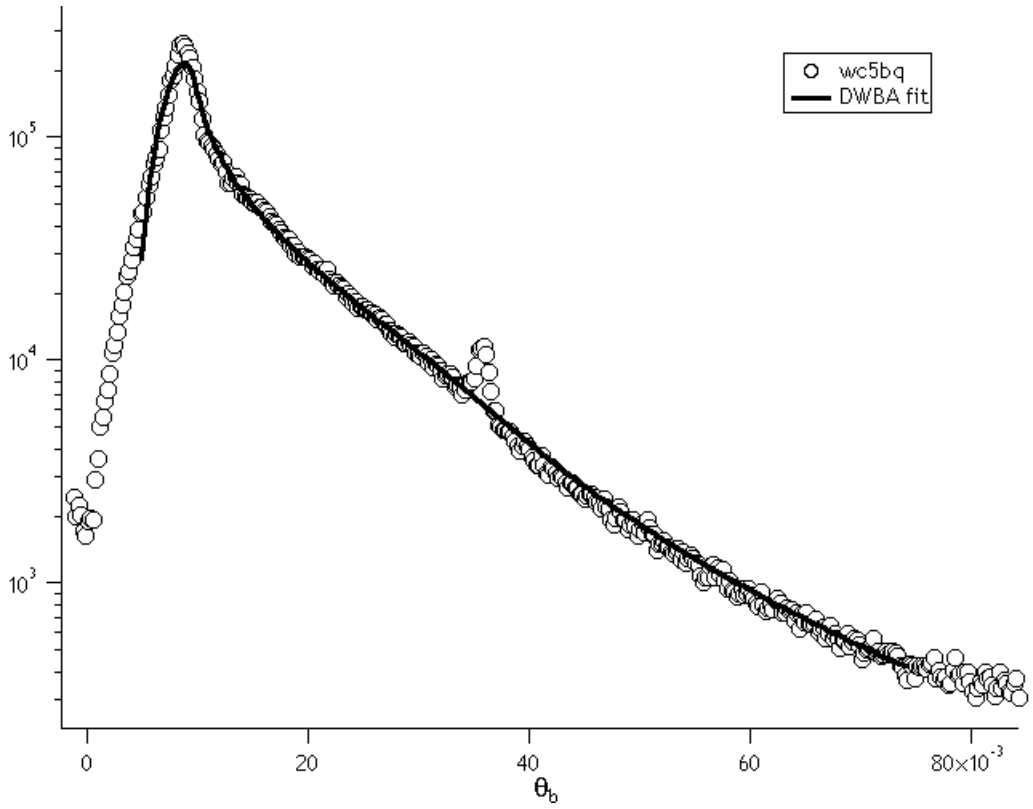

Figure 2. DWBA fit to GISAXS from amorphous WC film with lower unbound carbon content.

GRAZING INCIDENCE SMALL ANGLE X-RAY SCATTERING STUDY OF IRRADIATION INDUCED DEFECTS IN MONOCRYSTALLINE SILICON

P. Dubcek [1,2], B. Pivac [2], O. Milat [3], S. Bernstorff [1], R.Tonini [4], F. Corni [4] and G. Ottaviani [4]

1.) Sincrotrone Trieste, SS 14 km 163,5, 34012 Bassovizza (TS), Italy
2.) Ruder Boskovic Institute, Bijenicka 54, 10000 Zagreb, Croatia
3.) Institute for Physics, Bijenicka 46, 10000 Zagreb, Croatia
4.) University of Modena, Physics Department, Via Campi 213a, 41100 Modena, Italy

Monocrystalline silicon samples have been He ion implanted at room temperature and at high doses (of the order of $2*10^{16}$ cm^{-2}) and in this way a high concentration of defects is introduced. At higher doses and/or temperatures also voids (bubbles) filled with He are produced. To investigate the dynamics of the bubble formation, the samples have been annealed isochronaly at discrete temperatures up to $900^{O}C$. The annealing at temperatures above $700^{O}C$ should cause He to effuse and the remaining voids to coalesce, producing empty bubbles with dimensions in the range 5-100 nm. The walls of these voids, supposedly perfectly clean, are of great scientific interest, either for fundamental or for applied research, e.g. impurities gettering (in situ substrate cleaning) in the process of integrated circuit production.

Structural defects were investigated using small angle X-ray scattering. Because the induced defects were expected to be present in a thin layer close to surface, grazing angle incidence was chosen due to its surface sensitivity.

Due to the defects introduced by irradiation, in as implanted sample, the in plane correlation range is reduced compared to that of the monocrystaline silicon and the interference contribution (high correlation between the sample surface and implantation range) is present indicating an uniform distribution of penetration depths.

The changes in the film composition can be followed by the change of annealing temperature (see figure 1.). At $350^{O}C$ the correlation contribution in the scattering is strongest (high oscilations in the scattering intensity). This is expected to be due to onset of defects aglomeration producing high electron density difference, since the voids are beginning to be formed. Also, this process begins probably at the highest defects density whose position is highly correlated to the sample surface.

At 600 ^{O}C, real bubbles should be formed, and after this temperature the density of the film starts to increase again because of the defects difusion towards film surface, as well as the formed voids. The shape of the bubbles should be the reason for increase of lateral (in plane) correlation length.

Somewhere at 800 ^{O}C the structural changes in the implanted film should be almost over, and the scattering is similar to the as implanted one, up to the interference contribution which is now reflecting a different effective film thickness.

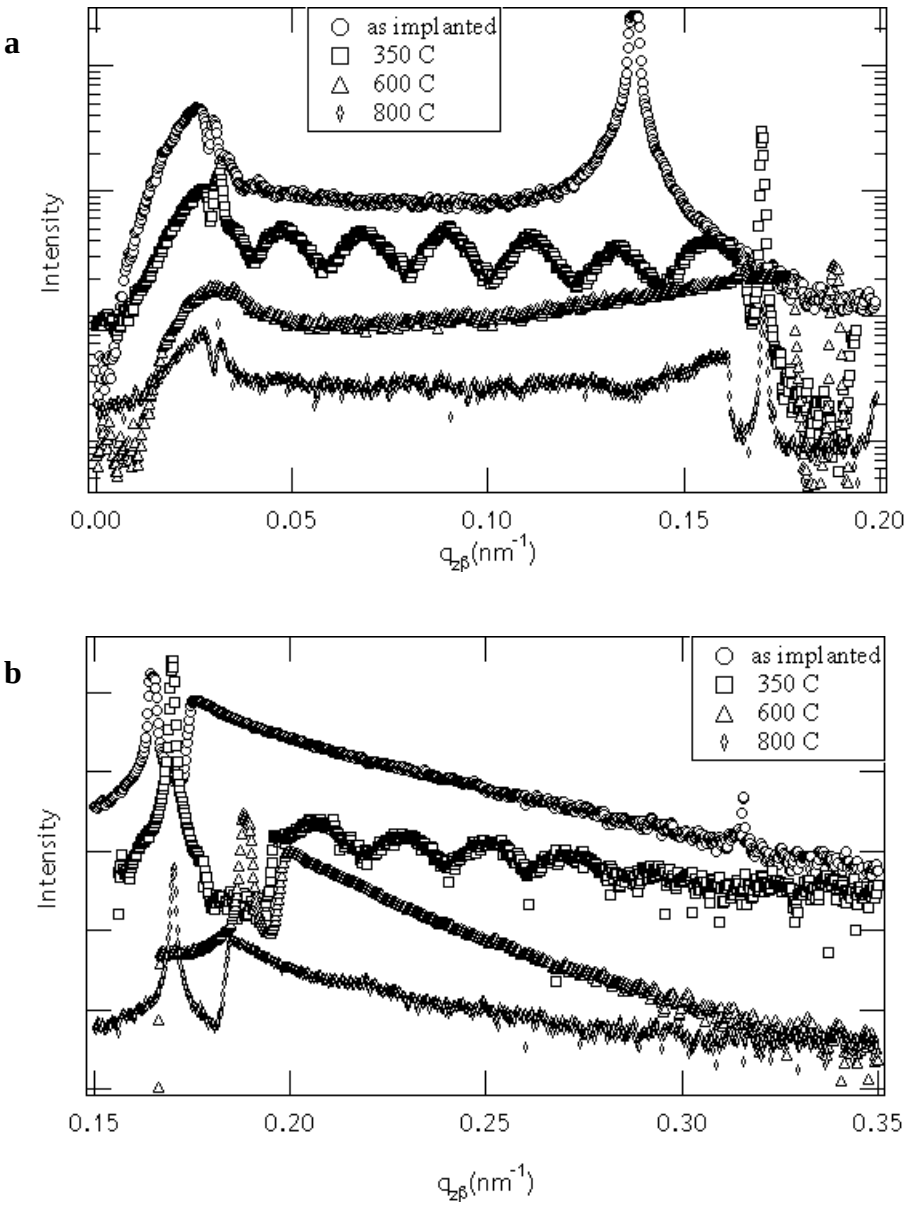

Figure 1. The GISAXS from He implanted silicon vs. angle to the sample surface, a) below and b) above the specular angle.

GRAZING INCIDENCE SMALL ANGLE X-RAY SCATTERING STUDY OF THE RAPID THERMAL CHEMICAL VAPOUR DEPOSITED SILICON

P. Dubcek [1,2], B. Pivac [2], O. Milat [3] and S. Bernstorff [1]

1.) Sincrotrone Trieste, SS 14 km 163,5, 34012 Bassovizza (TS), Italy.
2.) Ruder Boskovic Institute, Bijenicka 54, 10000 Zagreb, Croatia.
3.) Institute for Physics, Bijenicka 46, 10000 Zagreb, Croatia.

Polycrystalline silicon is widely used in modern microelectronic devices e.g. as a dielectric in interconnections, in gates of field-effect transistors, resistors and other passive applications, as well as an active semiconducting material in a variety of photovoltaic devices. The morphology and surface topography of such layers strongly influence device performances, especially in thin layered structures with fine device geometry. Structural properties, influenced by deposition and processing parameters, can have a significant effect on the electrical properties of the layer for a given doping level.

Polycrystalline silicon films are typically produced by chemical vapour deposition technique. The rapid thermal chemical vapour deposition (RTCVD), a new developed technique used for the deposition of such samples, is a variant of chemical vapour deposition in a lamp-heated rapid thermal processing reactor. This technique is very interesting in microelectronics as it offers the possibility of single wafer processing, including in-situ sequential treatments such as cleaning, dielectric growth, and deposition of multiple layers. Moreover, this technique is attracting more and more interest in material production for solar cells application.

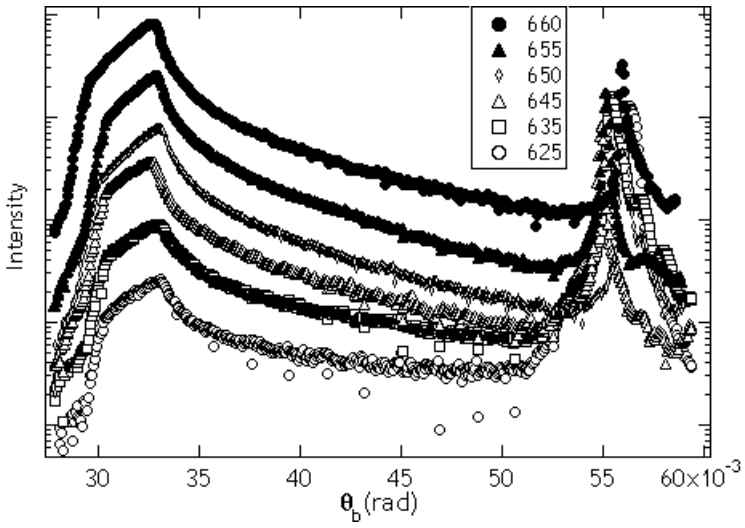

Figure 1. The GISAXS from RTCVD polisilicon vs. angle to the sample surface with the substrate temperature as the parameter. The curves are vertically offset for clarity.

The RTCVD polycrystalline silicon samples, grown from silane in hydrogen as a carrier gas, on monocrystalline silicon substrate, were investigated using grazing incidence small angle X-ray scattering (GISAXS). The scattering data are shown in figure 1 for the substrate temperature range from 625 to 660 ^{O}C. Due to the technique of the preparation, the polisilicon surface was poorly correlated to the monocrystalline substrate, and lateral coherence range was in the order of few tens of nm, as deduced from the distorted wave Born approximation (DWBA) treatment of the data, although the polycrystalline surface is not expected to fulfil

the normal surface height distribution implied in this approximation. These properties of the surface did not vary a lot in the temperature range investigated.

There is an increase of surface roughness parameter with temperature (deduced again from DWBA, see figure 2), which is correlated more to the grains surface roughness, than to the grain sizes. The grain boundaries are expected to be contaminated with hydrogen, present in the process of growth.

On the other hand, relative X-ray reflectivity (measured as the intensity of the specular peak divided by Yoneda peak intensity) is strongly dependant on the substrate temperature parameter. This could be explained with the grain sizes and/or possible preferred orientation parameter, as well as the hydrogen inclusion in the matrix, highly depending on the temperature parameter.

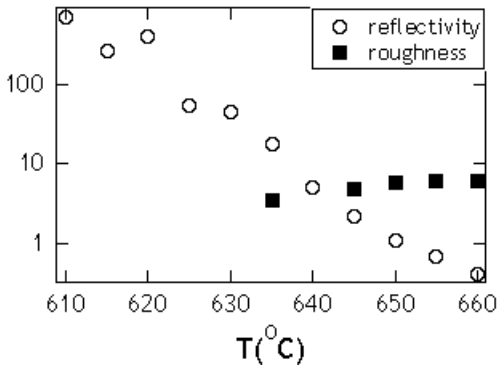

Figure 2. The relative X-ray reflectivity and relative surface roughness vs. substrate temperature.

MORPHOLOGY DEVELOPMENT OF PHYSICAL NETWORKS IN TRIBLOCK COPOLYMER GELS UNDER THE INFLUENCE OF EXTERNAL FIELDS

R. Kleppinger[1], S.Bernstorff[2] and H. Amenitsch[3]

1) FOM Institute AMOLF, Kruislaan 407, 1098 SJ Amsterdam, The Netherlands
2) Sincrotrone Trieste, S.S. 14 km 163.5, Basovizza, 34012 Trieste, Italy
3) IBR, Steyrergasse 17, 8010 Graz, Austria

The strong incompatibility between the constituting blocks of copolymers provides a strong driving force towards the formation of self-assembled microstructures in bulk or in solution with characteristic length scales determined by the dimensions of the block segments. In contrast to solutions of diblock copolymers, where micelles interact via entanglements of their corona chains, the micellar structures formed by triblock copolymers in a midblock selective solvent are interconnected. Vitrification of the microdomains below their glass temperature reticulates the microstructure and therefore the mechanical properties of such systems are strongly dependent on temperature.
In-situ studies of the microstructure during dynamic mechanical experiments clearly revealed that vitrification of such systems proceeds via an intermediate viscoelastic state with the latter being characterized by the presence of a highly ordered morphology. In analogy to micellar solutions of diblock copolymers, the full development of these morphologies requires high chain mobility. In case of micellar networks, however, the competition between the evolution of a highly ordered microstructure and the vitrification of the network junctions makes the final morphology of the gel extremly sensitive to the sample history.
The experiments at the ELETTRA SAXS beamline were therefore performed in two steps. In a first series of experiments, the effect of temperature and shear conditions on the polycrystalline morphologies were studied, using a temperature-controlled shear stage with parallel plate geometry at the SAXS setup that was equipped with the PHOTONICS CCD detector. Based on the experiments, a general orientation diagram could be established, indicating that the polycrystalline morphologies are transformed into a highly ordered twinned BCC morphology when subjecting them to shear within a certain range of shear amplitudes. If shear amplitudes are too low, the shear field is not able to break the gel and to allow for reorganization into a highly ordered structure, whereas very high shear amplitudes destroy any long range order in the system.
The second set of experiments was based on samples that were oriented under well-defined shear conditions and uniaxially deformed after vitrification at room temperature. The experimental setup consisted of a PC-controlled, miniaturized tensile tester, being placed in the SAXS setup that was equipped with the CCD camera in order to record the diffraction pattern from the deformed microstructures with high time resolution (100ms) during the deformation of the systems. Selected series of scattering patterns are visualized in [1]. They demonstrate that relatively small macroscopic sample deformation results in affine-type network deformation, whereas large deformations result in plastic deformation of the samples. The latter is supported by time-resolved scattering experiments which have been performed during hysteresis experiments.

We highly appreciate financial support from the European Union via the EU-TMR program.

References:

[1] Kleppinger, R., Valenca, A., Bernstorff, S., Amenitsch, H. (1999): In-Situ Studies on Mesoscopic Order of Thermoplastic Elastomer Gels *ELETTRA Newsletter* **33**; a series of scattering pattern, recorded during deformation is shown at http:\\www.elettra.trieste.it\science\newsletter

FINE STRUCTURE OF ORGANISED SOLUTIONS AND LYTROPIC MESOPHASES / POLYMORPHIC AND MESOMORPHIC BEHAVIOUR IN WATER-SURFACTANT SYSTEMS

C. La Mesa

Dept of Chemistry, Univ. La Sapienza, P.le A. Moro 5, 00185 Roma

Part 1. Experimental Report for the Year 1998. One day of measurements (three units) was given from Elettra to support the project. Due to the reduced measurement time, the investigation on viscous isotropic liquid crystalline phases could not be performed. Measurements were performed on different lyotropic liquid crystal systems, indicated below.

- The reverse hexagonal phase of the system composed by water, ethylene glycol, **EG**, and **Aerosol OT**. Spacings typical of hexagonal phases (with ratio 1:1/3:1/2) were observed in all cases. The radii of the rods and areas per molecule were calculated from the observed spacings. The working temperature was 25 °C.
- A few selected samples relative to the system water-hexadecyltributylphosphonium sulfate, **CTBPS** (the derivative of a phase transfer catalyst) were investigated. **CTBPS** forms a lamellar phase in a wide, central part of the phase diagram, between a micellar and a reverse micellar solution. Related spacing were measured. Part of this work has been reported in the paper „*Role of Counterions in the Catalytic Activity and Phase Equilibria of Phosphonium Salts in Water*." by G. Cerichelli, C. La Mesa, L. Lucchetti & G. Mancini, **Langmuir**, 2000, 16, page. 166-71. A more detailed analysis on the system is still in progress.

Part 2. Experimental Report for the Year 1999. One day of measurements (three units) was given from Elettra to support the project. Measurements were performed on lyotropic liquid crystals formed by water and sodium taurodeoxycholate, **NaTDC** (a steroidal surfactant present in significant amounts in the bile of mammals). Previous evidence on the formation of liquid crystalline phases was inferred from SAXS scattering and NMR measurements performed in collaboration with a Swedish group (see „*Formation of a Liquid Crystalline Phase in the Water –Sodium Taurodeoxycholate System*." by H. Edlund, A. Khan and C. La Mesa, **Langmuir**, 1998, 14, page 3691-97). Investigation was focused on the following aspects of the above system:

- The region of existence of the liquid crystalline phase in the water-**NaTDC** system is small and thermal transitions to a micellar phase take place at 35 °C. **SAXS** measurements were performed as a function of temperature, from 15 to 45-50 °C. **SAXS** results support previous data inferred from ^{2}**H** NMR and electrical conductance findings.
- A peculiar feature was observed. Depending on the concentration of **NaTDC** in the mixture, swelling or shrinking of the main spacing occurs.
- Spacings typical of reverse hexagonal phases (with ratio 1:1/3:1/2) were observed. The radii of the rods and areas per molecule were calculated. They are in agreement with previous information.
- A few selected samples in other water-bile salt systems were investigated too. Part of the work performed at the SAXS Beam-line was used to support experimental measurements reported in the paper: „*Liquid Crystals and Phase Equilibria in Binary Bile Salt-Water Systems*." By E.F. Marques, H. Edlund, A. Khan & C. L Mesa, **Langmuir**, 2000, 16, in the press.
- A manuscript, keeping the title „*Bile Salts Form Lyotropic Liquid Crystals.*„ is still in preparation. Information on the puzzling swelling- shrinking behaviour of the liquid crystalline phases occurring in the water-**NaTDC** system is there discussed in some detail.
- An oral contribution on the same item was presented at the National Meeting of the Colloid and Interface Division of the Italian Chemical Society, Rome (1999). Another oral contribution is being presented at the National Congress of the Italian Chemical Society, to be held in Rimini on June 2000.

PHASE DIAGRAM OF THE LYOTROPIC LIQUID CRYSTAL SODIUM 3,4,5, - TRIS(ω - ACRYLOYLOXYUNDECYLOXY)BENZOATE

R. Resel[1], U. Theissl[1], C. Gadermaier[1], G. Leising[1], M. Kriechbaum[2] H. Amenitsch[2] D. Gin[3] and R. Smith[3]

1.) Institut für Festkörperphysik, Technische Universität Graz, A-8010 Graz, Austria
2.) Institut für Biophysik und Röntgenstrukturforschung, Österreichische Akademie der Wissenschaften, A-8010 Graz, Austria
3.) Department of Chemistry, University of California, 94720 Berkeley, California, USA

One way to prepare an optical active nanocomposite material is based on the lyotropic liquid crystal sodium 3,4,5 – tris (ω - acryloyloxyundecyloxy)benzoate. This amphiphilic molecule forms lyotropic liquid crystals which serves as matrix for optical active molecules. A polymerization procedure stabilizes the matrix and the optical active molecules are fixed within this matrix and separated from each other [1].
The chemical structure of the investigated molecule is given in Figure 1. The shape of the molecule - built by a small polar headgroup and three long extended tails - forces this molecule to form a reversed hexagonal structure. Typical diffraction pattern of a hexagonal lattice was observed for samples with different water content from 8% to 20%. The main diffraction peak of the diffraction pattern at different water content is depicted in Figure 2. Additional to the sharp diffraction peak a broad correlation peak of less intensity appears at an angle of about $2\Theta = 2.6°$. The intensity of this broad diffraction peak increases with the water content. This broad correlation peak is referred to an isotropic phase which is apparently also present besides the reversed hexagonal phase. The insert of Figure 2 gives the transition temperature T_{tr}. This temperature is the melting temperature of the reversed hexagonal structure which is the change from the reversed structure to an isotropic state.
We conclude that the best stability of the reversed hexagonal structure is at a low water content of 8% and at room temperature. Higher water contents as well as higher temperatures pushes the system closer to the stability boundary of the reversed hexagonal phase [2].

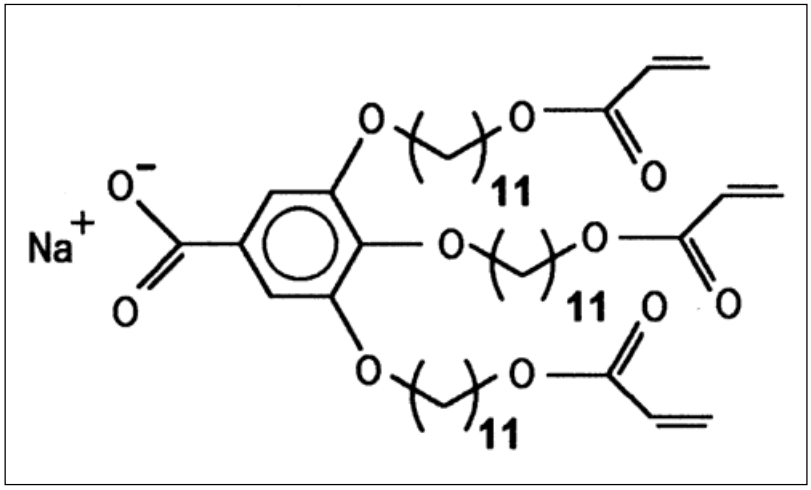

Figure 1. Molecular Structure of the lyotropic liquid crystal sodium 3,4,5 – tris (ω - acryloyloxyundecyloxy)benzoate

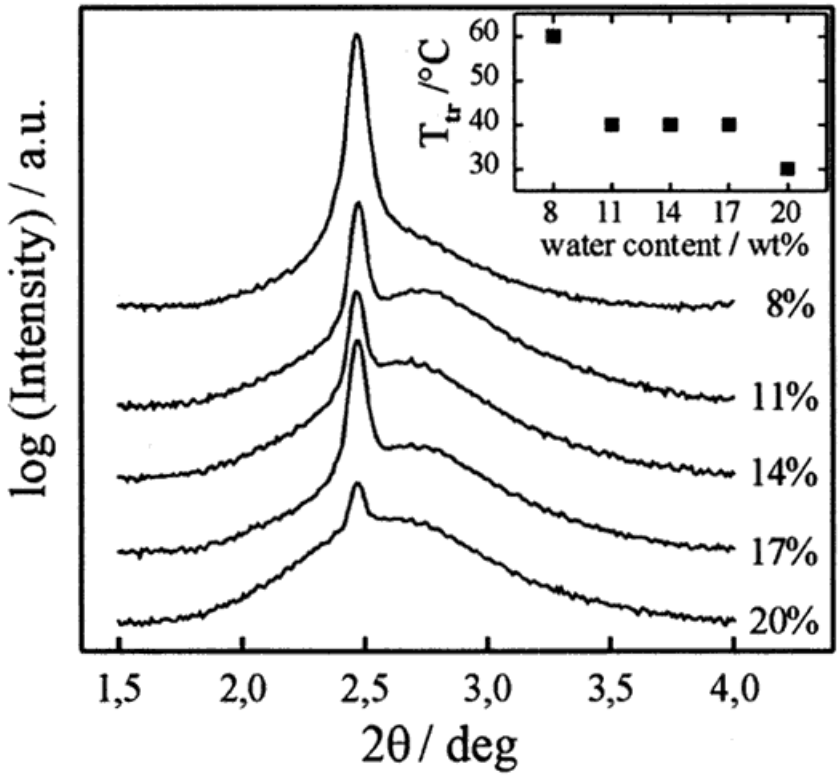

Figure 2. X-ray diffraction patterns of the lyotropic liquid crystal phases at 30°C prepared with different water content. For clarity the experimental curves are vertically shifted relative to each other; the intensities are given in logarithmic scale. The insert gives the transition temperature (T_{tr}) from the reversed hexagonal phase to the isotropic phase as a function of the water content.

References:

[1] Gin, D., Smith, R., Deng, H. & Leising, G. (1999): Synthesis of PPV nanocomposites using lyotropic liquid crystal monomers, Synth. Met. **101**, 52-55.

[2] Resel, R., Theissl, U., Gadermaier, C., Zojer, E., Kriechbaum, M., Amenitsch, H., Gin, D., Smith, R. & Leising, G. (2000): The H_2 – phase of the lyotropic liquid crystal sodium 3,4,5 – tris (ω - acryloyloxy-undecyloxy)benzoate, Liquid Crystals **27**, in print.

STRUCTURAL PROPERTIES OF POLY(VINYLQUATERPHENYLENES) IN SOLUTION

A. Valenca[1], W. Ruland[1], J.H. Wendorff[1], R. Kleppinger[2], K. Amenitsch[3], S. Bernstorff[4]

1.) Institute of Physical and Macromolecular Chemistry, Philipps-University, Hans-Meerwein-Strasse, D-35032 Marburg, Germany
2.) FOM-Institute for Atomic and Molecular Physics, Kruislaan 407, 1098 SJ Amsterdam, The Netherlands
3.) Institute of Biophysics and X-Ray Structure Research, Austrian Academy of Sciences, Steyrergasse 17, A-8010 Graz, Austria
4.) Sincrotrone Trieste, ELETTRA, Strada Statale 14 km 163.5, Trieste, Italy

Poly(vinylquaterphenylenes) (PQP) are members of a novel class of synthetic polymers with a complex chain architecture, consisting of a flexible backbone with laterally attached rigid side-chains. Computer simulations using quantum mechanical methods and forcefield-based simulations reveal an interesting structure in which – due to a high rotational energy barrier – a coplanar orientation of the side-chains is strongly favored. The generation of polymer chain models on the basis of a rotational isomeric state model and equilibration using molecular dynamics leads to rigid brush-like molecules.

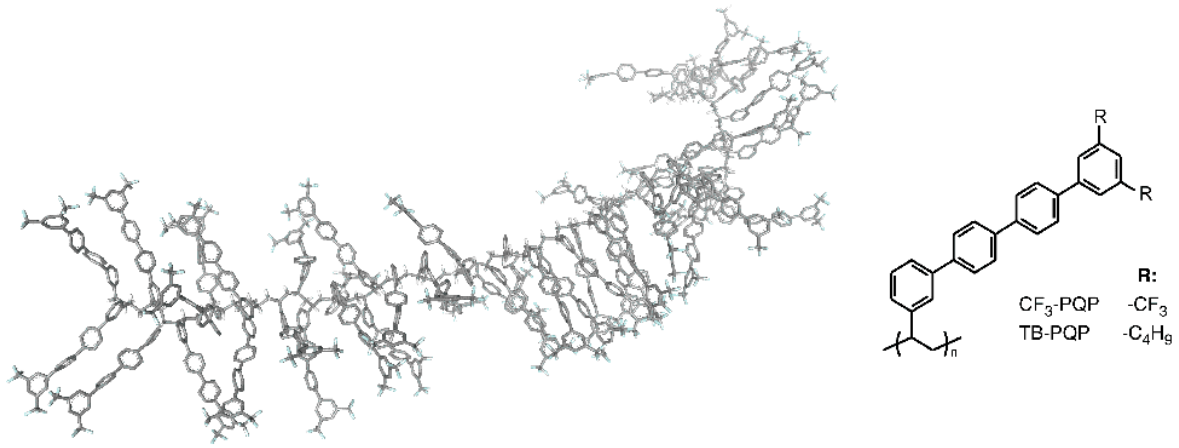

Figure 1. Conformation of a PQP-chain.

In order to obtain experimental information on the chain conformation SAXS experiments were carried out on solutions of various PQP samples with differently terminated side-groups and chain lengths in the range of 25 to 200 repeat units. The polymer concentration was varied between 0.5 and 2 w%. To exclude specific solvent effects the measurements were carried out in different solvents such as tetrahydrofurane and toluene.

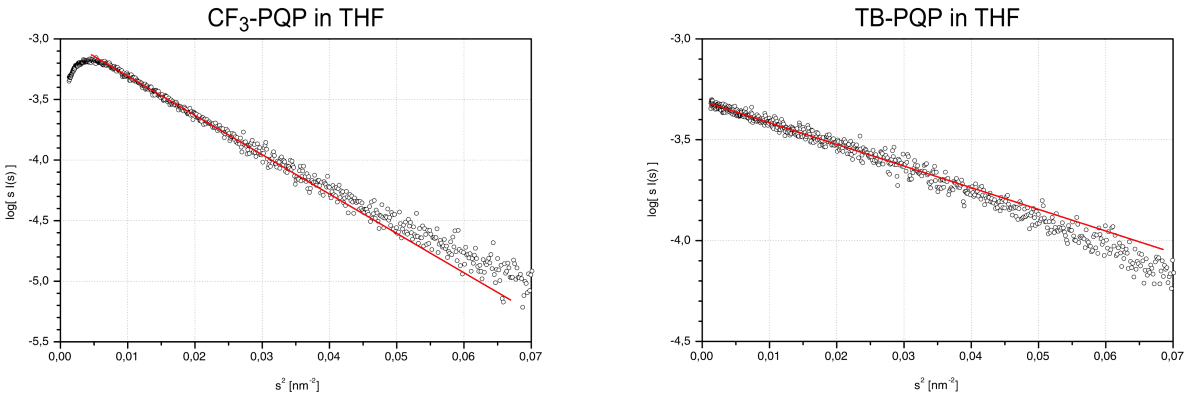

Figure 2. Scattering curves of PQPs in solution

The data show the characteristic scattering behavior of rod-like molecules where the radii of gyration of the cross-section R_c can be obtained from a log[s I(s)] vs. s^2 plot. In order to compare the experimental values to our predicted structures the inhomogeneous electronic density distribution along the side-chains and the scattering contrast must be taken into account. This can be accomplished by using a model where the PQP side-chains are separated into discrete building blocks. Corrected electronic densities with respect to the solvent can then be calculated using the molecular volumes of these structural segments.

With these corrected values the cross sectional radii of gyration for brush-like polymer models as predicted by molecular modeling can be calculated. The resulting values for R_c are in good agreement with the experimentally obtained data.

Table 1. Experimental and calculated R_c values.

	R_c,exp [Å]	**R_c, calc [Å]**
TB-PQP	7.4	7.9
CF3-PQP	13.2	13.6

INVESTIGATION ON THE FORMATION OF SUPERSTRUCTURES IN OPTICALLY ACTIVE POLY(NORBORNENE DERIVATIVES)

K. Viertler[1], A. Wewerka[1], H. Amenitsch[2], M. Rappolt[2] and F. Stelzer[1]

1.) Institute for Chemistry and Technology of Organic Materials, Strehmaierg. 16, Graz, Austria.
2.) Insitute of Biophysics and X-ray Structure Research, Austrian Academy of Sciences, Steyrerg. 17, Graz, Austria.

Ring Opening Metathesis Polymerization (ROMP) employing well defined transition metal alkylidene catalysts has repeatedly presented itself as a clean and efficient method to obtain highly functionalized polymers. Due to the living polymerization mechanism they usually show narrow molecular weight distributions and sometimes highly regular backbone structures [1]. It has been repeatedly proposed, that poly(7-oxanorbornene) [2] and poly(norbornenederivatives) [3] tend to form helical superstructures. However, the data published up to now are only the results of thermodynamic calculations and molecular modelling. To our knowledge no experimental prove for the formation of such helices has been reported yet.

Liquid crystalline polymers can be used as anisotropic materials for various applications [4]. Several side chain liquid crystalline polymers (SCLPs) [5] in which the mesogenic groups are attached to the polymer backbone e. g. polyacrylates [6], poly(vinylether) [7] or polysiloxanes [8] by flexible spacer groups have been prepared. Recently new materials based on poly(norbornene)[9]- and poly(cyclooctene) [10] - core units have been prepared *via* ROMP.

Over the last few years several optically active norbornene and 2-azanorbornene derivatives have been synthesized and polymerized by our group. The results have been reported in various publications [11]. Since thermodynamic calculations indicated, that these chiral polymers are especially likely to form helical superstructures, it is of great interest to investigate such samples by small angle X-ray measurements.

Recently we started our work on a new class liquid crystalline polymers. Optically active mesogenic groups such as cholesterol are connected to the poly(norbornene) backbone through flexible spacers with various lenghts. Investigations by optical polarized light microscopy and differential scanning calorimetry showed, that cholesteric mesophases are formed. Characteristic for such phases is a helical order of the mesogenic groups. Based on these data, we are highly interested in finding out about whether the alignment of the mesogenic groups has an influence on the order of the polymer backbone. Of special interest is whether the helical order of cholesteric mesogenes induces a similar structure in the main chain.

The monomers shown in Fig. 1 are known to undergo ROMP with various ”Schrock type” molybdenum alkylidene initiators [12] and a ruthenium alkylidene initiator introduced by Grubbs [13].

The norbornene derivatives were prepared in enantiomerically pure form, so that after the coupling of the optically active cholesterol unit two different diastereomers are obtained.

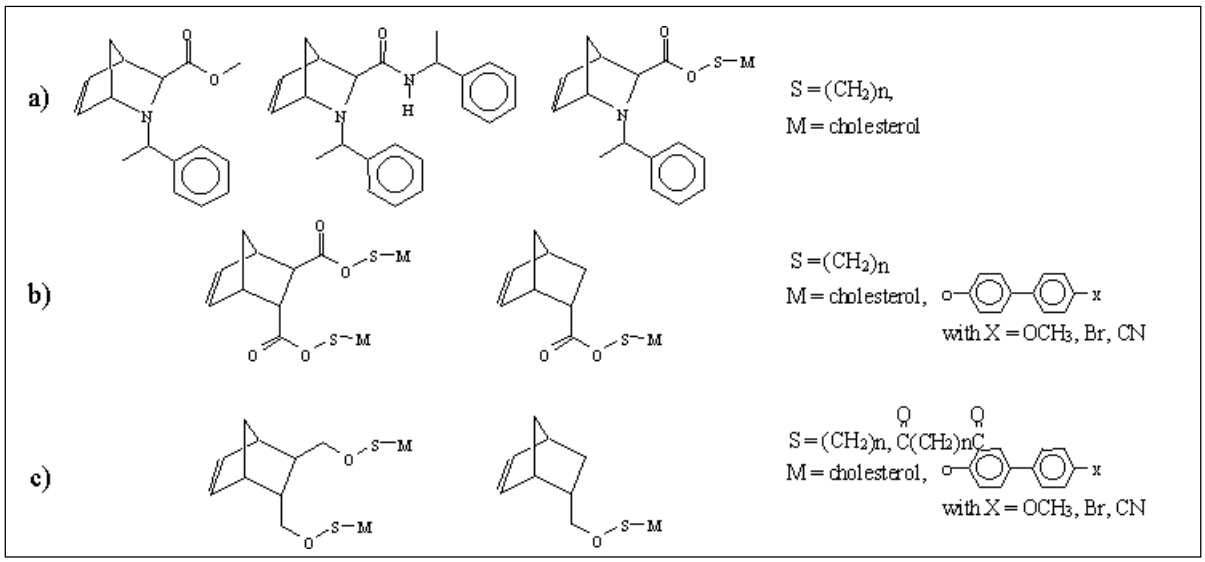

Figure 1. Chiral monomers to be polymerized *via* ROMP.

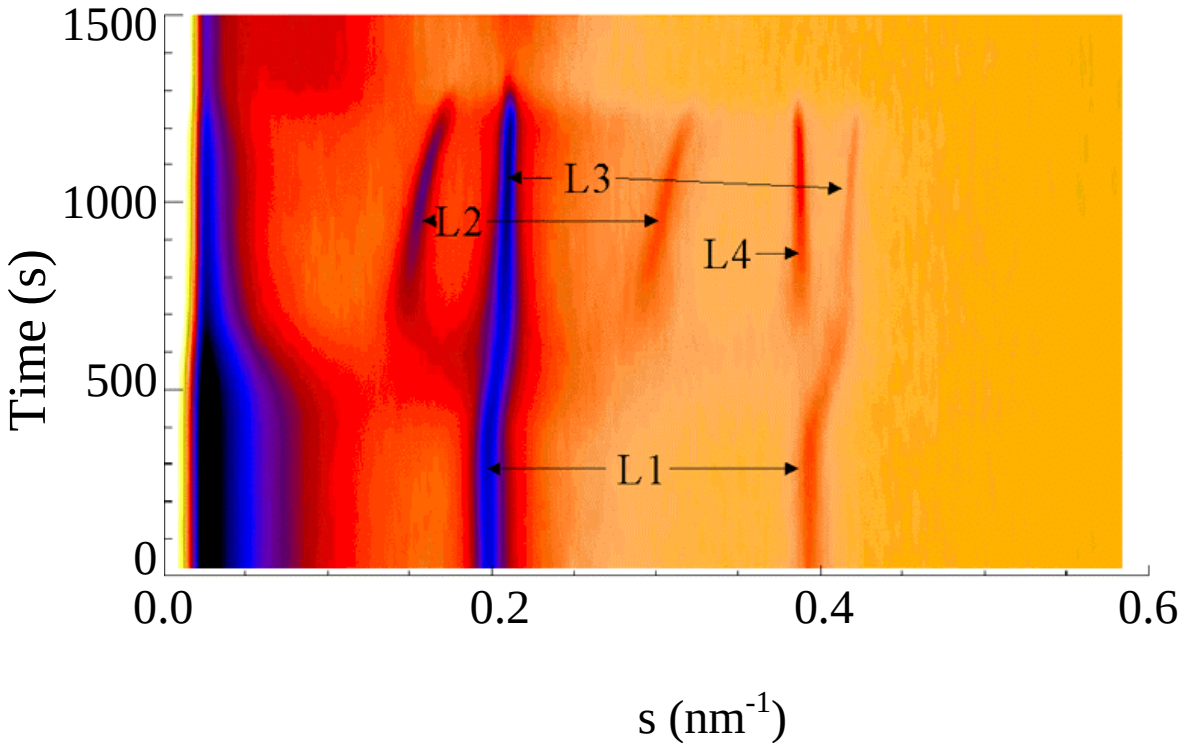

Figure 2. Temperature resolved measurement of PNB in the range between 26 and 210 °C (heating rate 9 °C/min). The lamellar phases L1, L2, L3, L4 are indicated corresponding to 5.06 nm, 6.57 nm, 5.0 nm and 2.57 nm, respectively.

These derivatives were investigated by fiber diffraction and classical SAXS. The fiber diffraction pattern showed the lamellar d-spacings but no layer lines indicating helical ordering. The temperature resolved SAXS measurements were performed in the temperature range between 26 and 210 °C and with a heating rate of 9 °C/min.
The phase behaviour of the polymer PNB derived of the disubstituted monomer, type C in fig. 1 with S = succinic acid and M = cholesteryl was investigated in detail. A typical diffraction

pattern is shown in Fig 2. indicating a complex temperature phase diagram. The lamellar phase L1 (d-spacing is 5.06 nm) undergoes a phase transition at 105 °C to the phases L2, L3 and L4. These new phases can be interpreted as an extended sidechain lamellas (L2: 6.57 nm), regular sidechain lamellas (L3: 5.0 nm) and an interdigitated phase (L4: 2.57 nm). After 100 s annealing at 210 °C these phases melt and the system forms an isotropic phase.
The temperature scans are able to give new insights in the thermal behaviour of these new poly(norbornene derivatives), which contain a more detailed picture than obtained by conventional DSC measurements.

References:

[1] a) Ivin, K.J. & Mol, J.C. (1997): *Olefin Metathesis and Metathesis Polymerization.* Academic Press, London. 1997; b) Breslow, D.S. (1993): *Prog. Polym. Sci.* **18**, 1141; c) Bazan, G.C., Schrock, R.R., Cho, H.-N. & Gibson, V.C. (1991): *Macromolecules* **24,** 4495.

[2] Novak, B.M. & Grubbs, R.H. (1988): *J. Am. Chem. Soc*. **110**, 960.

[3] O´Dell, R., McConville, D.H., Hofmeister, G.E. & Schrock, R.R. (1994): *J. Am. Chem. Soc*. **116**, 3414.

[4] Ciferri, A., Krigbaum, W.R. & Meyer, R.B. (1982): *Polymer Liquid Crystals.* Academic Press, New York.

[5] McArdle, C.B. (1989): *Side Chain Liquid Crystal Polymers*. Blackie and Son Ldt., Glasgow-London.

[6] Cecobert, G., Soyer, F. & Dubois, J.C. (1985): *Polym. Bull. (Berlin)* **14**, 179.

[7] Chiellini, E., Dossi, E., Galli, G., Solaro, R. & Gallot, B. (1995): *Macromol. Chem. Phys.* **196,** 3859.

[8] Mallon, J.J. & Kantor, S.W. (1989): *Macromolecules* **22**, 2070.

[9] a) Komiya, Z., Pugh, C. & Schrock, R.R. (1992): *Macromolecules* **25**, 3609; b) Ungerank, M., Winkler, B., Eder, E. & Stelzer, F. (1995): *Macromol. Chem. Phys.* **196**, 3623; c) Winkler, B., Ungerank, M. & Stelzer, F. (1996): *Macromol. Chem. Phys.* **197,** 2343; d) Ungerank, M., Winkler, B., Eder, E. & Stelzer, F. (1997): *Macromol. Chem. Phys.* **198**, 1391.

[10] Winkler, B., Rehab, A., Ungerank, M. & Stelzer, F. (1997): *Macromol. Chem. Phys.* **198**, 1417.

[11] a) Schitter, R.M.E., Jocham, D., Saf, R., Mirtl, C., Stelzer, F. & Hummel, K. (2000): *J. Mol. Cat*., in print*;* b) Schitter, R., Steinhäusler, T. & Stelzer, F. (1997): *J. Mol Cat*., A. Chemical **115**, 11; d) Steinhäusler, T., Stelzer, F. & Zenkl, E.(1994): *Polymer* **35** (**3),** 616; e) Steinhäusler, T. &Stelzer, F.(1994): *J. Mol. Cat***. 90**, 53.

[12] Murdzek, J.S. & Schrock, R.R. (1987): *Organometallics*, **6**, 1373.

[13] Schwab, P., Grubbs, R.H. & Ziller, J.W. (1996): *J. Am. Chem. Soc*, **118**, 10.

STRUCTURAL INVESTIGATION OF NEAR SURFACE –LAYERS IN SILICON PLATELETS FOR SOLAR CELLS [1]

M. Zehetbauer[1], J.T. Bonarski[2], I. Kopacz[1], S. Bernstorff[3] and H. Amenitsch[4]

1.) Institute of Materials Physics, University of Vienna, Austria
2.) Institute of Metallurgy and Materials Science, Polish Acad. of Sciences, Krakow, Poland
3.) Sincrotrone ELETTRA, Trieste, Italy
4.) Institute of Biophysics & X-Ray Structure Research, Austrian Academy of Sciences, Graz, Austria

It has been shown that the formation of damaged and/or amorphized layers plus a suitable heat treatment can strongly increase the photovoltaic efficiency of silicon solar cells. However, the optimum combination of the microstructural parameters being the distribution, dimension and fraction of both the amorphized areas as well as the internal stresses connected, is still unknown. For characterization of such microstructure, the authors make use of a special diffraction method: It is based on the fact that the cyclic (harmonics) components caused by the phenomenon of extinction will not completely attenuate when the perfect crystal structure is disturbed by defects, such as amorphized lattice areas, internal stresses and/or atomic lattice defects [2]. By careful analysis of these disturbances, detailed information on the microstructural parameters mentioned can be obtained.

In frame of the proposal, measurements on Si <001> single crystal samples with buried amorphized layers have been performed. Both wide-angle diffraction patterns as well as (001)-pole figures within the range $\varphi = 0 \div 360^{o} / \Delta\varphi = 20^{o}$ and $\psi = 0 \div 3^{0} / \Delta\psi = 0.3^{0}$ have been carried out. For each sample position of registered pole figure a line profile of (004) Si reflection was measured, see Fig. 1. The registered profiles of the (004) diffraction line enabled to evaluate structural details of the Si <001> single crystals with their disturbed (damaged and amorphous) layers implanted [2]. The effective localisation depth of strong damages from P^{+} implantation was evaluated to be 0.4 to 0.5μm. This depth almost corresponds to two times the mean free path of the P^{+} -ions. The area of elastic deformations was found to extend to a depth of about 1.3 μm where the transition area between damaged and amorphous layer is situated; the strain in this transition layer is of compressive nature and amounts to about $4x10^{-3}$ maximum. In the deeper transition layer between amorphous zone and unaffected crystal, the strains are tensile ones and vary in between 3 and $5x10^{-4}$. The thickness of this transition layer revealed to be about 0.2-0.4 μm. The diffuse loss parameter μ_d (which is a measure of the defect density) equals to about 12.7 cm^{-1} in the Si crystal, which seems somewhat too large when compared to the literature.

Besides the above structural disturbances, some angular misorientation (ca. 0.25°) between the [001] axis and normal of sample surface was evident. This misorientation slightly varied by ± 0.02° across the sample surface. Furthermore, differences in crystallographic orientation in all near-surface areas of the crystal were observed. This is shown in Fig. 2, where the changes of pole figure values as well as modulations of the intensities are demonstrated. This result indicates that strongly defected areas are present in the sample-near-surface zones.

References:

[1] Bonarski, J.T., Zehetbauer, M., Swiatek, Z., Fodchuk, I.M., Kopacz, I., Bernstorff, S. & Amenitsch, H.(1999): Synchrotron Investigation of the Near Surface Areas in Silicon Solar Cells Modified by P^{+} Ion Implantation and Thermal Treatment, *Europ.Conf. on Photovoltaics*, Oct.25-27, Cracow, Poland; to be published in: *Opto-Electronics Review* (2000)

[2] Servidori, M. (1987): Characterization of lattice damage in ion implanted silicon by multiple crystal x-ray diffraction, *Nuclear Instruments and Methods in Physics Research* **19/20**, 443-449.

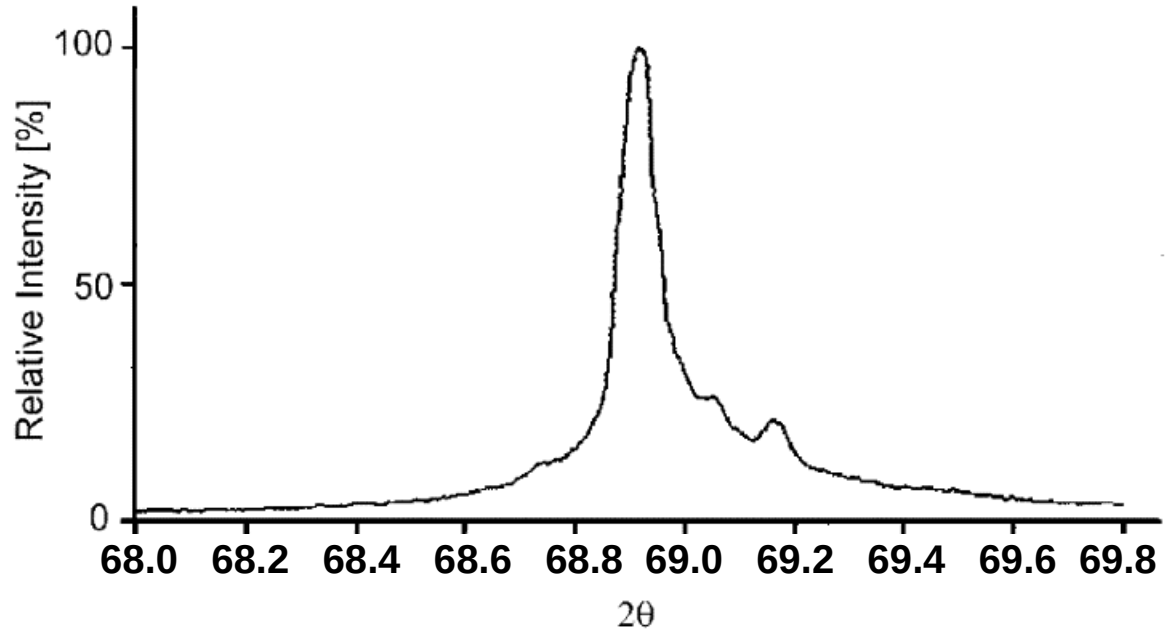

Figure 1. One of several (004) line profiles measured for Si <001> single crystal with buried amorphized layer. Visible right-side components of the profile are the sequential harmonics of diffraction effect non-perfectly attenuated due to the disturbed crystal structure from implantation of P^+ ions.

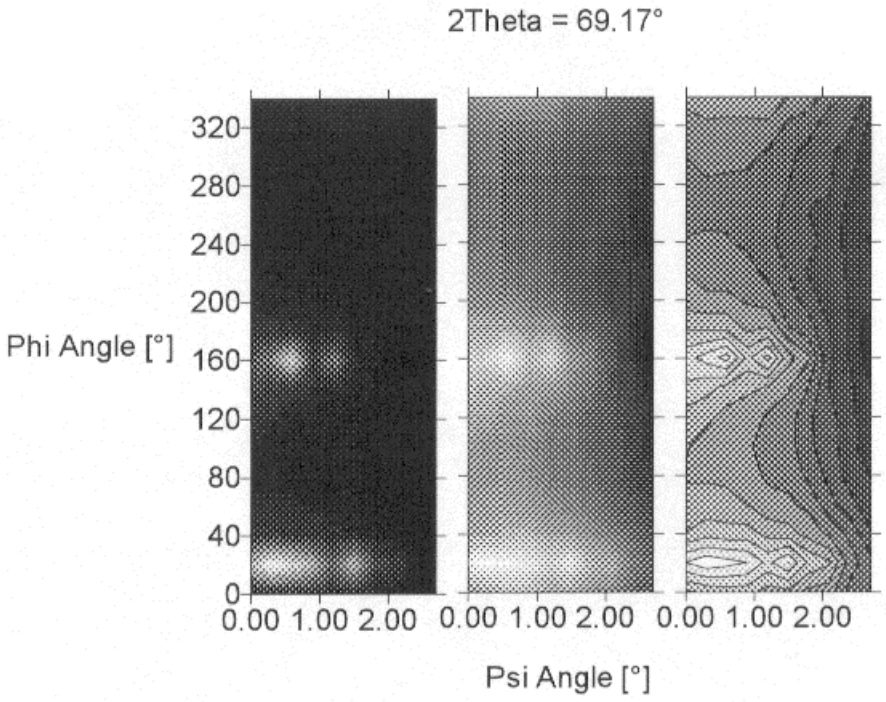

Figure 2. Pole figure image (range: Ψ = 0-3°, φ = 0-360°) for investigated Si <001> crystal sample presented in a line scale (left), logarithmic scale (middle) and isolines (right).

DISLOCATION DENSITIES & LONG RANGE INTERNAL STRESSES IN TORSIONALLY DEFORMED FCC METALS

M. Zehetbauer[1], T. Ungar[2], R. Pippan[3], E. Schafler[1], I. Kopacz[1], E. Szekely[3], H. Amenitsch[4] and S. Bernstorff [5]

1.) Institute of Materials Physics, University of Vienna, Austria
2.) Institute of General Physics, Eötvös University Budapest, Hungary
3.) Erich Schmid Institute of Materials Science, Austrian Academy of Sciences, Leoben, Austria
4.) Institute of Biophysics & X-Ray Structure Research, Austrian Academy of Sciences, Graz, Austria
Sincrotrone ELETTRA, Trieste, Italy

Samples of polycrystalline Cu, Al and Ni have been subjected to X-ray Bragg Peak Profile Analyses (XPA) which had been deformed in torsion and cut by 45° before, since both the normal strains and stresses are expected to be maximum here in torsional deformation. Deformation by torsion provides a spectrum of different deformation degrees in layers parallel to the torsion axis having different distances from the center of the sample. Since XPA with synchrotron radiation (SXPA) allows for a sufficiently high spatial resolution of order 100 μm, it is possible to perform SXPA-scans across the 45° cross section of only ***one*** sample and to get information on the evolution of dislocation density and internal stresses as a function of deformation.

Among the large amounts of data to be evaluated (in total, more than 300 line profiles by two reflections (200), (311) were measured), those of Ni were considered as the first because of an interesting comparison of results of torsioned samples with those from rolled ones [1]. The results of both and a common discussion have been recently published [2]: Assuming a simply statistical arrangement of dislocations, the dislocation density as measured by XPA does not coincide with measurements of the residual electrical resistivity although the latter has been corrected for possible influence of deformation induced vacancies (Fig. 1). However, by assuming the dislocations to arrange in dipolar dislocation walls, and to rearrange into tilt dislocation walls at large deformations, a good coincidence with resistivity data could be achieved (Fig.1). Moreover, these findings well correlate with the results of [1], where this special transformation has been concluded from SXPA measurements from microbeam scans across single grains on the surface of cold-rolled Ni samples. The iterative character of rolling deformation, however, seems to affect the deformation dependent evolution of dislocation density at high deformation degrees. There has been observed a degeneration of dislocation density and long range internal stresses, in contrast to the findings in samples continuously deformed by torsion where the dislocation density and long range internal stresses steadily grow (Fig. 2). Since in Cu no such effects have been observed [3], it is concluded that (i) the higher stacking fault energy and (ii) the higher concentration of vacancies being available during cold work conditions of Ni, strongly enhance the occurrence of marked recovery processes in between single rolling passes leading to the degeneration of parameters observed.

References

[1] Zehetbauer, M., Ungar, T. et al. (1997): Annual Report 1996/97 of the Austrian SAXS beamline at ELETTRA, 44-49.
[2] Schafler, E., Zehetbauer, M., Kopacz, I., Ungar, T., Hanak, P., Amenitsch, H. & Bernstorff, S. (1999): *Phys. Stat. Sol.* A **175 (2)**: 501.
[3] Zehetbauer, M., Ungar, T., Kral, R., Borbely, A., Schafler, E., Ortner, B., Amenitsch, H. & Bernstorff, S. (1999): *Acta Mater* **47 (3)**: 1053.

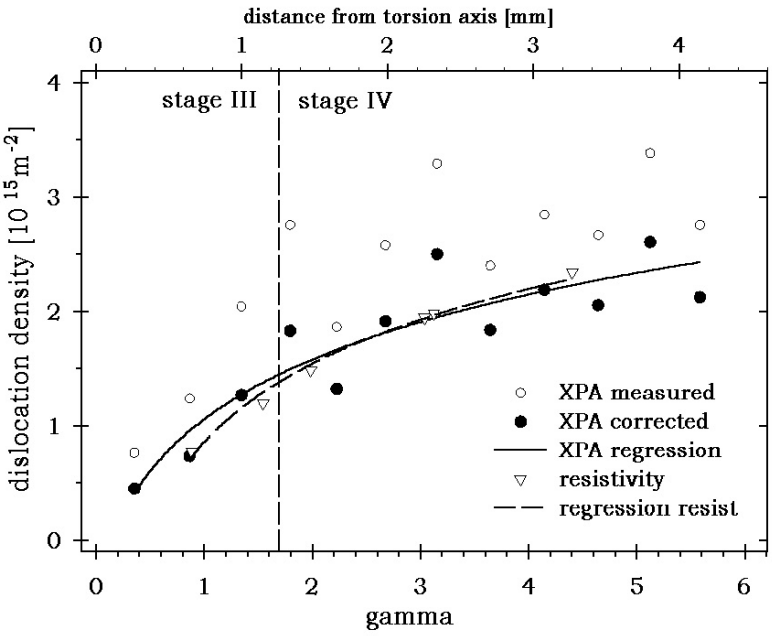

Figure 1. Evolution of dislocation density in torsionally deformed Ni, versus resolved shear strain. The full points represent the results of the X-ray measurement after appropriate correction (see text). The measuring error is of the order of the symbol size. The triangles indicate the values as determined by residual electrical resistivity measurements, where the measuring error is smaller than the symbol size. The solid line results from a non-linear regression of the X-ray data.

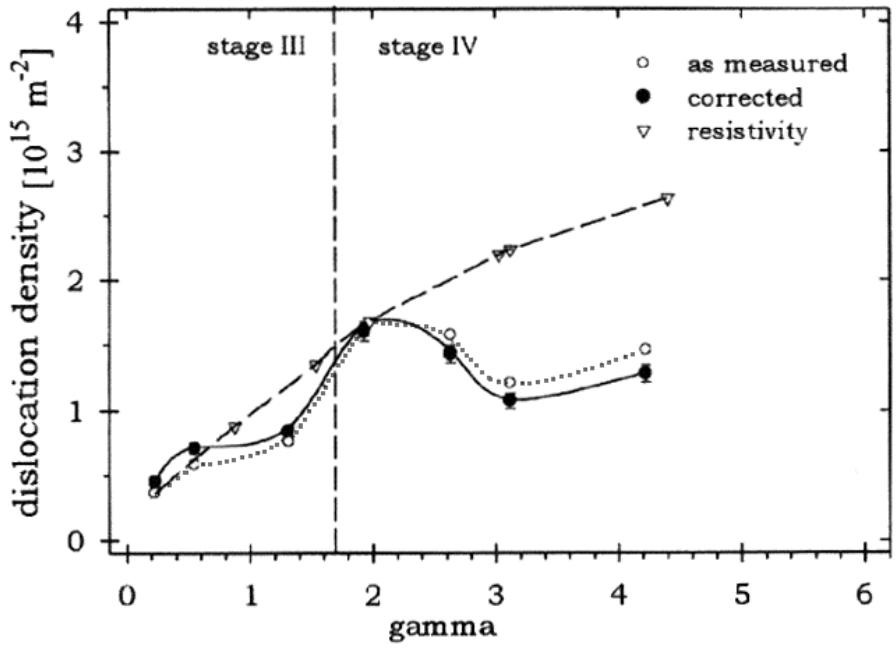

Figure 2. Evolution of dislocation density in cold rolled and torsionally deformed Ni, as a function of resolved shear strain. The full points represent the results of the X-ray measurement after appropriate correction. The triangles indicate the values as determined by SXPA measurements along the 45°-cross section of the torsionally deformed sample; they nicely fit to the results of residual electrical resistivity measurements. The bars represent the standard deviation of mean of all data measured during an one-grain scan.

MICROSTRUCTURAL PARAMETERS DURING PLASTIC DEFORMATION OF FCC METALS AS OBSERVED BY IN-SITU SYNCHROTRON BRAGG PEAK PROFILE ANALYSIS [1]

M. Zehetbauer[1], T. Ungar[2], R. Pippan[3], E. Schafler[1], P. Hanak[2], I. Kopacs[1], S. Bernstorff [4] and H. Amenitsch[5]

1.) Institute of Materials Physics, University of Vienna, Austria
2.) Institute of General Physics, Eötvös University Budapest, Hungary
3.) Erich Schmid Institute of Materials Science, Austrian Academy of Sciences, Leoben, Austria
4.) Sincrotrone ELETTRA, Trieste, Italy
5.) Institute of Biophysics & X-Ray Structure Research, Austrian Academy of Sciences, Graz, Austria

In this project it has been undertaken to measure the evolution of dislocation density ρ^* as well as of long range internal stress $\Delta\sigma \equiv |\Delta\sigma_w - \Delta\sigma_c|$ (for definitions, see [2]) during plastic compression of Cu and Al. Four Cu and two Al polycrystalline samples have been monitored during deformation. A special mini-compression device has been constructed and mounted on a large two-cradle goniometer with three rotational and two lateral axes, the latter in order to follow the same sample region (focus about 500 μm) during the whole period of experiment. The high intensity of Synchrotron radiation has been used to realize 1 minute - "flashlights" during deformation. This measuring time revealed to be short enough to neglect the deformation induced changes in microstructure during the measurement, but sufficiently long to provide well resolved Bragg profiles. After strain intervals of 10% having collected more than 10 measurements in dynamic mode, the deformation machine has been stopped, and the microstructural parameters ρ^* and $\Delta\sigma$ have been measured in (quasi-)static mode. In Fig. 1 where the stress-strain characteristics of a Cu sample being plastically deformed in compression is shown, these interruptions can be recognized by the small stress drops indicated. The deformation could be performed up to true strains $\varepsilon \approx 1.5$ when the sample got too small to achieve any scattering. The unloading process is indicated by the dotted line. In Fig. 2 it can be clearly seen that the dislocation density dynamically measured is about a factor 1.5 – 2 larger than that measured in (quasi-) static mode, which itself exceeds that of unloaded state by another 30%. In Fig. 3 the long range internal stresses are shown as a function of plastic strain as they resulted from measurements in (quasi-) static mode. The values lie up to a factor 5 (!) higher than those measured in unloaded state previously [2]. Altogether, it can be concluded that the ρ^* and $\Delta\sigma$ values ***during*** deformation distinctly exceed those being present *after* deformation. This result will certainly attract much interest in the community of plasticity theoreticians which have been still designing models adapted to statically measured microstructural parameters instead of dynamically measured ones, due to the lack of experiments like that reported here.

In comparing Figs. 1-3, at about a true strain $\varepsilon \approx 1$, a sudden decrease in dynamical dislocation density can be seen which is accompanied by a slight one in static dislocation density as well as in long range internal stress. It seems that the transformation of cell wall dislocations from a dipole to a tilt arrangement [2-4] is much more reflected in the dynamic dislocation evolution than in the (quasi-)static and/or unloaded state where some of dislocations experience an additional rearrangement due to relaxation and/or unloading [1].

References:

[1] Zehetbauer, M., Ungar, T., Pippan, R. et al., in preparation for publication in Scripta mater (2000).
[2] Zehetbauer, M., Ungar, T., Kral, R., Borbely, A., Schafler, E., Ortner, B., Amenitsch, H. & Bernstorff, S. (1999): *Acta mater*. **47 (3)**: 1053.
[3] Müller, M., Zehetbauer, M., Borbély, A. & Ungàr, T. (1996): *Scripta metall.mater.* **35**: 1461.[4] Ungar, T. & Zehetbauer, M.(1996): *Scripta metall.mater.* **35**:1467.

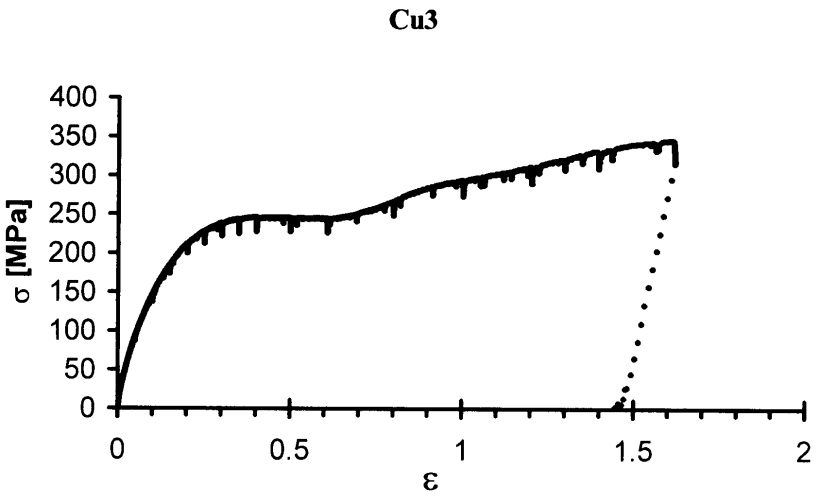

Figure 1.

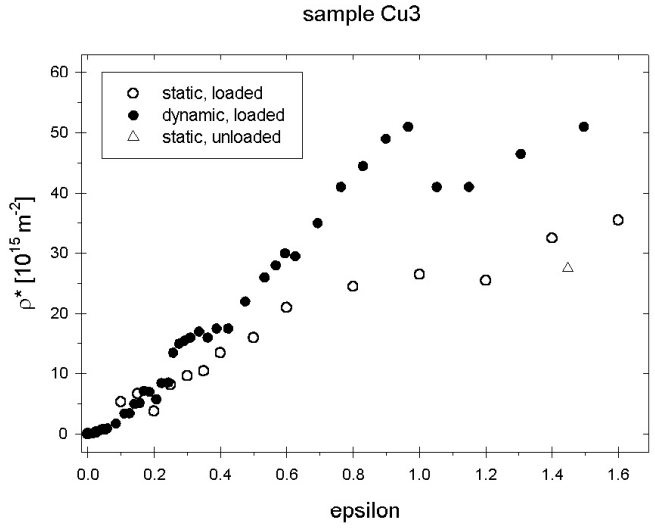

Figure 2.

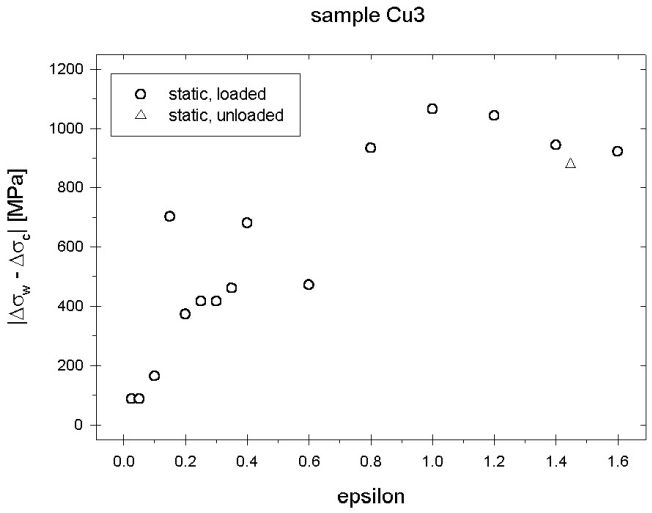

Figure 3.

4. Chemistry

SOLUBILIZATION OF OIL IN SILICATE-SURFACTANT MESOSTRUCTURES

P. Ågren[2], M. Lindén[1], S. Karlsson[1] and H. Amenitsch[3]

1.) Department of Physical Chemistry, Åbo Akademi University, Porthansgatan 3-5, FIN-20500, Finland.
2.) Max-Planck Institut für Kohlenforschung, Kaiser-Wilhelm Platz 1, D-45470, Mülheim an der Ruhr, Germany.
3.) Institute of Biophysics and X-Ray Structure Research, Austrian Academy of Sciences, Steyrergasse 17/VI, A-8010 Graz, Austria.

The solubilization of n-hexane and toluene by silicate-surfactant hexagonal, mesophases has been studied by time resolved in situ synchrotron small angle X-ray scattering. The addition of different oils, i.e., hexane, octane and toluene, in the synthesis mixture, produced bimodal silicate-surfactant composite mesophases. The composite mesophases have different d-spacings depending on the amount and type of oil. This coincides nicely with the fact that oil can be solubilized in the micellar core, thus increasing the size of the micellar aggregate. Aromatic compounds, like toluene, are solubilized in larger amounts in aqueous solutions of ionic surfactants. This effect originates both from the smaller molecular volume and the higher polarity of aromatic compounds. Due to the higher polarity, aromatic compounds can solubilize both in the micellar core and in the palisade layer. As a result, the micellar core-water interaction energy will decrease and lead to an increase of the solubilization of aromatic compounds in micellar aggregates, compared to the corresponding saturated hydrocarbons. In our study, the well-ordered hexagonal phase expanded only slightly with increasing reaction time and amount of oil, in the presence of hexane and octane. However, a pronounced swelling of the well-ordered hexagonal phase in the presence of toluene was observed with both increasing reaction time and increasing amount of toluene. The pronounced swelling with time of the whole hexagonal structure can be seen in Figure 1.
It is suggested that the extent of solubilization be mainly governed by the oil solubility in the continuous phase. The availability of the oil will largely influence the phase behavior and the long-range order of the silicatropic mesophase. While the addition of n-hexane to the synthesis results in a loss of order, a substantial amount of toluene can be solubilized without affecting the long-range order. Many of the observed effects can be rationalized based on time-dependent changes in the properties of the system due to silicate hydrolysis and condensation reactions, in addition to the water solubility of the solubilizate. Much more oil can be solubilized in silicatropic systems than in aqueous solutions of ionic surfactant.

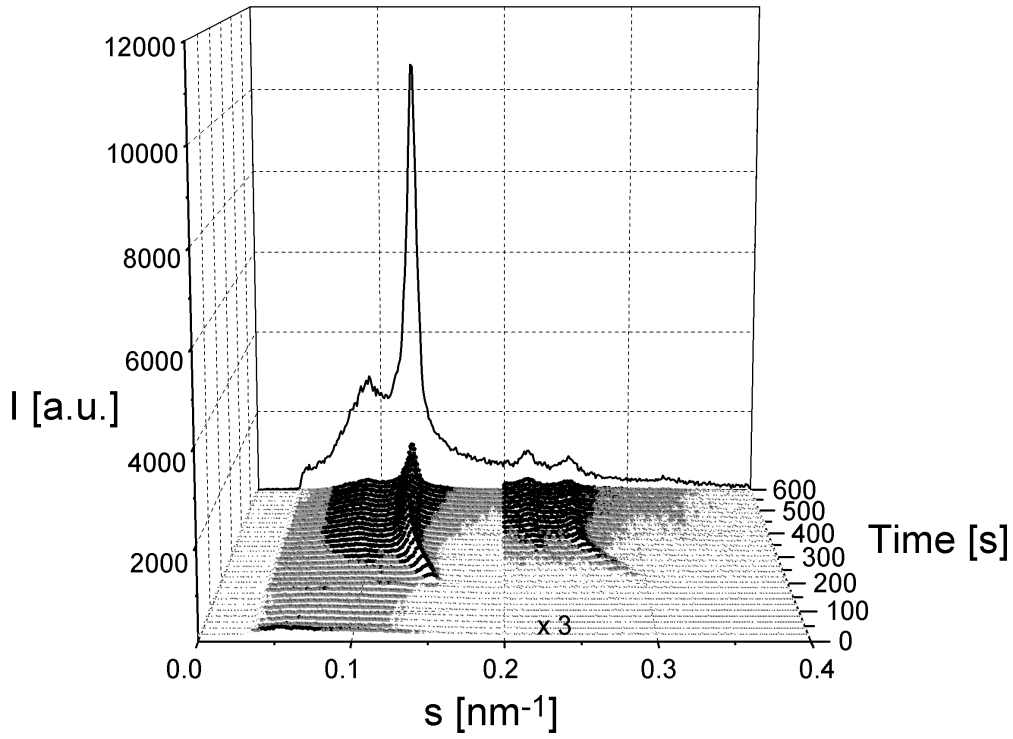

Figure 1. An in situ synchrotron XRD pattern of the development of a silicate-surfactant composite mesophase in the presence of toluene, mtoluene/mCTAB = 5.85. Note the multiplication of the intensity scale in the s range 0.2 – 0.4 1/nm.

SAXS STUDY OF SODIUMN-DODECANOYL-L-PROLINATE IN D_2O

H. Amenitsch[1], S. Borocci[2], G. Mancini[2] and M. Rappolt[1]

1.) Institute of Biophysics & X-Ray Structure Research, Austrian Academy of Sciences, Graz, Austria.
2.) Centro CNR di Studio sui Meccanismi di Reazione, c/o Dip. di Chimica"LaSapienza", 00185 Roma, Italia.

Introduction: We have recently reported about the high extent of organisation of the chiral anionic surfactant sodium N-dodecanoy-L-prolinate **1** [1, 2]. 1H and 13C NMR experiments demonstrated that, analogously to other amidic surfactants [3], compounds **1** aggregates in water in separate domains on the basis of the E/Z stereo-chemical code [1]. Moreover, a 1H NMR investigation carried out in the presence of an aromatic solute put in evidence a selective interaction of the Z domains with the solute [2]. Some of the obtained evidences could suggest that the E and Z domains were separate aggregates more than regions belonging to the same aggregate.

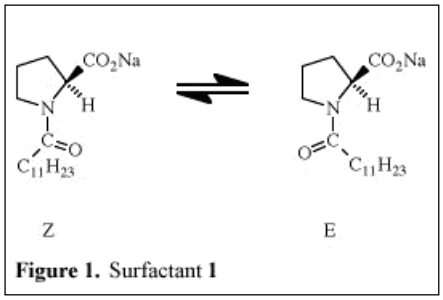

Figure 1. Surfactant **1**

Small angle X-rays experiments have been made both on aqueous micellar solutions and on liquid crystalline phases in order to detect a) the possible presence of two different micellar populations, and b) to check if the organisation in E/Z domains remains also in more organised phases. Experiments were carried out on D_2O solutions, because 1H and 2H and 13C NMR spectra were previously run on the same samples. The percentage content of the examined samples is reported in Table 1.

Table 1. Percentage concentration of the examined samples

Sample	Concentration %
1	1.8
2	2.6
3	5.1
4	7.0
5	11.5
6	19.7
7	38.0
8	41.4
9	51.9
10	71.8
11	76.0
12	90.8

Samples 1-8: Normalised patterns concerning samples 1-6 are reported in Fig. 2. It can be observed a broad distribution at around s = 0.33 nm^{-1}, which is due to the form factor. At 19.7% also inter-particle interference is visible (arrow). Patterns 1-5 have been treated in regime of isolated particles and fitted according to a spherical micelle model Fig. 3 [4]. According to this fit the hydrocarbon core should have a diameter of about 3 nm and an outer diameter of about 4.5 nm. According to the patterns and to the used model, there is only evidence for a certain size distribution of the micelles rather than two distinct populations. At higher concentrations (samples 7 & 8), it can be observed, that inter particle interference becomes dominant at ~ 0.23 nm^{-1} (Fig 4).

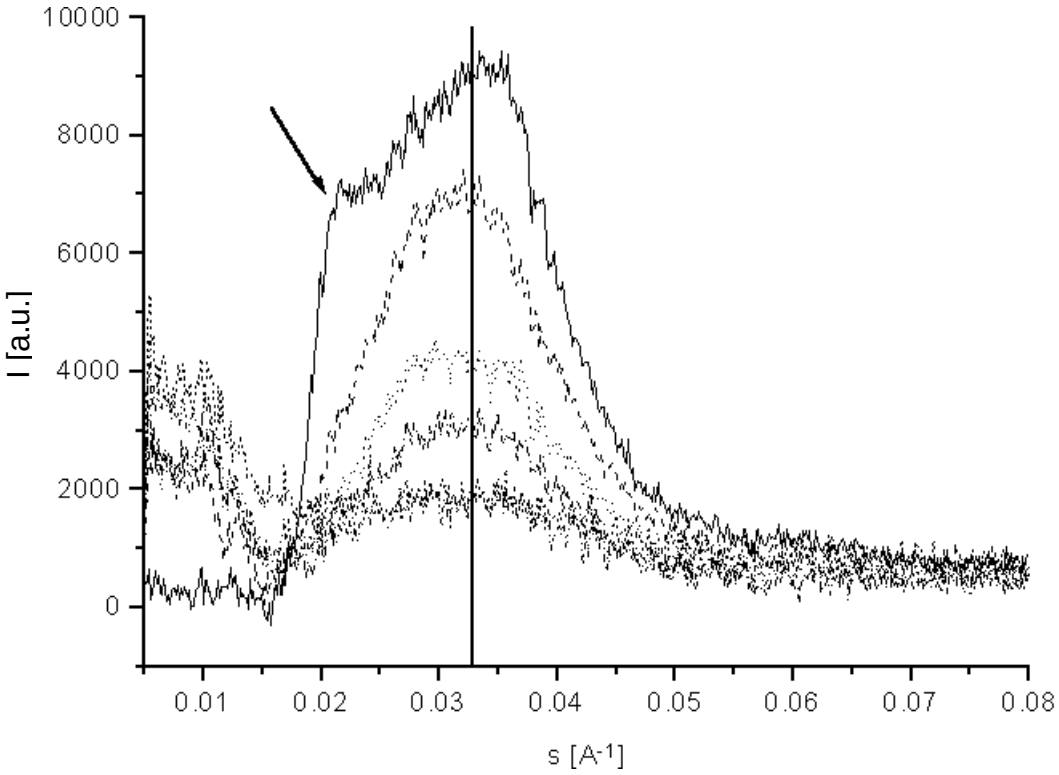

Figure 2. From bottom to top: X-ray scattering pattern of samples 1 - 6.

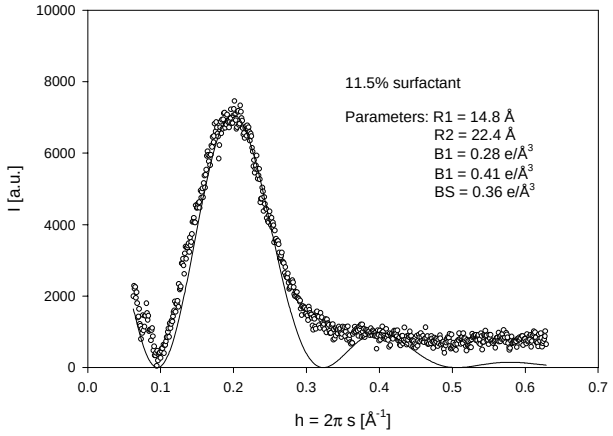

Figure 3. Model of the form factor of the 11.5% surfactant sample.

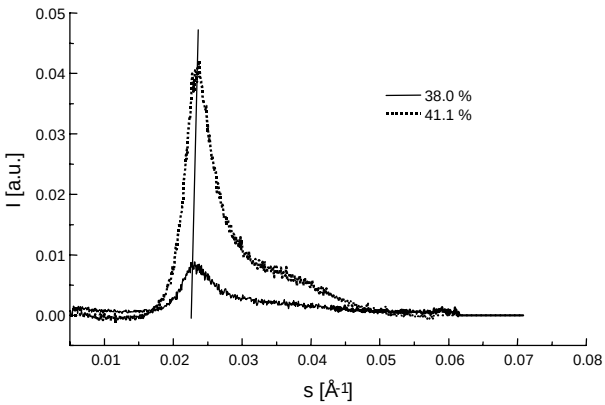

Figure 4. X-ray scattering pattern of samples 7 and 8.

Samples 9-12: (Fig.5) One pure hexagonal phase is observed between 25 and 90 °C with a = $\sqrt{3}/2*s_{10}$ = 4.3 nm at a concentration of 51.9% (A). Probably, two cubic phases are visible at a concentration of 71.8% at 25 °C (B). Below 25 °C a lamellar crystalline phase is observed (d-spacing 2.85 nm). Above the cubic phase region three molten lamellar phases are visible (e.g., C, D). Their d-spacings are 3.3, 2.8 and 3.1 nm, respectively. Depending on the concentration the lamellar crystalline phase (d-spacing 2.85 nm) co-exists

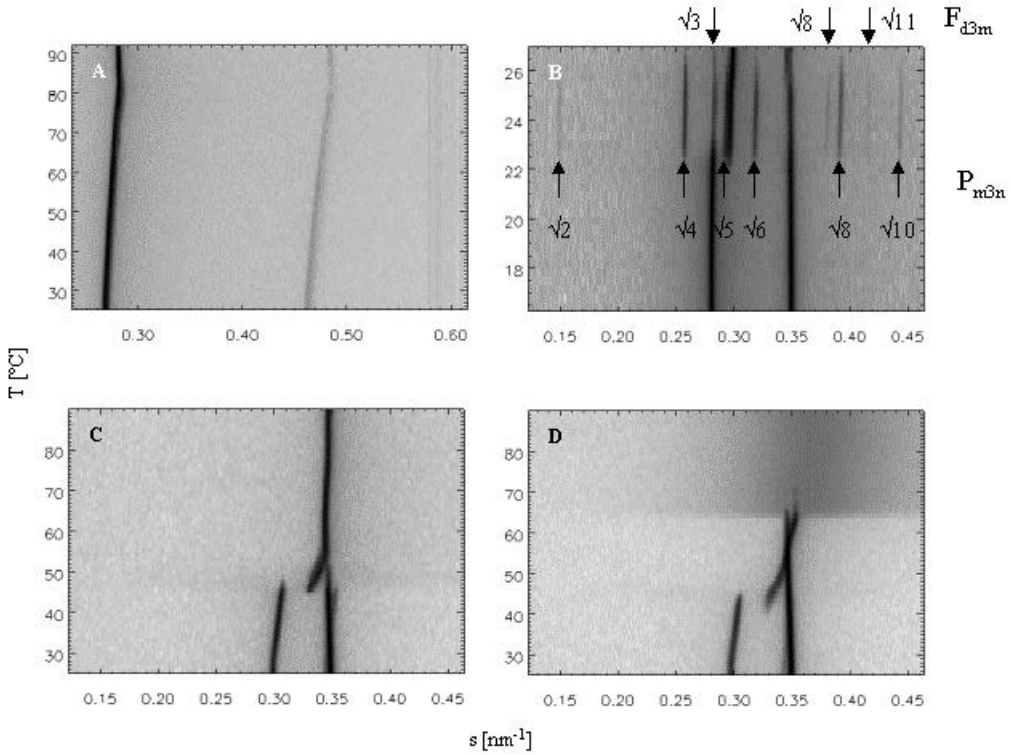

Figure 5. Diffraction patterns of samples 9-12 (A-D) at various temperatures.

with the cubic phase (sample 10, B) or is still existent at even higher temperature with two of the molten lamellar phases (sample 11, C) or even with the last formed lamellar phase (sample 12, D). At 70 °C in the most concentrated sample one micellar phase with interfering particles is seen. Being formed at high temperatures from the third lamellar phase, it is likely to be of inverted type.

The SAXS patterns of the liquid crystal phases show in some cases the possibility that the organisation in domains holds across all the phase diagram. In the case of the hexagonal phase only one phase is observed, on the other hand we observe two cubic and at least two lamellar phases at the same temperature. If we accept the hypothesis of E and Z isomers organising in separate phases, the evidence of the hexagonal case could be ascribed to E and Z rods organised in a single hexagonal lattice. NMR experiments are still going on in order to have a more complete picture of the phase diagram of surfactant 1.

References:

[1] S. Borocci, G. Cerichelli, L. Luchetti, G. Mancini,(1999):Conformational Behaviour of Aqueous Micelles of SodiumN-Dodecanoyl-L-prolinate. *Langmuir* **15**, 2627-2630.
[2].J. Bella, S. Borocci, G. Mancini, (1999):Recognition in Organized Aggregates Formed by a Chiral Amidic Surfactant *Langmuir* **15**, 8025-8031.
[3] G. Cerichelli, L. Luchetti, G. Mancini, (1997): Conformational Behaviour of Aqueous Micelles of Sodium N-Dodecanoyl-N-methylglicinate. *Langmuir* **13**, 4767-4769.
[4] T.Zemb, P. Chaprin, (1985): Micellar Structure from Comparison of X-ray and Neutron Small-Angle Scattering. *J. Physique* **46**, 249-256.

SAXS/WAXS STUDY OF REAL-TIME CRYSTALLINE DENSITY AND CRYSTALLINITY EVOLUTION OF PEO IN PEO/PMMA BLENDS

J. Baldrian[1], M. Horký[2], M. Steinhart[1], P. Laggner[3], H. Amenitsch[3] and S.Bernstorff[4]

1.) Institute of Macromolecular Chemistry, Academy of Sciences of the Czech Republic, Heyrovsky Sq.2, 162 06 Prague, Czech Republic
2.) Faculty of Nuclear Sciences and Physical Engineering, Czech Technical University, V Holešovickách 2, 180 00 Prague 8, Czech Republic
3.) Institute of Biophysics and X-ray Structure Research, Austrian Academy of Sciences, Steyergasse 17, 8010 Graz, Austria
4.) Sincrotrone Trieste, Basovizza, 34012 Trieste, Italy

The simultaneous real-time SAXS/WAXS measurements at ELETTRA offered a very useful possibility – to see the development of the structure on two levels of dimensions characterizing the molecular structure (WAXS) and long-range order (SAXS). Our first step of such study was concentrated on the early stages of structure formation in a PEO/PMMA blend which proceeds after a temperature jump from 80 °C, homogeneous melt to crystallization temperature. The structure formation in this system starts with spinodal decomposition, which is followed by crystallization [1].

This study is aimed at a better understanding of structure formation during crystallization. The isothermal melt crystallization of a PEO3000/PMMA4000 blend at 40 °C was studied. From scattering curves, the real-time changes of SAXS scattering invariant Q_{SAXS} and WAXS crystallinity Cr were obtained. It was shown [2,3] that crystallization concerns the PEO component only, PMMA is completely segregated outside the PEO phase.

The relation between invariant Q_{SAXS} and crystallinity Cr is

$$Q_{SAXS} = Cr(1-Cr)(\rho_{cr} - \rho_{am})^2 = Cr(1-Cr)(\Delta\rho)^2, \qquad (1)$$

where ρ_{cr} and ρ_{am} are respectively the electron densities of the crystalline and amorphous phases and Cr is the volume crystallinity. From Fig.1 it follows that the measured Q_{SAXS} values pass through a maximum. The reason is, that product Cr(1-Cr) has a maximum for the volume crystallinity 0.5 and crystallinity of PEO crosses this value during crystallization. In such case, it is possible to put the relative crystallinity values obtained from WAXS into absolute scale, volume fractions. In Fig.1, the time dependence of Q_{SAXS} and Cr(1-Cr) are compared. The different courses of these parameters reflect real-time changes of the square electron density difference (1). The square root of the ratio

$$\sqrt{Q_{SAXS}/Cr(1-Cr)} \approx \rho_{cr} - \rho_{am} = \Delta\rho \qquad (2)$$

represents development of electron density difference between the crystalline and amorphous phases of PEO. Since the amorphous density of PEO does not change during crystallization, $\Delta\rho$ is proportional to the real-time development of density of the crystalline phase. Using the known density of amorphous phase (1.124 gcm^{-3}) and the crystallographic density of the crystalline phase (1.239 gcm^{-3}), the changes in crystalline density of PEO can be reasonably scaled. The result of scaling is plotted in Fig.2. During crystallization, the density of the crystalline phase changes in two steps.

During spinodal decomposition, the homogenous one-phase polymer blend separates in two noncrystalline phases with different concentrations of PMMA molecules and probably also two pure PEO phases differing in the content of crystallizable and noncrystallizable stems of PEO molecules. In the first step of crystallization, the crystalline density and crystallinity of PEO very steeply grow, but the lamellar periodicity does not change. The phase-separated regions, which are able to crystallize, form very thin and very distorted crystalline lamellae

separated by thick amorphous interlayers. The density and thickness of crystalline lamellae increase very quickly at this stage. When the lamellar structure corresponding to the thermodynamic conditions of crystallization is practically settled, a second step starts, a very slow growth of crystalline density and crystallinity. In this step, the structure of the crystalline phase gradually improves and crystallinity grows very slowly.

Research supported by Grant Agency of the Czech Republic No.:106/99/0557

References:

[1] Baldrian, J.,Horky, M.,Steinhart, M.,Laggner, P.,Amenitsch & H., Bernstorff S.: Time-resolved SAXS/WAXS study of phase behaviour and nucleation in polymer blends. *J.Polym.Sci.,Polym.Phys.* in preparation.

[2] Baldrian ,J., Horky, M., Sikora, A., Steinhart, M., Vleek, P., Amenitsch, H. & Bernstorff S.(1999): Time-resolved SAXS study of crystallization of poly(ethylene oxide)/poly(methyl metacrylate) blends. *Polymer* **40**, 439-445.

[3] Baldrian, J., Horky, M., Steinhart, M., Sikora, A., Vleek, P., Amenitsch, H. & Bernstorff S.: Time-resolved SAXS/WAXS study of polymer blends crystallization. *Proc. SPIE Int. Soc. Opt. Eng.*, in press.

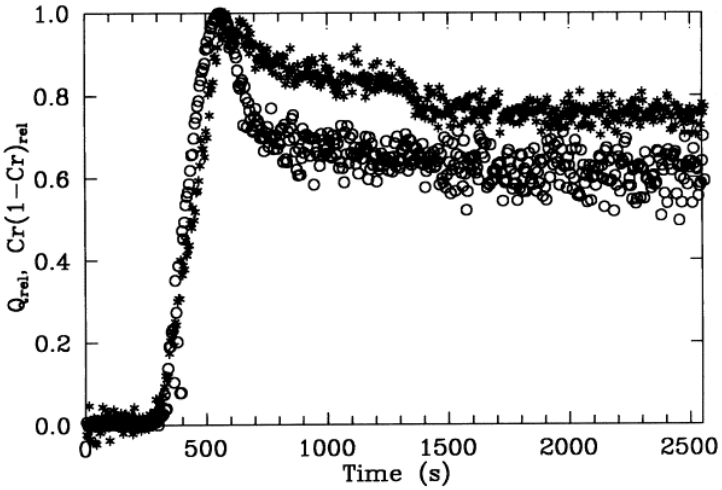

Figure 1. Comparison of real-time changes of scattering invariant Q_{SAXS} (*) and crystallinity term Cr(1-Cr) (o) during isothermal melt-crystallization of PEO3000/PEO4000 blend at 40 °C

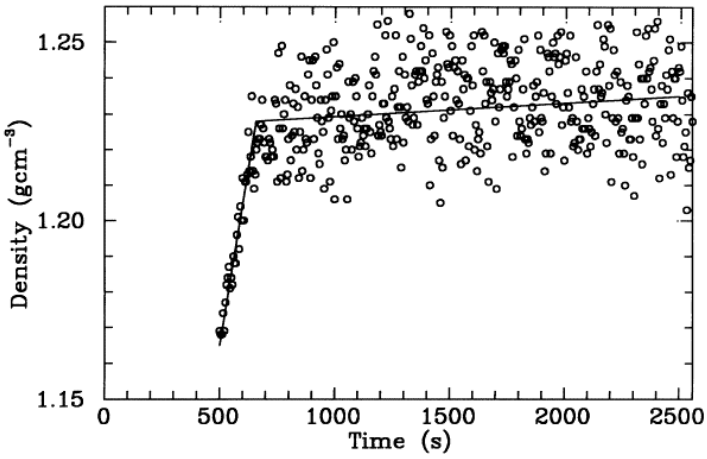

Figure 2. Real-time evolution of crystalline density of PEO in PEO3000/PMMA4000 blend during isothermal melt-crystallization at 40 °C

EMULSIFICATION BY TEMPERATURE CHANGE FOLLOWED BY TIME RESOLVED SAXS

J. Caelles[1], I. Carrera[1] , H. Amenitsch[2] and R. Pons[1]

1.) IIQAB, CSIC, Jordi Girona 18-26, Barcelona 08034, .Spain
2.) Institute for Biophysics and X-ray Structure Research, Austrian Academy of Sciences, Graz Austria.

Emulsions are present in a wide range of products and processes, e.g. pharmaceuticals, papermaking, cosmetics, paints, etc (1). Understanding the processes of emulsification can allow for a better control of their properties. Low energy emulsification methods have attracted increasing interest, not only because of energy savings, but also as a way to control their properties (e.g. particle size and stability). Two promising methods of emulsification have been proposed. a) Phase transition by temperature change (2) and b) phase transition by mixing two different phases (3).

We have followed the process of spontaneous emulsification by temperature change from a one-phase solution. Through the heating process the equilibrium system has several structures. Those can be followed by their scattering patterns. In figure 1 a sample which initially has a bicontinuous structure (L3 phase) is heated to 40ºC at which the system corresponds to an emulsion that at equilibrium separates in two phase (almost pure water and a water-in-oil microemulsion). The peak appearing at q~0.4nm-1 corresponds to the microemulsion structure peak. As the temperature increases the intensity at low q (corresponding to the bicontinuous structure) decreases its intensity. At the same time the slope at this low q increases tending to a q-4 behaviour. This low q behaviour corresponds to the Porod limit due to the water-microemulsion interfaces that constitute the emulsion droplets.

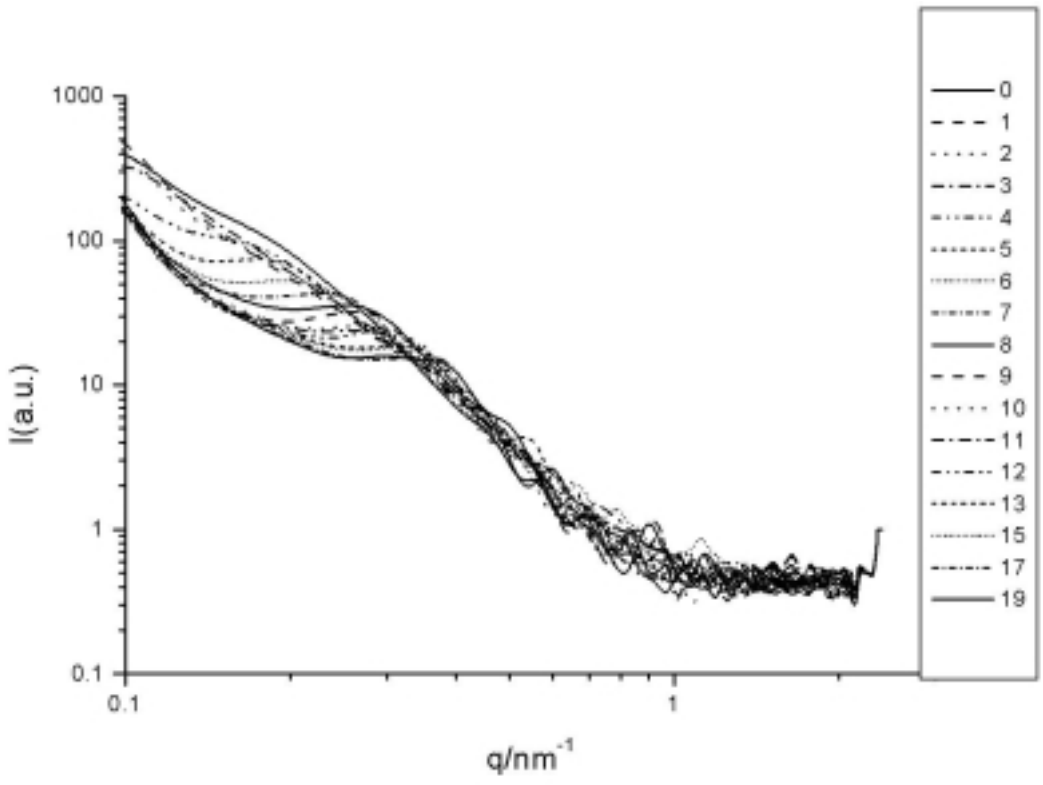

Figure 1. X-ray scattering pattern of emulsion formation from 7ºC to 40ºC as a function of time.

Figure 2 shows the spectra of three emulsions prepared from different initial temperature. The intensity at low q is slightly different, suggesting a bigger total interface (lower radius) for the sample that was heated from 7º. On the other hand, the microemulsion peak shifts to higher q the higher the initial temperature. This means that at this time (about 5 minutes) the microemulsion phase has not yet reached equilibrium.

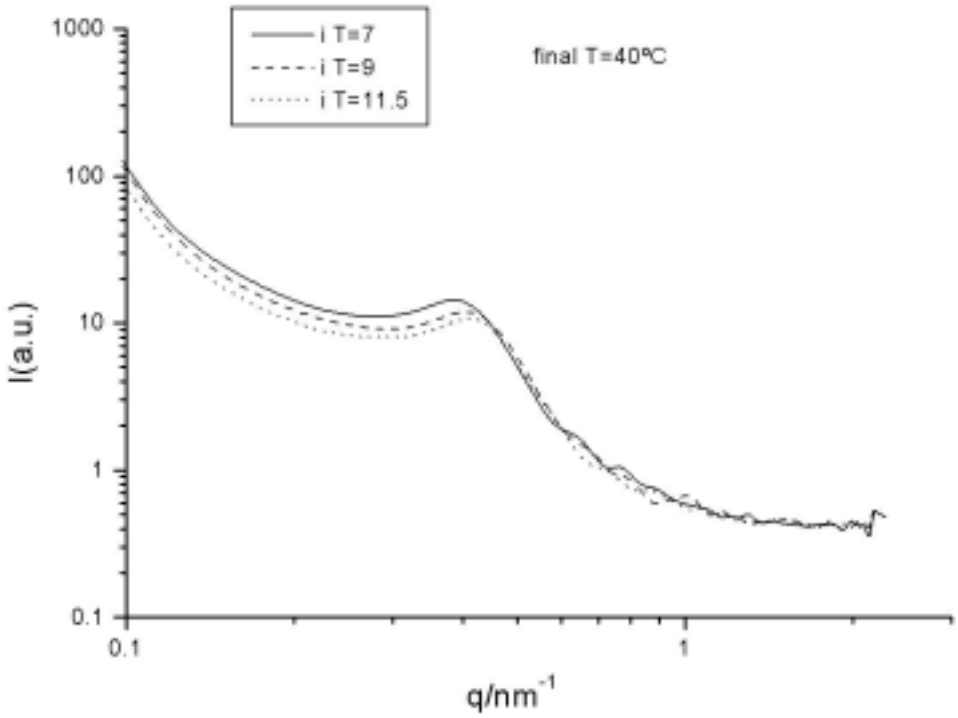

Figure 2. X-ray scattering pattern of emulsions after 5 min. formed at 40ºC from three different initial temperatures.

References:

[1] Becher, P. (Ed.) (1983): "Encyclopedia of Emulsion Technology", Vol 1.Marcel Dekker Inc., N.Y..

[2] Shinoda, K., Saito, H. (1969): *J. Colloid Interface Sci*. **30**: 258.

[3] Miller, C.A. (1988): "Spontaneous Emulsification Produced by Diffusion- A Review", *Colloids Surfaces* **89**: 29.

SAXS STUDIES ON NEW POLYSACCHARIDES DERIVATIVES

R. Gianni[1], F. Delben[1], G. Liut[1], R. Rizzo[1], A. de Nooy[2], S. Bernstorff[3] and P. Dubcek[3]

1.) Dipartimento di Biochimica, Biofisica e Chimica delle Macromolecole, Universita' di Trieste, Via L. Giorgieri 1, 34127 Trieste, Italy.
2.) Dipartimento di Chimica, Universita' "La Sapienza", Piazzale A. Moro 5, 00185 Roma, Italy
3.) Sincrotrone Trieste, S.S. 14 km 163.5 in Area Science Park, 34012 Basovizza, Trieste, Italy

Aqueous gels are materials of technological relevance and their use is continuously increasing [1,2]. The formulation of chiral matrices in biotechnology and the synthesis of "molecularly imprinted matrices" are among the most advanced uses. In addition to this, there is a need for the so-called "intelligent materials" which are able to give specific responses (e.g. volume changes, rapid contractions, etc) as a function of external stimuli. In this picture, polysaccharidic gels are particularly relevant.

Synthetically modified fungal polysaccharides were obtained in our laboratory in order to produce new polymeric chains exhibiting either positive or negative charge density. The research was aimed at the synthesis of polymers able to interact within each other and possibly to give rise to gelling systems. Scleroglucan, exhibiting $\beta(1\rightarrow3)$ linked saccharidic units, was selected as representative of a rigid rod-like chain, whilst pullulan, containing both $\alpha(1\rightarrow4)$ and $\alpha(1\rightarrow6)$ linked glucose units, was representative of flexible chains.

Carboxylated and aminated polysaccharide chains were obtained first producing cyanoethyl-derivatives and either hydrolysing or reducing them, as the second step. Alternatively, carboxyethyl and aminopropyl derivatives were obtained by direct SN_2 substitution. The chemical characterisation of the semi-synthetic polysaccharides was carried out by means of NMR, FT-IR, potentiometric titration and elemental analysis. Possible modifications of the polymer molecular weight were detected by means of high pressure gel permeation chromatography.

Both the equilibrium and rheological solution properties of the derivatives obtained strongly depend on the conformational behaviour of the polymeric chain. In addition to this, it is well known that the gelling ability of polysaccharides depends on their capacity to assume ordered secondary structures. We used the SAXS beamline at the ELETTRA synchrotron machine to get information on the shape of both the native and the modified macromolecules in different solvents. The results obtained on native and cyanoethylated scleroglucan are hereafter reported.

Both polymers exhibited a linear behavior of the angular dependence of the scattering curves when $\mathbf{log(I*h)}$ was plotted as a function of $\mathbf{h^2}$ (Fig. 1). Therefore, the polymers investigated could be considered as rigid rods. The slope of the straight line gave the value of the dross-sectional radius, $\mathbf{R_c}$. For a uniform rod of radius $\mathbf{R}$, $\mathbf{R_c}$ is given by $\mathbf{R_c=R/\sqrt{2}}$. The diameters of the rods ($\mathbf{D=2R}$) are reported in Table 1.

X-ray diffraction data obtained on scleroglucan fibres [3] showed that the dimensions of the hexagonal cell containing the triple helix structure were 17.3 Å for both **a** and **b** axes located in a plane perpendicular to the fibre axis. This number represents the distance between two triple-helix axes in adjacent cells and can be considered, in good approximation, as the diameter of the triple-helix rod. The figures obtained for scleroglucan by SAXS measurements both in water and in 0.01 M NaOH, where the polymer is present as triple helix, are in very good agreement with the crystallographic findings (Table 1). The **R** value obtained for native scleroglucan in dimethylsulfoxide (7.0 Å, Table 1) could be consequently considered as the diameter of the scleroglucan single chain.

Cyanoethyl-scleroglucan exhibited low **R** values: 9.6 Å at pH 11.5 and 7.3 in DMSO (Table 1). Therefore, even in 0.01 M NaOH, where native scleroglucan is able to give a triple-helix

structure, the cyanoethylated sample exhibited a rod diameter only slightly higher than that found in DMSO. In agreement with capillary viscosity data, this increase of the polymer chain diameter very likely indicates the presence of some molecular aggregation which, at pH values lower than 10, is responsible for micro-gel formation. The physico-chemical properties of the gel obtained are still under investigation.

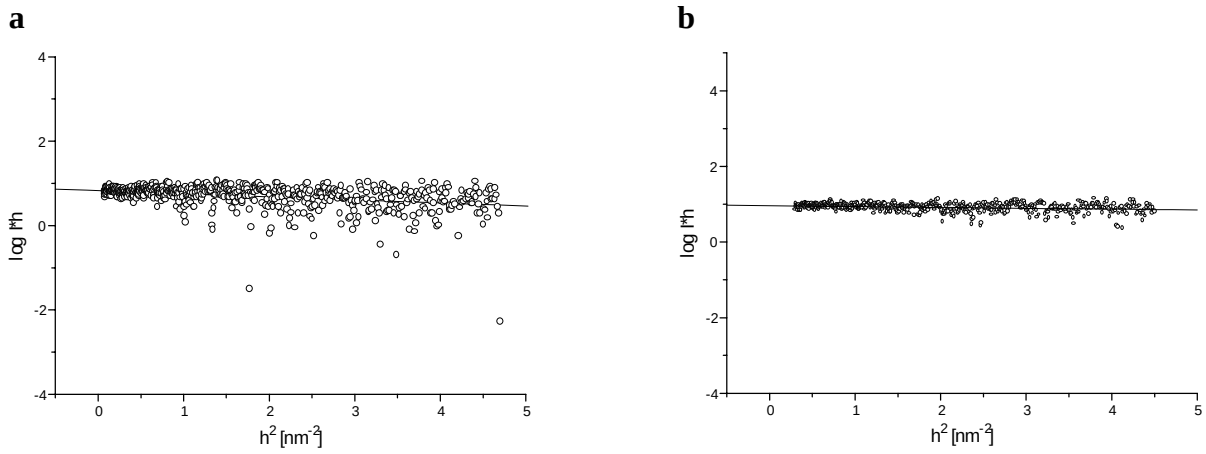

Figure 1. Guinier plots for: **a**) native scleroglucan (polymer concentration: 0.25 w/v in 0.01 M NaOH); **b**) cyanoethyl scleroglucan (polymer concentration: 0.3 % w/v in 0.01 M NaOH)

Table 1. Diameters of the polymer chain cylinders as determined by SAXS.

Sample	**Polym. Conc. (%w/v)**	**Solvent**	**D (Å)**
Native scleroglucan	0.15	Water	17.8-19.1
Native scleroglucan	0.25	0.01 M NaOH, (pH 11.5)	16.4
Native scleroglucan	0.25	DMSO	7.0
cyanoethyhl scleroglucan	0.30	0.01 M NaOH (pH 11.5)	9.6
cyanoethyhl scleroglucan	0.30	DMSO	7.3

References:

[1] Yalpani M. (Ed.). (1987): *Industrial Polysaccharides. Genetic engineering, structure/properties relations and applications*. Elsevier, New York.

[2] Whistler R.L. & BeMiller J.N. (Eds.). (1993): *Industrial gums*. Academic Press, San Diego.

[3] Bluhm T., Deslandes Y., Marchessault R.H., Perez S. & Rinaudo M.. (1982): *Carbohydr. Res.* **100**, 117-130.

KINETICS OF LIPOSOME-SURFACTANT INTERACTION: A STUDY BASED ON SMALL ANGLE X-RAY SCATTERING

O. López[1], M.Cócera[1], A. de la Maza[1], H. Amenitsch[2] and R. Pons[1]

1.) IIQAB-CSIC, Jordi Girona 18-26 08034 Barcelona, Spain
2.) Institute of Biophysics & X-Ray Structure Research, Austrian Academy of Sciences, Graz, Austria.

Liposomes are lipid-water systems, which have come into widespread use as a simplified model of biological membranes and delivery systems. In this sense, the study of their interaction with surfactants (understood as the vesicle to micelle transition) is currently attracting much interest. In previous papers we investigated this transition vesicle to micelle induced by surfactants from a structural viewpoint [1,2] that raised a number of questions about the kinetics. Dynamic Light Scattering and Freeze fracture electron microscopy were performed to investigate this kinetic aspect [3,4]. In these works, the time needed for the formation of mixed micelles could be detected. However, these techniques were unable to detect the initial adsorption of surfactant monomers due to the fast rate of this process.

In order to elucidate this problem, the use of a more sensitive technique, in which the experimental timescale was short enough to detect the initial steps of the interaction liposome-surfactant, was necessary. Thus, the SAXS instrument at ELETTRA for time resolved was used. The experiments were performed using a stopped flow cell that it allowed us to study in detail the evolution with time of liposome solubilization.

Three different populations of liposomes slightly charged (non-ionic, anionic and cationic behaviour) and three types of surfactants (non-ionic, anionic and cationic) were used. The diffraction spectra were obtained every 0.1 sec for the first 50 sec of interaction liposome-surfactant, every 0.5 sec for the following 150 sec, and from this time to the end every 1 sec. The kinetic was studied for 6-8 min at 25 ^{o}C. In addition, X-ray diffraction experiments of solutions containing pure liposomes and pure micellar solutions were carried out. In general terms, the X-ray diffraction patterns indicate that both the adsorption of surfactant on the liposomes and the release of mixed micelles from the vesicle surface depends on the liposome and surfactant electrostatic charges. This fact is observed in Fig. 1, which shows x-ray spectra corresponding with two systems composed by liposomes containing phosphatidic acid (slightly negative charge) and two surfactants, the cationic dodecyl trimethylammoniun bromide, DTAB, (Fig. 1A) and the anionic sodium dodecyl sulfate, SDS, (Fig. 1B). These spectra were taken some minutes after mixing liposomes and surfactant, as is indicated in the legend. When the liposome and the surfactant had got different charges, our results seem to indicate a faster adsorption of surfactant and a slower of mixed micelle release than in the case of liposome and surfactant equally charged. This fact could be attributted to a balance between the repulsion/attraction electrostatic effect of the particles formed during the solubilization process. These results offer a promising approach that could enhance our understanding on the stabilization of surfactant-lipid vesicles and surfactant-lipid micelles.

References:

[1] López O., de la Maza A., Coderch L., López-Iglesias C., Wehrli E., Parra J.L.,Direct formation of mixed micelles in the solubilization of phospholipid liposomes by Triton x-100, 1998, FEBS Lett., 426, 314-318.
[2] López O., Cócera M., Wehrli E., Parra J.L., de la Maza A., Solubilization of liposomes by sodium dodecyl sulfate: New mechanism based on the direct formation of mixed micelles, 1999, Arch. Biochem. Biophys., 367(2), 153-160.

[3] López O., Cócera M., Pons R., Azemar N., de la Maza A., Kinetic studies of liposome solubilization by sodium dodecyl sulfate based on a dynamic light scattering technique, 1998, Langmuir, 14(16), 4671-4674.
[4] López O., Cócera M., Pons R., Azemar N., López-Iglesias C., Wehrli E., Parra J.L., de la Maza A.,Use of a dynamic light scattering technique to study the kinetics of liposomes solubilization by Triton X-100, 1999, Langmuir, 15(13), 4678-4681.
[5] López O., Cócera M., de la Maza A., Amenitsch H., Pons R., in preparation

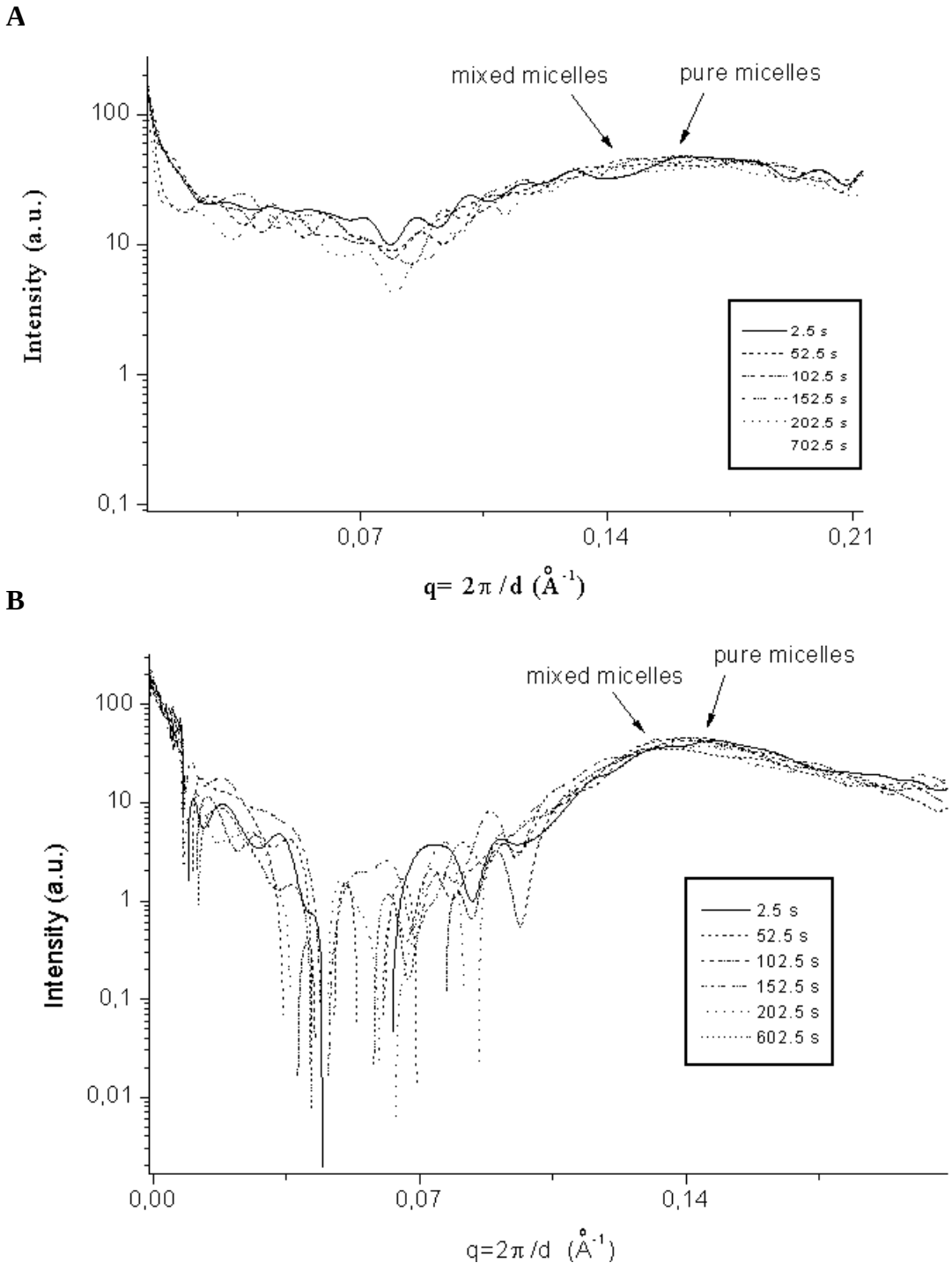

Figure 1. Time resolved X-ray patterns corresponding with two systems: liposome-DTAB (A) and liposome-SDS (B)

TIME-RESOLVED SAXS AND WAXS STUDIES OF CRYSTALLIZATION OF PEO INDUCED BY HIGH PRESSURE

M. Steinhart[1], J. Baldrian[1], M. Kriechbaum[2], M. Horký[3], H. Amenitsch[2], P. Laggner[2] and S. Bernstorff[4]

1.) Institute of Macromolecular Chemistry, Academy of Sciences of the Czech Republic, Heyrovsky Sq.2, 162 06 Prague, Czech Republic
2.) Institute of Biophysics and X-Ray Structure Research, Austrian Academy of Sciences, Steyrergasse 17, 8010 Graz, Austria
3.) Faculty of Nuclear Science and Physical Engineering, Czech Technical University, Prague, V Holešovickách 2, 180 00 Prague 8, Czech Republic
4.) Sincrotrone Elettra, Basovizza, 34012 Trieste, Italy

Crystalline low-molecular poly(ethylene oxide) PEO exhibits a stable structure where the polymer chains are integrally folded (IF) or fully extended (EC) in lamellas. Our time-resolved SWAXS synchrotron measurements based on isothermal crystallization from melt at various temperatures below the melting point have verified interesting behavior in the early stages of crystallization. It has been shown that an intermediate structure characterized by Bragg distances corresponding to non-integrally folded chains (NIF) shortly appears[1]. Further, we have been able to make conclusions about the priority-in-time of microphase separation to crystallization from simultaneous dynamic SAXS and WAXS measurements[2].
Precise evaluation of these effects is, however, biased by the development of temperature in time and existence of its gradients in the case of isothermal crystallization after a temperature jump. This led us to perform measurements where temperature is kept constant and crystallization is induced by a pressure change. In this approach thermodynamic conditions within the sample are more homogeneous and equilibrium is reached considerably faster. Moreover using the possibility of depressurizing, also effects accompanying melting are easily accessible.
Due to the stage of development of high-pressure experiment our measurements were affected by mixing of the sample with the pressurizing medium. In our particular case PEO dissolves in water. This leads to difficulties in reproducibility of experiments. In spite of that we came to some interesting conclusions as follows:

a) crystallization behavior depends both on temperature and history of the sample
b) at a temperature sufficiently close to the melting point NIF structure appears even after repeated pressurizing while at lower temperatures only IF or EC peaks are measurable after the second and higher pressurizing cycle
c) with increasing temperature the crystallization is slower and melting faster but the latter strongly depends on history of the sample
d) during melting the structure visible in the SAXS region disappears faster than that visible in the WAXS region

These results indicate that it is very likely that after solving the problem of separation of the sample from the pressurizing medium valuable data on the crystallization and melting effects will be obtained, especially, by comparing the behavior in the SAXS and WAXS region.

Research supported by the Grant Agency of the Czech Republic (Grant No. 106/99/0557)

References:

[1] Baldrian, J., Horky, M., Steinhart, M., Sikora, A., Vleek, P., Amenitsch, H. & Benstorff, S.(1999): Time-resolved SAXS study of crystallization of poly(ethylene oxide)/poly(methyl metacrylate) blends. *Polymer* **40**,439-445.

[2] Baldrian, J., Horky, M., Steinhart, M., Laggner, P., Vlyek, P., Amenitsch, H. & Benstorff, S. (1999): Ordering phenomena in PEO/PMMA blends during crystallization. 11th International Conference on Small-Angle Scattering, Abstract p.193.

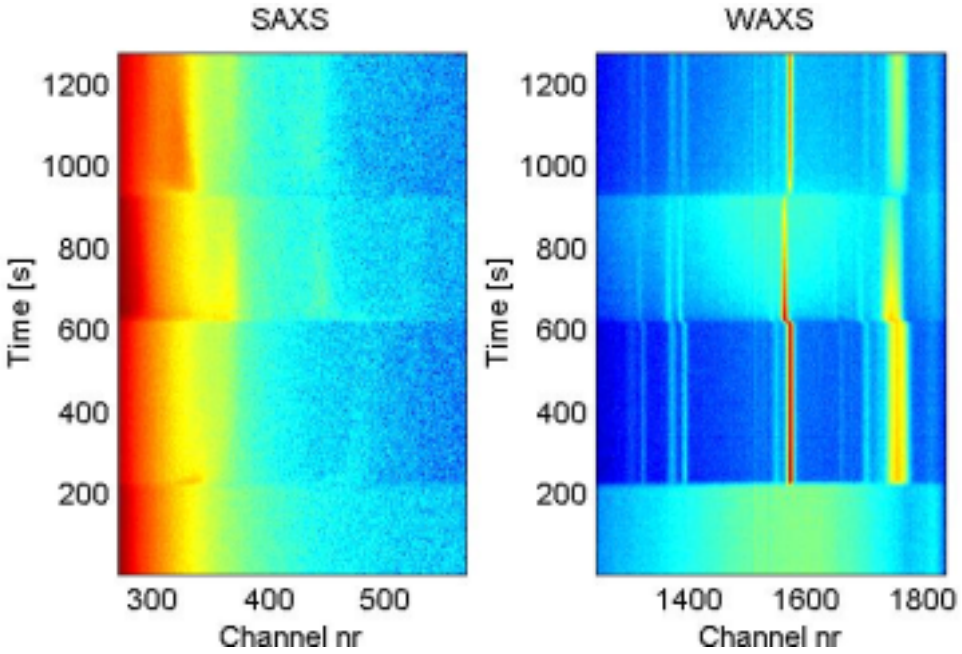

Figure 1. Time-resolved SWAXS measurement at 52° C with pressure jumps between 1 bar and 2 kbar. After the first pressurizing at 210 s the NIF structure shortly appears around the channel 330. It eventually recrystallizes to the IF structure. After depressurizing at 625 s the sample melts. In the WAXS region immediate expansion of the structure followed by much slower melting can be seen. After the second pressurizing at 900 s the structure develops differently than after the first one.

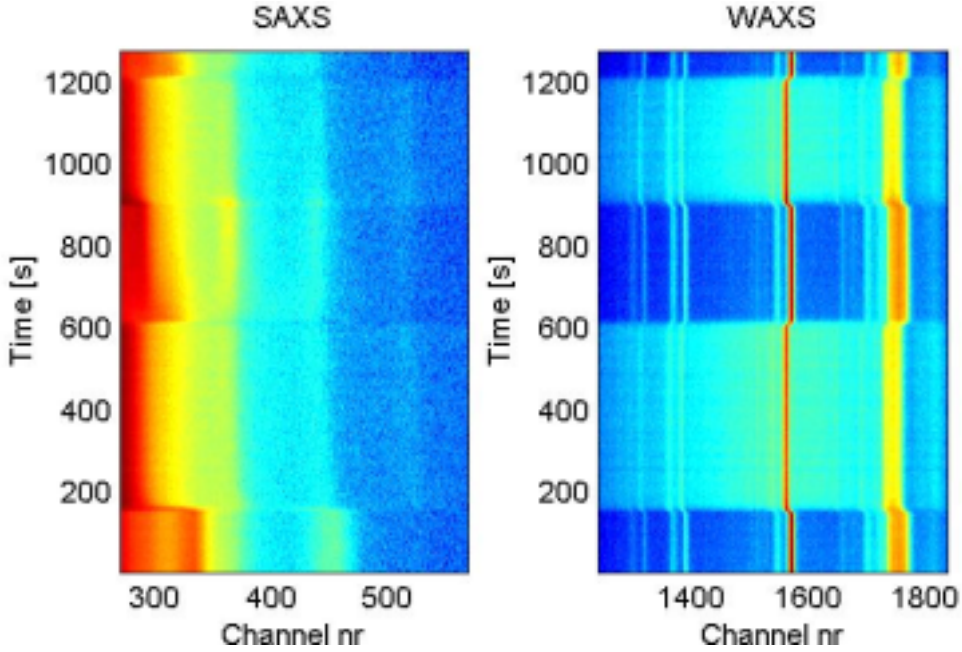

Figure 2. Similar experiment at 50° C. After depressurizing at 150 s and 900 s fast melting is visible only in the SAXS region while WAXS shows mainly the expansion. After pressurizing at 600 s and 1200 s the same structure is reached.

AGGREGATION PROCESSES OF BLOCK COPOLYMERS IN AQUEOUS SOLUTION

R. Triolo[1], A. Triolo[2], F. LoCelso[1], L. Crapanzano[1] and C. Di Giovanni[1]

1.) Dipartimento di Chimica Fisica, Universita' di Palermo, V.le delle Scienze, Parco d'Orleans II I-90128 Palermo, Italy
2.) BENSC - HMI Berlin Glienickerstr. 100 D-14109 Berlin, Germany

Polymeric surfactants are currently attracting a great deal of interest, because of their commercial relevance and novel physical behavior. In particular PolyEthylene Oxide (PEO) – based block copolymers are of extreme interest due to their potential (and in some case, effective) application for drug release in vivo and similar smart applications. Consequently a detailed knowledge of the nature of the phase diagram is requested for these materials, to understand and possibly foresee their properties in unusual conditions as a function of different external parameters (e.g. temperature, pressure, salt content etc).

We report on SAXS experiments run over aqueous solutions of two PEO-based block copolymers, namely PEO-PMMA and PEO-PS. This kind of systems shows the well-known behavior of micellar aggregation when the solvent is selective towards one of the two different moieties of the coblock. In particular the high affinity of PEO chains towards water induces the formation of classical core-shell micelles, with a PEO shell and a hydrophobic PS or PMMA core. We have investigated this behavior by means of Small Angle Neutron Scattering at few selected temperatures in the range 20-70 C and in a wide composition range 0.01-20 % w/w. Most of these investigations have been also conducted as a function of the contrast, by simply changing the ratio D_2O-H_2O of the solvent. This approach allows a detailed characterization for the structural model of these aggregates at the different temperatures, in terms of micellar core and shell sizes, composition of the two regions, amount of solvent inside the micellar aggregate etc. [1]. Once this detailed information is fully available, a complete interpretation of the large information coming from synchrotron based measurements would be easily obtained. In other words, we are now in the process of applying the SANS based structural model (which has been based on a contrast investigation, and then is highly reliable), to the SAXS patterns we have been collecting scanning the temperature from 20 to 90 C. In this way any detail in the mesoscopic size scale should be characterized in a large temperature range which corresponds to the one where these solutions would be of practical use.

During the SAXS beam time we were able to collect data over a large composition range (0.06 – 20 % w/w) for two kinds of block copolymers, namely PEO-PMMA 1000-1000 and PEO-PS 1000-1000, where the numbers refer to the molecular weight of the different moieties. In Figure 1 and 2, we report the temperature dependence of the SAXS pattern for 20 % w/w solutions of PEO-PS and PEO-PMMA coblocks. The existence of a well-defined interference peak corresponding to the micellar structural organization can be evidenced. A detailed knowledge of the structural parameters of these aggregates is highly interesting for a number of reasons. We have recently been awarded with a scholarship for running a series of X-ray PCS measurements on these very solutions. These measurements would be run at the coherent SAXS station at ESRF, and they would provide slow dynamics details of the motion of the aggregates. This information would nicely compare with viscosity and light scattering measurements, which are currently in progress.

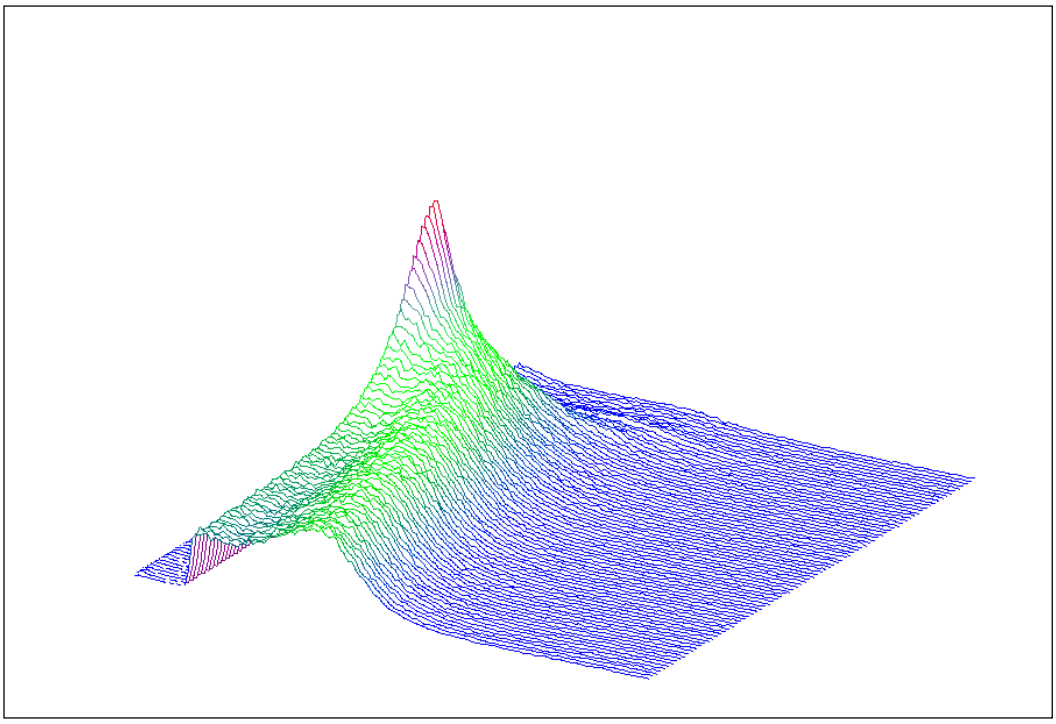

Figure 1. Temperature dependence of the SAXS profile for a PEO-PMMA 1k-1k aqueous solution at 20% w/w concentration.

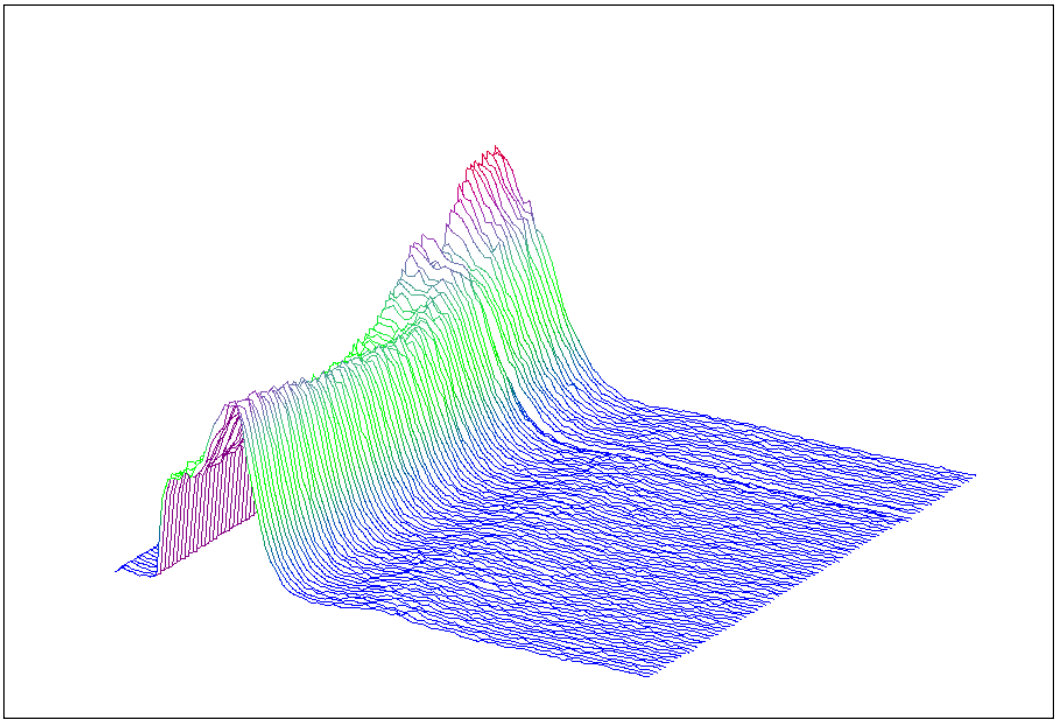

Figure 2. Temperature dependence of the SAXS profile for a PEO-PS 1k-1k aqueous solution at 20% w/w concentration.

References:

[1] see e.g. Triolo, R. et al. (1996): *Science* **274**, 2049.

IPP BLENDS: PHASE DIAGRAM AND CRYSTALLIZATION KINETICS VIA COMBINED SAXS-WAXS TECHNIQUES

R. Triolo[1], A. Triolo[2], F. LoCelso[1], L. Crapanzano[1] and C. Di Giovanni[1]

1.) Dipartimento di Chimica Fisica, Universita' di Palermo, V.le delle Scienze, Parco d'Orleans II I-90128 Palermo, Italy
2.) BENSC - HMI Berlin Glienickerstr. 100 D-14109 Berlin, Germany

Taking advantage of the high brilliance of synchrotron sources it is nowadays possible to thoroughly investigate the nature of the phase diagram of complex systems in very rapid experiments. In particular, in the case of polymer materials, due to the slow dynamics of the entangled molecules, only a pseudo-equilibrium phase diagram can be obtained; however, even in this situation a considerable amount of information can be derived.
In the reported experiments we investigated a large amount of samples of pure isotactic polypropylene and its blends with small additive molecules. In particular, we studied 4 different samples of iPP, which were obtained with different procedures (by means of different Montell catalysts) and blends of iPP with hydrogenated cyclo-pentadiene (HOCP) and hydrogenated stryrene-co-indene (HSI) in different amounts. The experiments have been carried on at the end of december so only limited time has been available for detailed data analysis, nevertheless relevant observation can be made even at this stage.

The investigation of the different neat iPP samples led to the discovery of interesting differences in the temperature dependence of the morphology both in the SAXS and in the WAXS patterns. In particular substantial differences exist in the WAXS region, see Figure 1, indicating that the different catalysts produced materials whose structural and thermodynamic properties are different. Attempts to relate these findings to other experimental evidences (i.e. results from DSC etc) are currently in progress.

We had already thoroughly investigated the morphology of iPP-HOCP blends by means of conventional SAXS and SANS [1,2]. This mixture revealed a complex phase diagram showing a miscibility gap. In order to gain further details concerning the nature of the phase diagram we run combined SAXS-WAXS measurements on iPP-HOCP mixtures applying a temperature profile from room temperature to 220^{o}C, see Figure 2. A detailed set of measurements is now available at different compositions of the mixtures. This refined composition grid allows to get a detailed picture of the shape of the miscibility and to relate its occurrence to the nature of the components. We are now in the progress of data interpreting, trying to relate the nature of the miscibility gap to the occurrence of thermodynamic transitions both for iPP and HOCP. In particular, by combining SWAXS with different other experimental techniques, we are now exploring the possibility that the overall miscibility gap might be related to the occurrence of relaxation features in the HOCP additive, as evidenced by NMR technique [3].

iPP-HIS mixtures have also been investigated by means of combined SAXS-WAXS. This system has been found to show interesting features in common with iPP-HOCP mixture, in particular it shows a miscibility gap very similar to the one reported for iPP-HOCP [4], see Figure 3. Accordingly we are now studying mixtures of the two systems, trying to compare them, aiming to find out the common elements, which determine the occurrence of a similar miscibility gap. We investigated the temperature dependence of the SAXS-WAXS pattern for a series of different compositions between 25 and 230^{o}C, aiming to characterize the phase

diagram features. Attempts to relate our recent findings to light scattering evidences [4] are currently in progress.

Unfortunately, it was not possible to develop the second portion of the proposed experiments, consisting in investigating the kinetics of crystallization on iPP-HOCP mixtures. This was due to technical problems at the station, which would have severely limited the amount of collected data, resulting in a waste of beam time. However recent improving at the beamline would now allow developing this kind of measurements, which would provide interesting information on the structural aspect of crystallization phenomena in polymers. Accordingly we are now going to apply for a continuation experiment fully devoted to crystallization phenomena.

Finally, we wish to report some successful feasibility tests, which we run at the SAXS beamline. We investigated the SWAXS pattern arising from poli di(n-alkyl) itaconates, (with alkyl=CH_3, $(CH_2)_nCH_3$, n=2, 10). These materials are polymers with very well defined sidechains, consisting of an alkyl chain of tunable length. We explored the dependence of the SWAXS pattern from the number of CH_2 units in the sidechain. For the first time, these materials have been structurally characterized and, although the reported measurements were only feasibility ones, interesting results have been obtained, see Figure 4. These latter are the subject of a communication sent to Macromolecules [5]. A more detailed investigation will be proposed, where a structural comparison between itaconates and poly (n-alkyl) metacrylates will be studied.

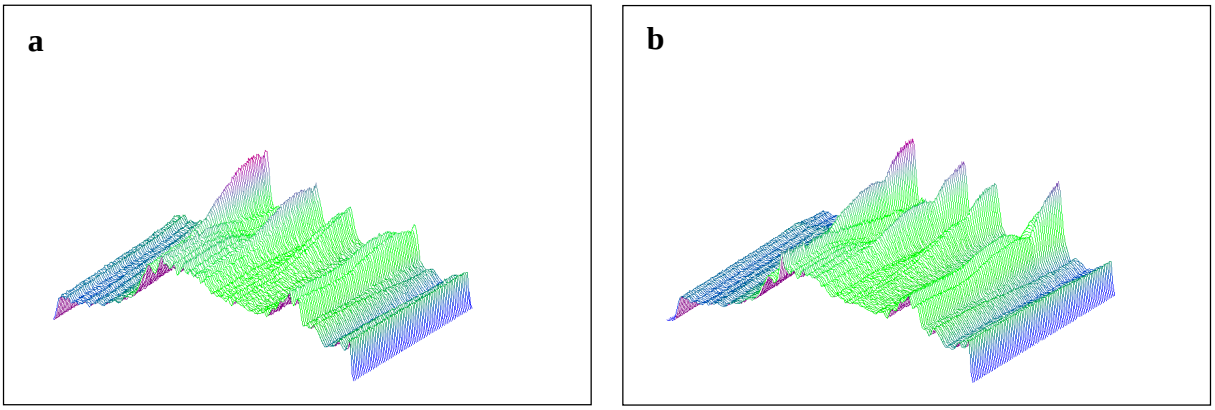

Figure 1. Comparison of the temperature dependence of the WAXS pattern for two different iPP samples, namely a) PS10 and b) Moplen35.

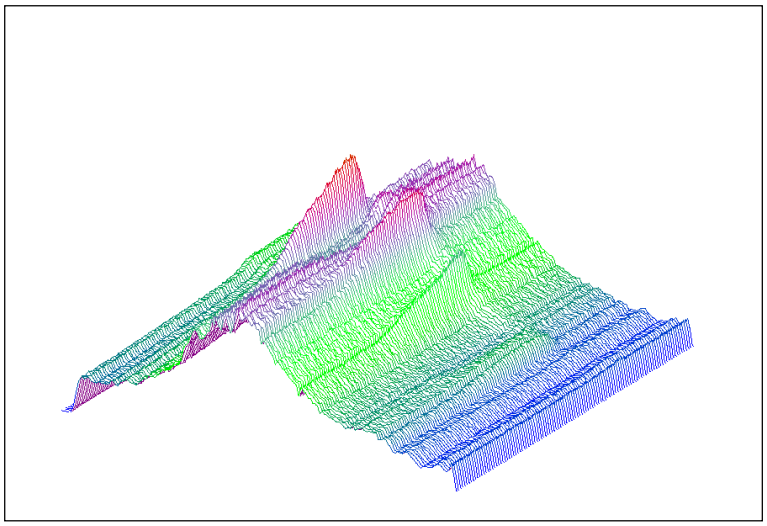

Figure 2. Temperature dependence of the WAXS pattern for a 50/50 iPP-HOCP blend: the developing of a WAXS peak occurs as the miscibility gap is entered.

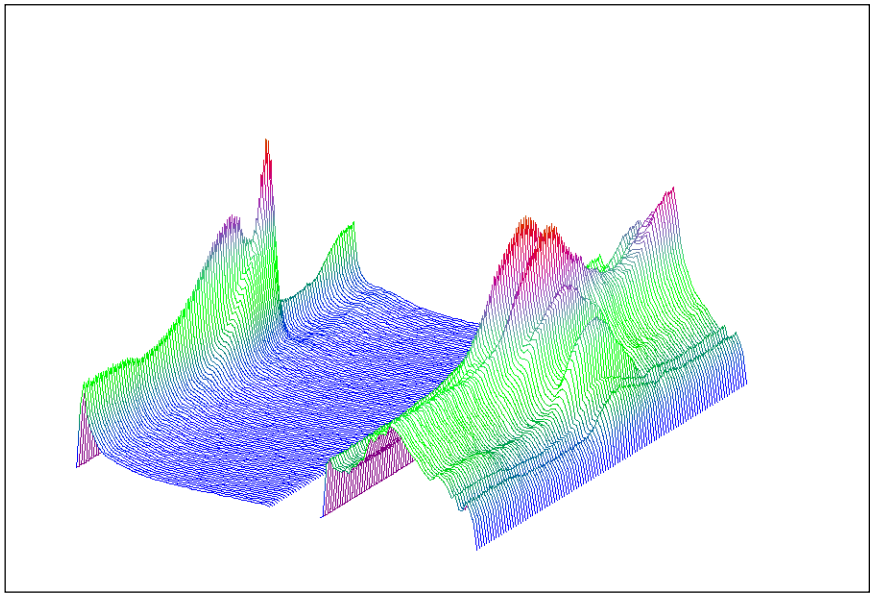

Figure 3. Temperature dependence of the SAXS-WAXS pattern for a 50/50 iPP-HSI blend: a dramatic structural evolution occurs when the miscibility gap is entered.

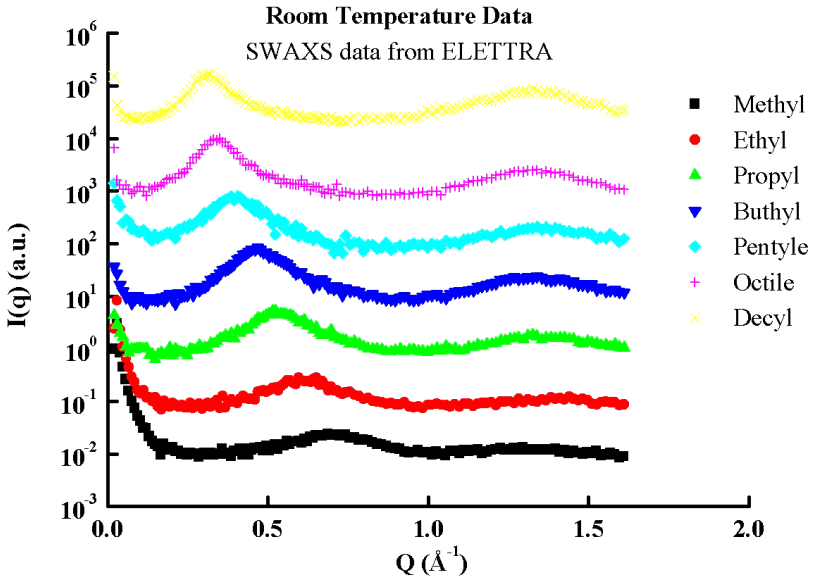

Figure 4. Room temperature SAXS-WAXS data collected for different itaconates with different length of the side chain, n. A linear dependence of the position of the first peak from n has been found [5].

References:

[1] Triolo, R. et al. (1998): *Polymer* **39**, 1697.
[2] Triolo, R. et al. (2000): *Polymer* **41,** 3751 and references therein.
[3] Triolo, R. et al. (2000): *Journal of Physical Chemistry* **B 104**, 510.
[4] Inoue et al.(1996): *Macromolecules* **29**, 4274.
[5] Triolo, R. et al., Macromolecules submitted.

5. Instrumentation

NEW X-RAY SURFACE DIFFRACTION CELL TO STUDY HIGHLY ALIGNED AND FULLY HYDRATED LIPIDS AND LB-FILMS UNDER VARYING SOLVENTS

H. Amenitsch[1], W. Jing[1], K. Lohner[1], M. Rappolt[1], S. Bernstorff[2] and P. Laggner[1]

1.) Insitute of Biophysics and X-ray Structure Research, Austrian Academy of Sciences, Steyrerg. 17, Graz, Austria.
2.) Sincrotrone Trieste, SS 14, Km 163.5, Basovizza, Trieste.

Lipids, especially phospholipids, are the main constituents of the biological membrane-matrix. Depending on the thermodynamic parameters (T, p, c) these lipids show a distinct morphology from lamellar, hexagonal to cubic phases.
Usually these systems are studied under physiological excess water conditions, which was up to now only possible with liposomes in solutions. The liposomes diffract like a rotational averaged powder pattern, which results in about 5 resolved diffraction orders. In contrary, highly aligned lipids on a Si or glass substrate show 10 to 20 orders. Unfortunately, the aligned lipids were hydrated in a 100% relative humidity environment, which gives rise to the so-called vapor pressure paradox, e.g. the d-spacing values reached under this conditions are always smaller, the transition temperatures are elevated and different mesophases are appearing compared with the liposomes [1].

Recently a neutron surface diffraction cell [2] has been developed, which allowed for the first time the study of aligned lipids or lb films under access water conditions. based on this cell a x-ray cell has been designed and tested at the austrian saxs beamline at elettra (see fig. 1).
Various lipids have been studied with this cell and the data show good agreement with the one measured with liposomes. A typical example of the obtained results is shown in fig. 2: a series of surface diffraction pattern of SOPE, which was ramped from 20 - 40 - 20 ºC with a rate of 1ºC/min. The diffraction peaks from the 2nd to the 6th order have been resolved clearly at fixed incidence angle ω (1.2º, for the notation see fig. 1). The upper resolution limit was just given by the dimension of the vacuum tube and the detector length. The phase transition L_β - L_α- L_β appearing at 25 ºC is clearly visible. The first diffraction order is strongly attenuated by the water layer and mylar window, and therefore, is not noticeable in the diffraction pattern.
The cell will be modified further to improve the performance and the user friendliness. The new cell will allow the following experiments:

- Stopped flow of the solvent on aligned lipids to study e.g. the influence of peptides on lipid bilayers.
- Highly aligned self-assembly of supramolecular structures on Si and Au surfaces e.g. lipid bilayer assembly, adsorption of surfactants on polymer surfaces or growth of S-layers on surfaces.
- Continuous flow.
- Shear alignment of supramolecular aggregates on surfaces, e.g., the adsorption of surfactants on polymer surfaces.

References:

[1] Tristram-Nagle St., et.al. (1998): *Biophysical Journal* **74**, 1421-1427.
[2] Katsaras, J. (1997): *Biophysical Journal* **73**, 2924.

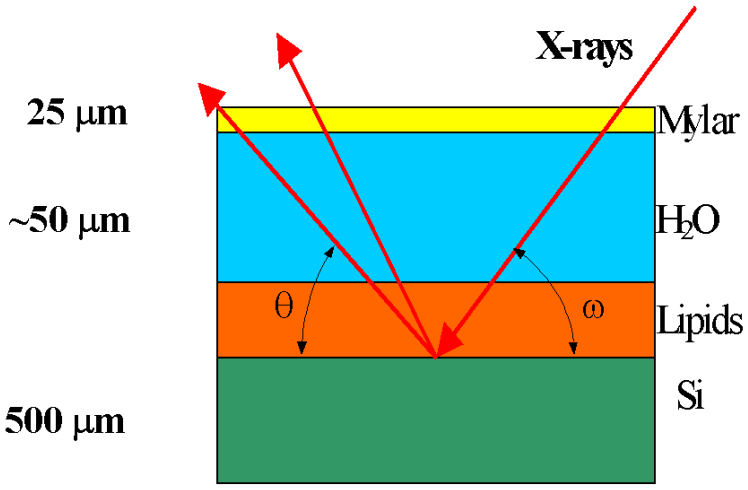

Figure 1. Sketch of the surface diffraction cell used for studying lipids under excess water conditions.

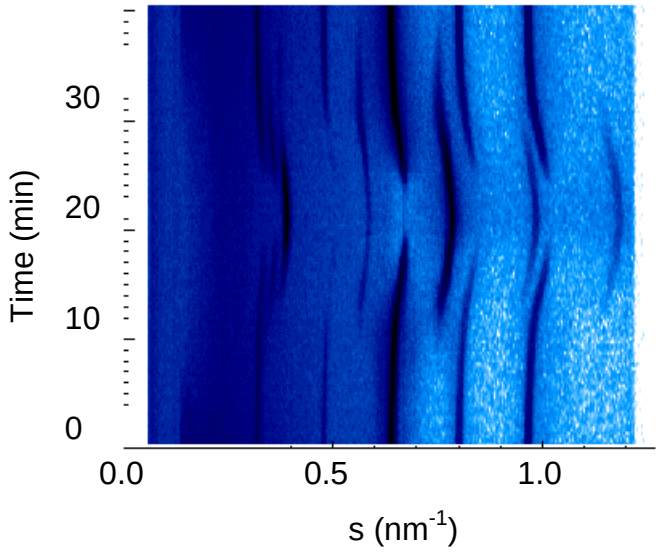

Figure 2. Surface diffraction pattern of SOPE ramped from 20 - 40 - 20 ºC with a rate of 1ºC/min showing the diffraction peaks from the 2nd to the 6th order at a fixed grazing angle (1.2º).

A MODIFIED 2D X-RAY DETECTOR FOR CRISTALLOGRAPHIC IMAGING

A. Orthen[1], H. Wagner[1], H. Amenitsch[2], S. Bernstorff[3], H.J. Besch[1], T. Hengstebeck[1], W. Meißner[1], R.H. Menk[3], N. Pavel[1], A. Sarvestani[1] and A.H. Walenta[1]

1.) Fachbereich Physik, Universität-GH Siegen, 57068 Siegen, Germany
2.) IBR, Steyrergasse 17, Graz, Austria
3.) ELETTRA, Sincrotrone Trieste, S.S.14 km 163.5, Basovizza, 34012 Trieste, Italy

During 1999 several modifications and measurements on the two dimensional single photon pixel detector prototype [1,2] have been carried out.
The basic working principle of this detector that comprises 7 x 7 cells covering a sensitive area of 28 x 28 mm² according to 140 x 140 digital interpolation pixels is illustrated in Fig.1. Due to the high electric field between the read out and the gas gain structure (MicroCAT) the primary charge is multiplied. This effect mainly depends on the geometrical distance. Thus a homogeneous distance is crucial for proper operation especially for large area detectors.
Small glass spacers (height about 200 µm), which are printed on the read out nodes by means of silk-screen printing provide this constant gap between the resistive anode and the MicroCAT. For test purposes the aforementioned prototype detector was only covered half by spacers in order to study disturbing effects in comparison to the uncovered part (Fig. 1).
An essential question, which arises when using insulating material within the detector, is the effect of charging up. For this reason several test series were started to study the properties of the glass spacers (Fig. 1). It has been shown that the energy resolution and the gas gain stay nearly constant for photon fluxes up to 10^7 photons/mm²/s (Fig. 2). The detector type used was able to produce gas gains up to $5 \cdot 10^4$. Furthermore, the local energy resolution amounts to less than 20% FWHM (at 8 keV and 0.1 mm² beam size). In comparison, the apparent global energy resolution was measured to be about 70% FWHM (at 6.4 keV and 28 x 28 mm² illumination area) and is mainly determined by the spatial dependency of the gas gain, as can be seen in Fig. 3.
No effect of the glass spacers on the spatial resolution was observed. It was measured utilizing a pencil beam of 180µm * 250 µm (Fig. 4) and can be quoted to be about 200µm (FWHM).
Besides the known images distortions that are due to the reconstruction algorithm [2] no additional artifacts were induced by the glass spacers as shown in Figure 5.

References:

[1] Besch, H.J., Junk, M., Meißner, W., Sarvestani, A., Stiehler, R. & Walenta, A.H. (1997) *Nucl. Instr. And Meth.* **A392**, 244.
[2] Sarvestani, A., Besch, H.J., Junk, M., Meißner, W., Menk, R.H., Sauer, N., Stiehler, R. & Walenta, A.H. (1998) *Nucl. Instr. And Meth.* **A410** 238.

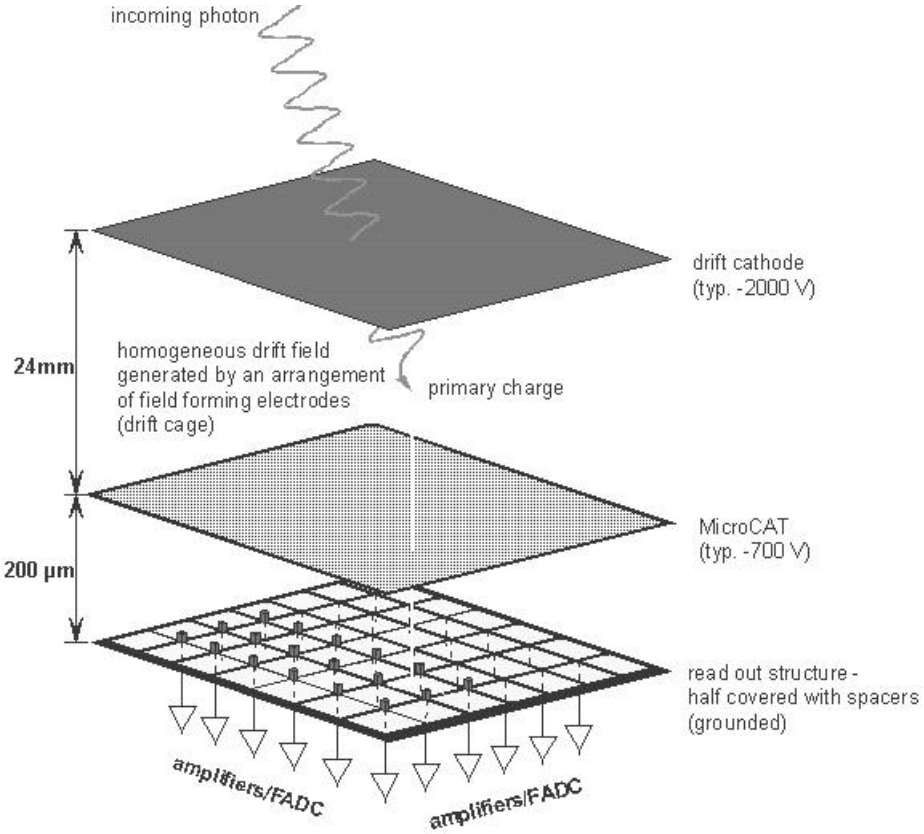

Figure 1. Profile of the relevant detector components. This scheme shows the read out structure only half covered with spacers. Further the high resistive centers and the low resistive cell borders are cognizable. Every read out node is connected to an amplifier/FADC-system.

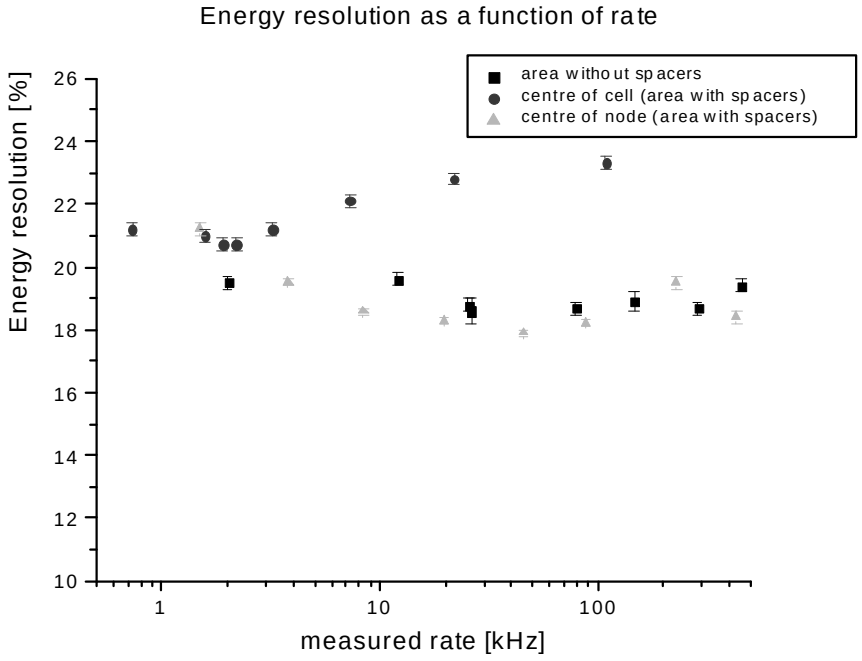

Figure 2. The energy resolution was measured at three different positions using a collimated pencil beam.

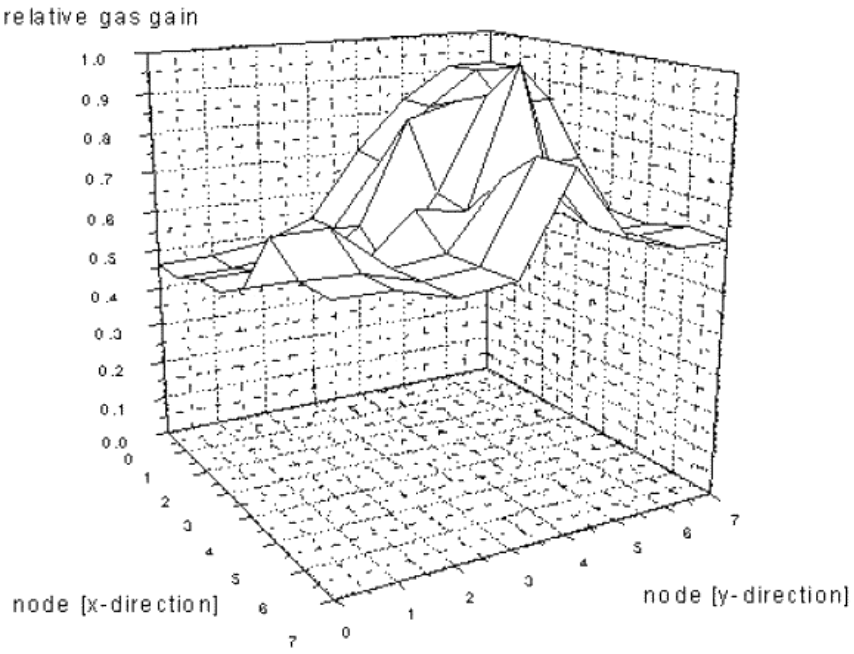

Figure 3. Relative gas gain as a function of the local position within the detection area.

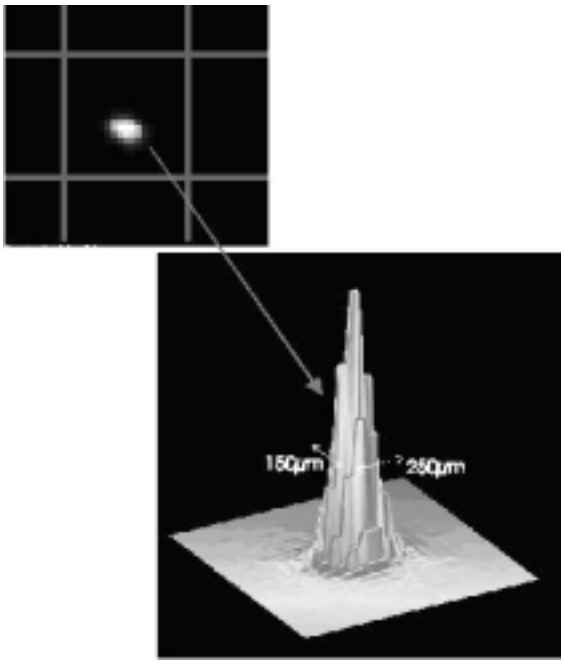

Figure 4. Collimated beam (250 x 150 µm²) with profile.

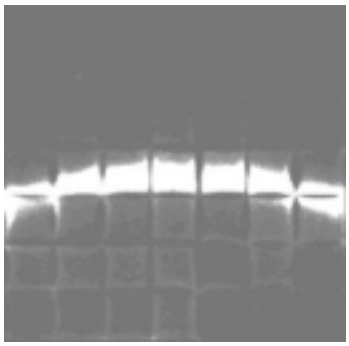

Figure 5. Part of a first-order diffraction ring of Ag-Behenate.

Publications

Publications in 1999

Patrik Ågren, Mika Lindén, Jarl B. Rosenholm, Robert Schwarzenbacher, Manfred Kriechbaum, Heinz Amenitsch, Peter Laggner, Juliette Blanchard and Ferdi Schüth
Kinetics of Cosurfactant-Surfactant-Silicate Phase Behavior. 1. Short-Chain Alcohols
J. Phys.Chem. B 103 (1999) 5943-5948.

H.Amenitsch, S. Bernstorff , M. Kriechbaum, D. Lombardo, H. Mio, G. Pabst, M.Rappolt, and P.Laggner
The Small Angle X-Ray Scattering Beamline at ELETTRA: A New Powerful Station for Fast Structural Investigations on Complex Fluids with Synchrotron Radiation
Nuovo Cimento D 20, (Dec 1998), 2181-2190

H.Amenitsch, M.Rappolt, P.Laggner, S. Bernstorff , R. Moslinger, E. Fleischmann, T. Wagner, S. Lax, E. Petru, K. Hudabiunigg and L. Dalla Palma
Synchrotron X-Ray Study at Trieste: No Correlation between Breast Cancer and Hair Structure
Synchrotron Radiation News, Vol. 12, No. 5 (1999) 32-34

Baldrian J., Horky M., Sikora A., Steinhart M., Vlèek P., Amenitsch H., Bernstorff S.
Time-resolved SAXS study of crystallization of poly(ethylene oxide)/poly(methyl methacrylate) blends
Polymer 40 (1999) 439-445

G. Balducci, L. Lucii, M. Linari, M. Reconditi, H. Amenitsch, S. Bernstorff, G. Piazzesi and V. Lombardi
Structural aspects of after-stretch potentiation studied by time-resolved X-ray diffraction on single frog muscle fibers
Biophys. J. 76, Abstract A33/Su-Pos9 (1999)

P. Laggner, H. Amenitsch, S. Bernstorff, P. Dubcek, M. Kriechbaum, R.H. Menk, M. Rappolt and G. Pabst
Österreichische SAXS Station bei ELETTRA in Triest: Forschung an Nano-Strukturen mit Synchrotron-Strahlung
Mitteilungsblatt der Österreichischen Physikalischen Gesellschaft (ÖPG) 1, 13-18 (1999)

P. Laggner, H. Amenitsch, M. Kriechbaum, G. Pabst, M. Rappolt
Trapping of Short-Lived Intermediates in Phospholipid Phase Transitions: The L_α-Phase.*
Faraday Discussion 111, 31-40 (1999)

S. Mazumder, D. Sen, I. S. Batra, R. Tewari, G. K. Dey, S. Banerjee, A. Sequeira, H. Amenitsch, and S. Bernstorff
Phase-Separation Kinetics of a Multicomponent Alloy
Phys. Rev. B 60, 822-830 (1999)

R.H. Menk, F. Arfelli, S.Bernstorff, D. Pontoni, A.Sarvestani, H.J. Besch, A.H.Walenta
A fast 1-D detector for imaging and time resolved SAXS experiments
Nucl. Instr. Meth. A 422 (1999) 698 - 703

R.H.Menk
Interference imaging and its application to material and medical imaging
Nuclear Physics B (Proc. Suppl.) (1999) 604 –609

R.H.Menk, A.Sarvestani
Novel Gaseous Imaging detectors for advanced biological diffraction studies
Synchrotron Radiation News Vol 12, No 4 (1999)

R.H.Menk, A.Sarvestani, H.J.Besch, A.H.Walenta
A fast integrating gaseous detector with single photon resolution
Proceedings of SPIE 3770 (1999) 57-63

M. Pregetter, R. Prassl, H. Amenitsch, F. Nigon, M. J. Chapman, P. Laggner
Time-Resolved X-Ray Diffraction of the Core Lipid Transition of Human Low Density Lipoproteins.
Atherosclerosis 144, 42 (1999)

M. Rappolt, G. Pabst, H. Amenitsch, S. Bernstorff, P. Laggner
Anomalous Thinning of Liquid Crystalline Phospholipid Bilayers: Comparison of Non-Equilibrium Perturbations with Salt Induced Features.
Biophys. J. 76, 1, 2/2, A139 (1999)

A.Sarvestani, H.Amenitsch, S.Bernstorff, H.J.Besch, R.H.Menk, A.Orthen, N.Pavel, M.Rappolt, N.Sauer, A.H.Walenta
Biological x-ray diffraction measurements with a novel two dimensional gaseous pixel detector
J.Synchrotron Radiation 6 (1999) 985-994

A. Sarvestani, H.J. Besch, R.H. Menk, N. A. Pavel, A.H. Walenta, Proceedings of the *A Novel High Rate Gaseous Pixel Detector for Time Resolved X-ray Diffraction Applications*
Proceedings of SPIE Vol 3448 (1999)

E.Schafler, M.Zehetbauer, I. Kopacz, T.Ungar, P.Hanak, H.Amenitsch and S.Bernstorff
Microstructural Parameters in Large Strain Deformed Ni Polycrystals as Investigated by Synchrotron Radiation
Phys. Stat. Sol. (a) 175, 501 (1999)

M. Steinhart, M. Kriechbaum, K. Pressl, H. Amenitsch, P. Laggner, S. Bernstorff
High-Pressure Instrument for Small- and Wide-Angle X-Ray Scattering. II. Time-Resolved Experiments
Rev. Sci. Instrum. 72/2, 1540-1545 (1999)

A.Turkovic, Z.Crnjak-Orel, P.Dubcek and H.Amenitsch
X-ray scattering measurements on nanosized TiO_2 micelles
Solar Energy Materials & Solar Cells 59, 387-392 (1999)

A.Turkovic, P.Dubcek and S. Bernstorff
Grazing-incidence small-angle and wide-angle scattering of synchrotron radiation on nanosized CeO_2 thin films
Materials Science & Engineering B58 (1999) 263-269

A.Turkovic, P.Dubcek, Z. Crnjak-Orel and S. Bernstorff
Small angle scattering of synchrotron radiation on nanosized CeO_2 and CeO_2-SnO_2 thin films obtained by sol-gel dip-coating method
NanoStructured Materials, Vol 11, No. 7, pp. 909-915 (1999)

M. Zehetbauer, T. Ungar, R. Kral, A. Borbely, E. Schafler, B. Ortner, H. Amenitsch and S. Bernstorff
Scanning X-ray Diffraction Peak Profile Analysis in Deformed Cu-Polycrystals by Synchrotron Radiation
Acta mater. 47 (1999) 1053-1061

Zizak, O. Paris, P. Roschger, H. Amenitsch, S. Bernstorff, K. Klaushofer, P. Fratzl,
Scanning – Saxs and –Waxs investigations of bone-cartilage interfaces
Calc. Tiss. Int. 64, Supplement 1, 108 (1999)

Publications in January - May 2000

Bagni, M.A., Cecchi, G., Colombini, B., Amenitsch, H., Bernstorff, S., Rapp, G., Ashley, C.C. & Griffiths, P.J.
14.5 nm meridional X-ray diffraction intensity changes associated with the myosin head elasticity and the quick recovery phase
Biophysical Journal 78 (1), A227 (2000)

G. Cerichelli, C. La Mesa, L. Lucchetti and G. Mancini
Role of Counterions in the Catalytic Activity and Phase Equilibria of Phosphonium Salts in Water
Langmuir 16 (2000) 166-71

P. Dubcek, O. Milat, B. Pivac, S. Bernstorff, H. Amenitsch, R. Tonini, F. Corni, and G. Ottaviani
GISAXS study of defects in He implanted silicon
Mater. Sci. & Eng. B 71, 292-296 (2000).

H.Grigoriew, A.Wolinska-Grabczyk, A.G.Chmielewski, H.Amenitsch and S.Bernstorff
SAXS study of the influence of ethanol on the microstructure of polyurethane-based membrane
Journal of Membrane Science 170, 275-279 (2000)

A. Gupta, N. Bhagat, G. Principi, A. Maddalena, N. Malhotra, B.A. Dasannaccharya, P.S. Goel, H. Amenitsch and S. Bernstorff
Nanocrystallization of amorphous alloys: comparision between furnace and current annealing
Intermetallics 8 (2000) 287-291

M. Linari, G. Piazzesi, L. Lucii, H. Amenitsch, S. Bernstorff, V. Lombardi
A time resolved X-ray diffraction study of the structural aspects of after-stretch potentiation in single frog muscle fibres
Pflügers Arch. 439, abstract R276/84, 2000

R.H. Menk, A.Sarvestani, H. Amenitsch, S.Bernstorff, H.J. Besch, A. Orthen, N. Pavel, M. Rappolt, N. Sauer and A.H.Walenta
Novel detector systems for time resolved SAXS experiments
J. Appl. Cryst. 33 (2000).778-781

R.H. Menk, A.Sarvestani, H.J. Besch, A.H.Walenta, H. Amenitsch and S.Bernstorff
Gas Gain Operations with Single Photon Resolution Using an Integrating Ionization Chamber in Small Angle X-Ray Scattering Experiments
Nucl.Instr.&Meth. A440 (2000) 181-190

R.Prassl, R. Schwarzenbacher, M.Kriechbaum, H. Amenitsch, M. J. Chapman, and P.Laggner
Low Resolution X-ray Crystallography on Human Low Density Lipoprotein
Biophys. J. 78(1), 484 (2000)

Michael Rappolt, Georg Pabst, Gert Rapp, Manfred Kriechbaum, Heinz Amenitsch, Christian Krenn, Sigrid Bernstorff and Peter Laggner
New evidence for gel-liquid crystalline phase co-existence in the ripple phase of phosphatidylcholines
Eur. Biophys. J. 29, 125 - 133 (2000)

M. Roessle, E. Manakova, I. Lauer, T. Nawroth, J. Holzinger, T. Narayanan, S. Bernstorff, H. Amenitsch and H. Heumann
Time-resolved small angle scattering: kinetic and structural data from proteins in solution
J. Appl. Cryst..33, 548-551 (2000)

Ilian Simidjiev, Svetla Stoylova, Heinz Amenitsch, Tamas Javorfi, Laszlo Must=E1rdy, Peter Laggner, Andreas Holzenburg, and Gyozo Garab
Self-assembly of large, ordered lamellae from non-bilayer lipids and integral membrane proteins in vitro
Proc. Natl Acad. Sci USA, Vol. 97, Issue 4, 1473-1476 (2000)

E.Schafler, M.Zehetbauer, P.Hanak, T.Ungar, T.Hebesberger, R.Pippan, B.Mingler, H.P.Karnthaler, H.Amenitsch and S.Bernstorff
Fragmentation in Large Strain Cold Rolled Aluminium as observed by Synchrotron X-Ray Bragg Peak Profile Analysis (SXPA), Electron Back Scatter Diffraction (EBSD) and Transmission Electron Microscopy (TEM)
Proc. NATO Adv.Res.Workshop "Investigations and Applications of Severe Plastic Deformation", ed. T.C.Lowe and R.Z.Valien, Kluwer Acad. Publ., The Netherlands (2000)

M.E. Vannicelli Casoni, L. Lucii, M. Linari, H. Amenitsch, S. Bernstorff, G. Piazzesi, V. Lombardi
Mechanical and structural evidences of an increased fraction of attached heads as responsible for after-stretch potentiation in frog single muscle fibers
Biophys. J. 78, abstract 231/1362-Pos (2000)

M.Zehetbauer
Strengthening Processes of Metals at Severe Plastic Deformation: Analyses with Electron and Synchrotron Diffraction
Proc. NATO Adv.Research Workshop "Investigations & Applications of Severe Plastic Deformation", ed. T.C.Lowe and R.Z.Valiev, Kluwer Acad. Publ., The Netherlands (2000)

I. Zizak, O. Paris, P. Roschger, S. Bernstorff, H. Amenitsch, K. Klaushofer, P. Fratzl
Investigation of bone and cartilage by synchrotron scanning SAXS and -WAXD with micrometer spatial resolution
J. Appl. Cryst. 33 (2000).820-823

Publications, in print

Baldrian J.,Horky M.,Steinhart M.,Sikora A.,Vlcek P.,Amenitsch H. and Bernstorff S.
Time-resolved SAXS/WAXS study of polymer blend crystallization
SPIE Int. Soc. Opt. Eng.

J.Bonarski, M.Zehetbauer, Z.Swiatek, I.M Fodchuk, I.Kopacz, S.Bernstorff and H.Amenitsch
Synchrotron Investigation of the Near-Surface Areas in Silicon Solar Cells Modified by P^+ Ion Implantation and Thermal Treatment
Proc of the European Conference on Photovoltaics, Oct. 25-27, 1999, Cracow, Poland Opto-Electronics Review

S. Gomez, R. Toffanin, S. Bernstorff, M. Romanello, H. Amenitsch, M. Rappolt, R. Rizzo and F. Vittur
Collagen Fibrils are differently organized in weight-bearing and not-bearing regions of Pig Articular Cartilage
Journal of Exp. Zoology

H.Grigoriew, A.G.Chmielewski and H.Amenitsch
Structural temperature transformation of the system: cellulose-water using time-resolved SAXS
Polymer

M. Linari, L. Lucii, M. Reconditi, M.E. Vannicelli Casoni, H. Amenitsch, S. Bernstorff, G. Piazzesi and V. Lombardi
A combined mechanical and X-ray diffraction study of stretch potentiation in single frog muscle fibres
J. Physiol.

E.F. Marques, H. Edlund, A. Khan and C. L Mesa
Liquid Crystals and Phase Equilibria in Binary Bile Salt-Water Systems.
Langmuir

Mazumder et al
Title: not communicted
Journal of Alloy & compounds

Pabst, G., Rappolt, M., Amenitsch, H. and Laggner, P
Structural information from multilamellar liposomes at full hydration: full q-range fitting with high quality X-ray data
Phys. Rev. E

O. Paris, I. Zizak, H. Lichtenegger, P. Roschger, K. Klaushofer and P. Fratzl
Analysis of the hierarchical structure of biological tissues by scanning X-ray scattering using a micro-beam
Cell. Mol. Biol.

G. Principi, A. Maddalena, A. Gupta, N. Bhagat, N. Malhotra, B.A. Dasannacharya, H. Amenitsch and S. Bernstorff
Furnace and current annealing of the amorphous $Fe_{72}Cu_1Nb_{4.5}Si_{13.5}B_9$ alloy
J. Appl. Phys.

Resel, R., Theissl, U., Gadermaier, C., Zojer, E., Kriechbaum, M., Amenitsch, H., Gin, D., Smith, R. and Leising, G.
The H_2 – phase of the lyotropic liquid crystal sodium 3,4,5 – tris (v-acryloyloxyundecyloxy)benzoate
Liquid Crystals

A.Turkovic
Grazing-incidence SAXS/WAXD on nanosized TiO_2 films obtained by ALE
Materials Science & Engineering B

Publications, submitted

Patrik Ågren, Mika Lindén, Jarl B. Rosenholm, Juliette Blanchard, Ferdi Schüth, Robert Schwarzenbacher, Manfred Kriechbaum, Heinz Amenitsch and Peter Laggner
Kinetics of Co-surfactant – Surfactant – Silicate Phase Behavior. 2. Short-chain Amines.
Langmuir

H. Amenitsch, S. Bernstorff, A. Bigi, N. Roveri and J. S. Shah
D-Periodicity in Intramuscular Collagen
Connective Tissue Research, in preparation.

Baldrian, J.,Horky, M.,Steinhart, M.,Laggner, P.,Amenitsch & H. and Bernstorff S.
Time-resolved SAXS/WAXS study of phase behaviour and nucleation in polymer blends
J.Polym. Sci. Polym. Phys.

A. Gamini, S. Paoletti, H. Amenitsch, S. Bernstorff, E. Theunissen, K. Bongaerts, H. Reynaers and G. Evmenenko
SAXS studies of temperature-induced conformational changes of k-carrageenan in salt solutions
Carbohydrate Research or to Polymer

Mika Lindén, Patrik Ågren, Stefan Karlsson, Patrick Bussian and Heinz Amenitsch
Solubilization of oil in silicate-surfactant mesostructures
Submitted to Langmuir.

Pabst, G., Rappolt, M., Amenitsch, H., Bernstorff, S. & Laggner, P.
X-ray kinematography of temperature-jump relaxation probes the elastic properties of fluid bilayers
Langmuir

M. Pisani, S. Bernstorff, C. Ferrero and P. Mariani
Pressure induced cubic-to-cubic phase transition on the monoolein hydrated system
J. Phys. Chem.

E.Schafler, M.Zehetbauer, I.Kopacz, B.Ortner, S.Bernstorff, H.Amenitsch, T.Ungar
Local Dislocation Densities and Internal Stresses by High Lateral Resolution Peak Profile Analysis in Plastically Deformed Polycrystalline Nickel
Scripta Mater.

E.Schafler, M.Zehetbauer, I.Kopacz, I. Altpeter, B.Ortner, H.Amenitsch, S.Bernstorff, T.Ungar
Messungen der Verteilung von Versetzungsdichten und inneren Spannungen in plastisch verformtem Ni mittels hochauflösender Synchrotron-Linienprofil-Analyse und magnetischer Mikroskopie
Scripta Mater.

D. Sen, S. Mazumder, R. Tewaris, P.K. De, H. Amenitsch and S. Bernstorff
Investigations on phase separation in zircaloy-2 fuel cladding tube
J. of Nuclear Materials

I. Simidjiev, S. Stoylova, H. Amenitsch, T. Javorfi, L. Mustardy, P. Laggner, A. Holzenburg and G. Garab
Self-Assembly of Large, Ordered Lamellae from Non-Bilayer Lipids and Integral Membrane Proteins in vitro
PNAS

M. Steinhart, M. Kriechbaum, K. Pressl, H. Amenitsch, P. Laggner and S. Bernstorff
High-Pressure Instrument for Small- and Wide-Angle X-ray Scattering. II: Time-Resolved Experiments
Rev. Sci. Instrum.

Satish Vitta
Ni50Nb50/C amorphous multilayers for "water window" soft x-rays - structure and stability
Journal Vacuum

M.Zehetbauer, T.Ungar, E.Schafler, S.Bernstorff, H.Amenitsch
Microscale Spatial Distribution of Dislocations and Long Range Internal Stresses in Cold Worked bcc Fe
Key Eng.Mater.

International Conferences and Workshops in 1999

Patrik Ågren
Influence of Non-Ionic Polymers and Cationic Surfactants on Silica Sols, Gels and Porous Ceramic Materials
Graduate School of Materials Research. Seminar 14.12.1999, Turku, Finland

P. Agren, H. Amenitsch, M. Linden, J. Rosenholm, R. Schwarzenbacher, M. Kriechbaum, P. Laggner, J. Blanchard, F. Schueth and S. Bernstorff
Synthesis of MCM-41 and MCM-50: A time resolved SAXS study of mesophase-formation
XI International Conference on Small-Angle Scattering (SAS99), Brookhaven National Laboratory, New York, USA, May 17 - 20, 1999 (talk)

Patrik Ågren, Mika Lindén, Jarl B. Rosenholm, Juliette Blanchard, Patrick Bussian, Ferdi Schuth, Heinz Amenitsch and Peter Laggner
Influence of short-chain alcohols and auxiliary organics on the formation of MCM-41 and MCM-50 structures
Graduate School of Materials Research. Seminar 20.5.1999, Turku, Finland

Patrik Ågren, Mika Lindén, Jarl B. Rosenholm, Juliette Blanchard, Patrick Bussian, Ferdi Schüth, Heinz Amenitsch and Peter Laggner
Kinetics of Surfactant - Silicate Composite Phase Behavior - Influence of Polar and Non-polar Additives
9th European Student Conference in Colloid and Polymer Chemistry (ESC'99), 29.6-2.7.1999, Nagu, Finland

Patrik Ågren, Mika Lindén, Jarl B. Rosenholm, Patrick Bussian, Juliette Blanchard, Ferdi Schüth, Heinz Amenitsch and Peter Laggner
Influence of Polar and Non-Polar Additives on the Formation of Surfactant -Silicate Mesophases - A Real-Time Synchrotron SAXS Study
13th Conference of the European Colloid and Interface Society, 12-17.9.1999, Dublin, Ireland (Poster)

P. Ågren, M. Linden, J. Rosenholm, P. Bussian, J. Blanchard, F. Schueth, H. Amenitsch, S. Bernstorff and P. Laggner
In-situ SAXS to study the influence of polar and non-polar additives on mesoporous MCM-materials
7th International Users‘ Meeting, ELETTRA, Trieste, Italy, 29. - 30.11.99 (poster)

Heinz Amenitsch, Patrik Ågren, Mika Lindén, Jarl B. Rosenholm, Robert Schwarzenbacher, Manfred Kriechbaum, Peter Laggner, Juliette Blanchard, Ferdi Schüth and Sigrid Bernstorff
Synthesis of MCM-41 and MCM-50: A Time Resolved SAXS Study of Mesophase -Formation
XI International Conference on Small-Angle Scattering, 17-20.5.1999, New York, USA (talk)

H. Amenitsch, S. Bernstorff, N. Bhagat, B.A. Dasannacharya, A. Gupta, N. Malhotra, A. Maddalena and G. Principi
Furnace and Current Annealing of Amorphous Fe72Cu1Nb4.5Si13.5B9 Alloy
7th International Users‘ Meeting, ELETTRA, Trieste, Italy, 29. - 30.11.99 (poster)

H. Amenitsch, S. Bernstorff, P. Dubcek, M. Kriechbaum, R.Menk, M.Rappolt, G.Pabst, and P. Laggner
ms and nm: The Small Angle X-ray Scattering Beamline at ELETTRA as a Tool for Fast Time Resolved Studies in the Nanometer-Scale
7th Congress of SILS (Societá Italiana Luce di Sincrotrone), Aquila, Italy, July 1-3, 1999 (talk)

H. Amenitsch, S. Bernstorff, P. Dubcek, M. Kriechbaum, R. Menk, H. Mio, G. Pabst, M. Rappolt, M. Steinhart and P. Laggner
Submillisecond time-resolved SAXS-experiments at ELETTRA on structural changes induced by rapid variations of external field parameters (e.g. pressure, temperature, tension, mixing)
XI International Conference on Small-Angle Scattering (SAS99), Brookhaven National Laboratory, New York, USA, May 17 - 20, 1999 (talk)

H. Amenitsch, S. Bernstorff, P. Dubcek, M. Kriechbaum, R. Menk, G. Pabst, M. Rappolt, M. Steinhart and P. Laggner
Time-Resolved Studies of Fast Triggered Jump Relaxations at the SAXS Beamline at ELETTRA
ESRF-ILL-CEA Workshop "Frontiers in SAXS and SANS", Grenoble, France, February 12 - 17, 1999 (poster)

H. Amenitsch, S. Bernstorff, R. H. Menk, H.J. Besch, A. Orthen, N. Pavel, A. Sarvestani, H. Wagner, A.H. Walenta
A fast one dimensional integrating detector with single photon resolution for SAXS experiments
7th International Users‘ Meeting, ELETTRA, Trieste, Italy, 29. - 30.11.99 (poster)

H. Amenitsch, A. Cesaro, F. Sussich and F. Princivalle
Polymorphic transformations of trehalose implied in anhydrobiosis
7th International Users‘ Meeting, ELETTRA, Trieste, Italy, 29. - 30.11.99 (poster)

Heinz Amenitsch, Martin Hainbuchner, Mario Villa, Matthias Baron, Patrik Ågren, Jarl B. Rosenholm, Helmut Rauch and Peter Laggner
A Time resolved USANS Study of Microstructure – Formation during the Synthesis of MCM-41 and MCM-50
XI International Conference on Small Angle Scattering. 17-20.5.1999, New York, USA (poster)

Amenitsch, P. Laggner, P. Ågren and M. Lindén
Space-time development of MCM - systems by combined SAXS and USANS: from deciseconds to hours, and from nano- to micrometers
48th Annual Denver X-ray Conference, 2-6.8.1999, Steamboat Springs, USA

H. Amenitsch, W. Jing, K. Lohner, M. Rappolt, S. Bernstorff and P. Laggner
New X-Ray surface cell to study highly aligned and fully hydrated lipids and LB-films under varying solvent conditions
7th International Users‘ Meeting, ELETTRA, Trieste, Italy, 29. - 30.11.99 (poster)

V.K. Aswal, P.S. Goyal, S. De, S. Bhattacharya, H. Amenitsch and S. Bernstorff
A direct observation of the counterion distribution around gemini micelles in aqueous solution

DAE Solid State Symposium, IGCAR, Kalpakkam, India, Dec. 20-24, 1999

J. Baldrian, M. Horky, M. Steinhart, P. Laggner, P. Vleek, H. Amenitsch and S. Bernstorff
Ordering phenomena in PEO/PMMA blends during crystallization
11th International Conference on Small-Angle Scattering (SAS99), Long Island, Upton, USA, Abstracts Book, p.193

J. Baldrian, M. Steinhart, M. Horky, P. Laggner, H. Amenitsch and S. Bernstorff
Structure Development in PEO/PMMA Blends during Crystallization
COST Workshop "Polymer Crystallization", Vught, Holland, 4. - 6. December 1999

J. Baldrian, M. Horky, M. Steinhart, P. Laggner, H. Amenitsch and S. Bernstorff
Real-time SAXS and SAXS/WAXS studies of polymer blends
7th International Users‘ Meeting, ELETTRA, Trieste, Italy, 29. - 30.11.99 (poster)

S. Bernstorff, P. Dubcek, S. Carrara, C. Nicolini, C. Paternolli, V. Erokhin, S. Paddeu, L. Valkova
Small-angle X-ray synchrotron study of structural reorganization in phthalocyanine containing Langmuir-Blodgett superlattices
7th International Users‘ Meeting, ELETTRA, Trieste, Italy, 29. - 30.11.99 (poster)

H.J. Besch, A. Orthen, N. Pavel, A. Sarvestani, H. Wagner, A.H. Walenta, S. Bernstorff, R. H. Menk and H. Amenitsch
Microsecond time resolved 2D x-ray imaging
7th International Users‘ Meeting, ELETTRA, Trieste, Italy, 29. - 30.11.99 (poster)

J.T. Bonarski, M.Zehetbauer, Z.Swiatek, I.M Fodchuk, I.Kopacz, S.Bernstorff and H.Amenitsch
Synchrotron Investigation of the Near-Surface Areas in Silicon Solar Cells Modified by P^+ Ion Implantation and Thermal Treatment
European Conference on Photovoltaics, 25-27 Oct. 1999, Cracow, Poland

P. Dubcek, O. Milat, B. Pivac, S. Bernstorff, H. Amenitsch, R. Tonini, F. Corni, and G. Ottaviani
GISAXS study of defects in He implanted silicon
EMRS 1999 Spring Meeting, June 1-4, 1999. Strasbourg, France, poster presentation

R. Gianni, F.Delben, G. Liut, R. Rizzo
Structural studies on modified microbial polysaccharides
10th European Carbohydrate Symposium, Galway, Ireland, July 11-16 1999 (poster)

R. Gianni, M. Miani, M. Nevyjel, F. Delben, G. Liut, R. Rizzo, S. Bernstorff, P. Dubcek, H. Amenitsch
SAXS Investigation of Native and Modified Polysaccharides
7th Congress of SILS (Societá Italiana Luce di Sincrotrone), Aquila, Italy, July 1-3, 1999 (poster)

R. Gianni, M. Miani, M. Nevyjel, F. Delben, G. Liut, R. Rizzo, S. Bernstorff, P. Dubcek and H. Amenitsch
SAXS Studies of Native and Modified Polysaccharides.

7th International Users‘ Meeting, ELETTRA, Trieste, Italy, 29. - 30.11.99 (poster)

H. Grigoriew, A. G. Chmielewski, H. Amenitsch and S. Bernstorff
Structural Temperature Transformation of the system: Cellulose - Water Using Time-resolved SAXS
7th International Users‘ Meeting, ELETTRA, Trieste, Italy, 29. - 30.11.99 (poster)

A. Gupta, N. Bhagat, G. Principi, A. Maddalena, N. Malhotra, B.A. Dasannaccharya, P.S. Goel, H. Amenitsch and S. Bernstorff
Nanocrystallization of amorphous alloys: comparision between furnace and current annealing
Workshop on Alloys and Intermetallic Compounds, Genova, March 25-27, 1999

A. Gupta, N. Bhagat, N. Malhotra, B.A. Dasannaccharya, G. Principi, A. Maddalena, P.S. Goel, H. Amenitsch and S. Bernstorff
Furnace and current annealing of amorphous FeCuNbSiB alloys
44th Annual Conference on Magnetism & Magnetic Materials, San Jose, California, November 15-18, 1999

Horky, M., Baldrian, J. & Steinhart M.
Phase behaviour of PEO/PMMA blends
Colloqium: STRUKTURA of the Czech Crystallographic Society, Hodonín u Kunstátu, 1999

M. Kriechbaum, M. Steinhart, P. Laggner, H. Amenitsch and S. Bernstorff
Time-resolved small-angle X-ray scattering studies of pressure-jump induced barotropic phase transitions of lipids
XI International Conference on Small-Angle Scattering (SAS99), Brookhaven National Laboratory, New York, USA, May 17 - 20, 1999 (poster)

M. Kriechbaum, M. Steinhart, H. Amenitsch, S. Bernstorff and P. Laggner
Time-Resolved Small-Angle X-Ray Scattering Studies of Pressure-Jump Induced Barotropic Phase Transitions of Phospholipids
7th International Users‘ Meeting, ELETTRA, Trieste, Italy, 29. - 30.11.99 (poster)

P. Laggner
Österreichische SAX-Beamline bei ELETTRA
EU-Synchrotron Round Table Meeting, Hamburg, Germany, 13.-14.12.99 (talk)

P. Laggner / M. Rappolt
Space-Time Development of MCM-Systems by Combined SAXS and USANS: From Deciseconds to Hours and from Nano- to Micrometers
47. Annual X-Ray Conf. Denver /USA 2.-6.8.99 (talk)

La Mesa et al
Bill Salts Form Lyotropic Liquid Crystals
National Meeting of the Colloid and Interface Division of the Italian Chemical Society, Rome 1999 (talk)

Mika Lindén, Patrik Ågren, Stefan Karlsson, Patrick Bussian, Heinz Amenitsch and Sigrid Bernstorff
In situ SAXS to study the solubilization of oil in mesoporous MCM-materials

Seventh International Users' Meeting. 29-30.11.1999, Trieste, Italy (Poster)

Mika Lindén, Patrik Ågren, Jarl B. Rosenholm, Juliette Blanchard, Patrick Bussian, Ferdi Schuth, Heinz Amenitsch and Peter Laggner
In situ synchroton SAXS study of the formation of surfactant - silicate mesophases in the presence of short-chain alcohols and auxiliary organics
COPSV. June 1999, Heidelberg, Germany (Poster)

Mika Lindén, Patrik Ågren, Jarl B. Rosenholm, Juliette Blanchard, Patrick Bussian, Ferdi Schüth, Heinz Amenitsch and Peter Laggner
In Situ Synchrotron SAXS Study of the Kinetically Controlled Formation of Surfactant - Silicate Mesophases in the Presence of Polar and Non- polar Additives
The IX National Symposium on Surface and Colloid Science. 30-31 August 1999, Espoo, Finland

K. Lohner, E. Staudegger and H. Amenitsch
Kinetics of Membrane Perturbation and Disruption by Antimicrobial Peptides
7th International Users‘ Meeting, ELETTRA, Trieste, Italy, 29. - 30.11.99 (poster)

L. Lucii, M. Linari, M. Reconditi, H. Amenitsch, S.Bernstorff, G. Piazzesi and V. Lombardi
Structural aspects of after-stretch potentiation studied by the time resolved X-ray diffraction on single frog muscle fibres
7th Congress of SILS (Societá Italiana Luce di Sincrotrone), Aquila, Italy, July 1-3, 1999 (poster)

L. Lucii, M. Linari, M. Reconditi, H. Amenitsch, S.Bernstorff, G. Piazzesi and V. Lombardi
Structural aspects of after-stretch potentiation studied by time resolved X-ray diffraction in single frog muscle fibres
V Scuola Nazionale Luce di Sincrotrone, S. Margherita di Pula, 27.9-8.10.1999 (poster)

S.S. Major,
Langmuir Blodgett multilayers and related nanostructures
DAE-BRNS Workshop on "Thin Film Multilayers", Oct. 1999, Mumbai, India.

P. Mariani, M. Pisani, L. Saturni, S.Bernstoff, C. Ferrero, M.Kriechbaum and M. Steinhart
Pressure induced cubic-to-cubic phase transition on the monoolein hydrated system
7th International Users‘ Meeting, ELETTRA, Trieste, Italy, 29. - 30.11.99 (talk and poster)

P.Mariani, F. Spinozzi and E. Maccioni
SAXS Studies of the Structural Properties of Carcinus Aestuarii Haemocyanin Proteins in Solution
XI International Conference on Small Angle Scattering (SAS99), Brookhaven National Laboratory, New York, USA, May 17 - 20, 1999

E.F. Marques; H. Edlund, H. Amenitsch, C. La Mesa and Ali Khan
Liquid Crystals and Phase Equilibria in Binary Bile Salt-Water Systems
7th International Users‘ Meeting, ELETTRA, Trieste, Italy, 29. - 30.11.99 (poster)

R.H. Menk, A.Sarvestani, H. Amenitsch, S.Bernstorff, H.J. Besch, A. Orthen, N. Pavel, M. Rappolt, N. Sauer and A.H.Walenta
Novel detector systems for time resolved SAXS experiments

XI International Conference on Small-Angle Scattering (SAS99), Brookhaven National Laboratory, New York, USA, May 17 - 20, 1999 (talk)

R.H.Menk, A.Sarvestani, H.J.Besch, A.H.Walenta
A fast integrating gaseous detector with single photon resolution
SPIE 1999, Denver, Colorado, USA

G. Pabst, M. Rappolt, H. Amenitsch, S. Bernstorff and P. Laggner
Structural Information from X-Ray Experiments on Unoriented Phospholipid Bilayers at Full Hydration by Means of an Inverse Fourier Method
7th International Users' Meeting, ELETTRA, Trieste, Italy, 29. - 30.11.99 (poster)

M. Pregetter, R. Prassl, H. Amenitsch, Nigon, M.J. Chapman, P. Laggner
Time-Resolved X-Ray Diffraction of the Core Lipid Transition of Human LDL
EAS Congress , Athen, Griechenland, 26.-29.5.99 (poster)

M. Pregetter, R. Prassl, P.Laggner
Kinetics of Core Lipid Transition of Human LDL: Time-Resolved Small-Angle X-Ray Scattering
Austr.Atherosclerose Soc. Meeting, Werfenweng, 23.-24.4.99 (poster)

M. Pregetter, R. Prassl , R. Schwarzenbacher, H. Amenitsch, M.J. Chapman, P. Laggner
Time-Resolved X-Ray Diffraction Displays the Kinetics of the Neutral Core Lipid Transition of Low Density Lipoprotein
XIII International Biophysics Congress, New Delhi, Indien, 19.-24.9.99 (poster)

M. Pregetter, R. Prassl, R. Schwarzenbacher, H. Amenitsch, and P. Laggner
Time-Resolved X-Ray Diffraction Displays in the Kinetics of the Neutral Core Lipid Transition of Low Density Lipoprotein
7th International Users' Meeting, ELETTRA, Trieste, Italy, 29. - 30.11.99 (poster)

M. Rappolt, H. Amenitsch, S. Bernstorff, P. Dubcek, M. Kriechbaum, R.Menk, G.Pabst, and P. Laggner
Austrian Small Angle X-ray Scattering (SAXS) Beamline at ELETTRA
Interregional Software and Telecom Business Meeting, Trieste, Italy, October 15, 1999 (talk)

M. Rappolt, G. Pabst, H. Amenitsch, S. Bernstorff and P. Laggner
Anomalous Thinning of Liquid Crystalline Phospholipid Bilayers: Comparison of Non-Equilibrium Pertubations with Salt-Induced Features
Ann.Meeting Biophys.Society 99, Baltimore/USA, 13.-17.2.99 (talk)

M. Rappolt, G. Pabst, H. Amenitsch, S. Bernstorff and P. Laggner
Probing Elasticity Changes due to Cholesterol Content in Phospholipid Bilayers by using a Temperature-Jump Technique
7th International Users' Meeting, ELETTRA, Trieste, Italy, 29. - 30.11.99 (poster)

M. Reconditi et al
Structural aspects of stretch-potentiation studied by X-ray diffraction in single frog muscle fibres
7th International Users' Meeting, ELETTRA, Trieste, Italy, 29. - 30.11.99 (poster)

M. Roessle
Time resolved small angle scattering – a powerfull method to obain kinetic and structural data form proteins in solution
Joint meeting of the Dutch and German Biophysical Socienties and the Biochemistry and Molecular Biology Society at Hünfeld, Germany 1999

A. Sarvestani, H.J. Besch, R.H. Menk, N. A. Pavel, A.H. Walenta
A Novel High Rate Gaseous Pixel Detector for Time Resolved X-ray Diffraction Applications",
SPIE 1999, Denver, Colorado, USA

E.Schafler, M.Zehetbauer, P.Hanak, T.Ungar, T.Hebesberger, R.Pippan, B.Mingler, H.P.Karnthaler, H.Amenitsch and S.Bernstorff
Fragmentation in large strain cold rolled Aluminium as observed by Synchrotron X-Ray Bragg Peak Profile Analysis (SXPA), Electron Back Scatter Diffraction (EBSD) and Transmission Electron Microscopy (TEM)
NATO Adv.Research Workshop "Investigations & Applications of Severe Plastic Deformation", August 2-6, 1999, Moscow, Russia

E.Schafler, M.Zehetbauer, P.Hanak, T.Ungar, T.Hebesberger, R.Pippan, B.Mingler, H.P.Karnthaler, H.Amenitsch and S.Bernstorff
Fragmentation in large strain cold rolled Aluminium as observed by Synchrotron X-Ray Bragg Peak Profile Analysis (SXPA), Electron Back Scatter Diffraction (EBSD) and Transmission Electron Microscopy (TEM)
7th International Users' Meeting, ELETTRA, Trieste, Italy, 29. - 30.11.99 (poster)

R. Schwarzenbacher, K. Zeth, K. Diederichs, A. Gries, G. M. Kostner, P. Laggner and R. Prassl
Crystal structure of human beta2-glycoprotein-1: Implications for phospholipid binding and the antiphospholipid syndrome
7th International Users' Meeting, ELETTRA, Trieste, Italy, 29. - 30.11.99

A.Turkovic
Rasprsenje sinhrotronskog svjetla na nanofaznim slojevima
Knjiga sazetaka, Drugi znanstveni sastanak Hrvatskog fizikalnog drustva, PMF, Zagreb 1.-3. prosinca 1999, p.100. (POSTER)

A.Turkovic, Z.Crnjak-Orel, P.Dubcek and H.Amenitsch
GISAXS and GIWAXS on Nanosized TiO_2 Micelles
Zbornik povzetkov, 6. srecanje strokovnjakov s podrocja vakuumske znanosti in tehnike iz Slovenije in Hrvatske, 17. junij 1999, Ljubljana, pp. 13-14. (LECTURE)

A.Turkovic, P.Dubcek, Z.Crnjak-Orel and S.Bernstorff
Grazing-incidence small-angle scattering of synchrotron radiation on nanosized CeO_2 and CeO_2-SnO_2 thin films obtained by sol-gel dip-coating method
MATH/CHEM/COMP '99, Inter-University Centre, Dubrovnik, Croatia 21-26 June 1999, Dubrovnik, p. 69 (INVITED LECTURE)

Satish Vitta

Ni50Nb50/C amorphous multilayers for water window soft x-rays - structure and stability
DAE-BRNS Workshop on "Thin Film Multilayers", Oct. 1999, Mumbai, India

I. Zizak, O. Paris, P. Roschger, S. Bernstorff, H. Amenitsch, K. Klaushofer and P. Fratzl
Investigation of bone and cartilage by Synchrotron Scanning SAXS and -WAXD with Micrometer Spatial Resolution
XI International Conference on Small-Angle Scattering (SAS99), Brookhaven National Laboratory, New York, USA, May 17 - 20, 1999 (talk)

Non-refereed Publications in 1999

R.Kleppinger, A.Valenca, S.Bernstorff, H.Amenitsch
In-situ studies on the Mesoscopic Order in Deformed Thermoplastic Elastomer Gels.
ELETTRA News 33, March 31, 1999

R. Schwarzenbacher, P. Jalili, H. Amenitsch, F. Nigon, M.J. Chapman, S. Bernstorff, P. Laggner and R. Prassl
The Austrian Small Angle X-ray Scattering Beamline goes Crystallography - Low Resolution Crystallography on Human Plasma Low Density Lipoprotein (LDL).
ELETTRA News 34, April 30, 1999

I. Zizak, O. Paris, P. Roschger, H. Amenitsch, S. Bernstorff, K.Klaushofer, P. Fratzl
Scanning SAXS/WAXD of Connective Tissue with 20 µm spatial resolution.
ELETTRA News Number: 36 - August 31, 1999
(http://www.elettra.trieste.it/science/news/volume36/EN60.html)

R.H. Menk, A. Sarvestani, H. Amenitsch, S. Bernstorff, H.J. Besch, A. Orthen, N. Pavel, M. Rappolt, N. Sauer and A.H. Walenta
State-of -the -Art Gaseous Imaging Detectors for time resolved SAXS experiments.
ELETTRA News 37, December 1, 1999

R. H. Menk, A. Sarvestani, S.Bernstorff, H.J. Besch , H.Amenitsch and A.H. Walenta
State-of-the-Art Gaseous Imaging Detectors for Advanced Biological Diffraction Studies
ELETTRA Highlights 1998/99

G. Pabst, M. Rappolt, H. Amenitsch, S. Bernstorff and P. Laggner
Non-Equilibrium Response-Kinetics of Phospholipid Bilayers in the Biologically Relevant L_α-Phase
ELETTRA Highlights 1998/99

M.Pregetter, R.Prassl, H.Amenitsch and P.Laggner
10 ms time-resolved x-ray diffraction of the core lipid transition of human Low Density Lipoproteins
ELETTRA Highlights 1998/99

Doctoral Theses

Patrik Ågren
Influence of Non-Ionic Polymers and Cationic Surfactants on Silica Sols, Gels and Porous Ceramic Materials
Department of Physical Chemistry, Åbo Akademi University, Turku, Finland 1999.

Diplom Theses (Tesi di Laurea)

Rita Farkas
Apolipoprotein AI: Faltung und Lipidbindung
TU Graz, May 1999

Leonardo Lucii
Il potenziamento da stiramento nel muscolo scheletrico studiato con metodi combinati di meccanica e diffrazione a raggi X con luce di sincrotrone
Università di Firenze, 9.9.1999

Udo Theissl
Nanostructured conjugated organic materials
Institut for Solid State Physics, Graz University of Technology, Austria, November 1999

Author Index